MICROCOPY RESOLUTION TEST CHART
NATIONAL BUREAU OF STANDARDS-1963-A

AFGL-TR-81-0018(I)

# ANALYSIS AND SIMULATION OF MULTISENSOR GRAVITY SURVEYS, VOLUME I

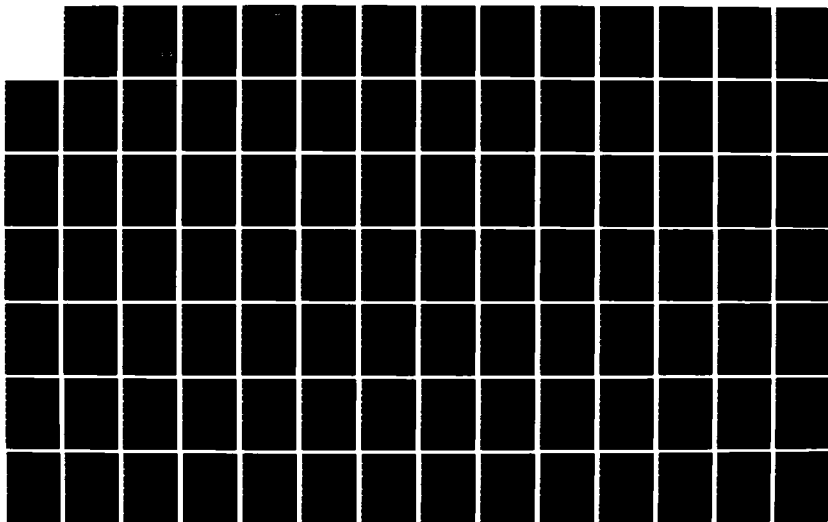Jacob D. Goldstein

AD-A160 388

The Analytic Sciences Corporation
One Jacob Way
Reading, Massachusetts 01867

Final Report
June 1977 - March 1981

1 December 1980; Modified 15 April 1985

DTIC
ELECTE
OCT 16 1985
B

Approved for public release; distribution unlimited

Prepared For:
**AIR FORCE GEOPHYSICS LABORATORY**
**AIR FORCE SYSTEMS COMMAND**
**UNITED STATES AIR FORCE**
**HANSCOM AFB, MASSACHUSETTS 01731**
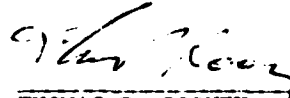
85 10 1 4

CONTRACTOR REPORTS

This technical report has been reviewed and is approved for publication.

THEODORE E. WIRTANEN
Contract Manager

THOMAS P. ROONEY
Chief, Geodesy & Gravity Branch

FOR THE COMMANDER

DONALD H. ECKHARDT
Director
Earth Sciences Division

This report has been reviewed by the ESD Public Affairs Office (PA) and is releasable to the National Technical Information Service (NTIS).

Qualified requesters may obtain additional copies from the Defense Technical Information Center. All others should apply to the National Technical Information Service.

If your address has changed, or if you wish to be removed from the mailing list, or if the addressee is no longer employed by your organization, please notify AFGL/DAA, Hanscom AFB, MA 01731. This will assist us in maintaining a current mailing list.

SECURITY CLASSIFICATION OF THIS PAGE (When Date Entered)

| REPORT DOCUMENTATION PAGE | | READ INSTRUCTIONS BEFORE COMPLETING FORM |
|---|---|---|
| 1. REPORT NUMBER<br>AFGL-TR-81-0018(I) | 2. GOVT ACCESSION NO.<br>AD-A140388 | 3. RECIPIENT'S CATALOG NUMBER |
| 4. TITLE (and Subtitle)<br>Analysis and Simulation of Multi-sensor Gravity Surveys, Volume I | | 5. TYPE OF REPORT & PERIOD COVERED<br>Final Report<br>June 1977-March 1981 |
| | | 6. PERFORMING ORG. REPORT NUMBER<br>TR-4423-4 |
| 7. AUTHOR(s)<br>Jacob D. Goldstein | | 8. CONTRACT OR GRANT NUMBER(s)<br>F19628-77-C-0152 |
| 9. PERFORMING ORGANIZATION NAME AND ADDRESS<br>The Analytic Sciences Corporation<br>One Jacob Way<br>Reading, Massachusetts 01867 | | 10. PROGRAM ELEMENT, PROJECT, TASK AREA & WORK UNIT NUMBERS<br>63701B<br>320432AA |
| 11. CONTROLLING OFFICE NAME AND ADDRESS<br>Air Force Geophysics Laboratory<br>Hanscom AFB, Massachusetts<br>Monitor/Theodore E. Wirtanen/LWG | | 12. REPORT DATE 1 Dec 1980;<br>Modified 15 April 1985 |
| | | 13. NUMBER OF PAGES<br>176 |
| 14. MONITORING AGENCY NAME & ADDRESS(If different from Controlling Office) | | 15. SECURITY CLASS. (of this report)<br>Unclassified |
| | | 15a. DECLASSIFICATION/DOWNGRADING SCHEDULE |

16. DISTRIBUTION STATEMENT (of this Report)

Approved for public release; distribution unlimited

17. DISTRIBUTION STATEMENT (of the abstract entered in Block 20, if different from Report)

18. SUPPLEMENTARY NOTES

Additional technical details and results are contained in
Scientific Report No. 4 AFGL-TR-81-0018(II)

19. KEY WORDS (Continue on reverse side if necessary and identify by block number)

| | |
|---|---|
| Gravity Surveys | Satellite-to-Satellite Tracking |
| Gravimetric Sensors | Gravity Gradiometer |
| Satellite Radar Altimeters | Gravity Field Model |

20. ABSTRACT (Continue on reverse side if necessary and identify by block number)

A new general methodology is developed for the determination of the statistics of multisensor survey residual gravity. The method is ideally suited for the design of multisensor surveys to achieve a desired level of gravity recovery accuracy. Survey types considered consist of any combination of satellite radar altimetry, high-low satellite-to-satellite tracking, shipborne or land-based gravimetry and airborne gradiometry. Several examples of the results obtained with the methodology are included. Keywords

DD FORM 1473 EDITION OF 1 NOV 65 IS OBSOLETE
1 JAN 73

UNCLASSIFIED

i SECURITY CLASSIFICATION OF THIS PAGE (When Data Entered)

# FOREWORD

This document contains the analysis, models and results obtained for the Air Force Geophysics Laboratory and the Defense Mapping Agency under Task 2 of Contract No. F19628-77-C-0152, "Integrated Gravity Studies."

| Accession For | |
|---|---|
| NTIS GRA&I | ✓ |
| DTIC TAB | ☐ |
| Unannounced | ☐ |
| Justification | |
| By | |
| Distribution/ | |
| Availability Codes | |
| | Avail and/or |
| Dist | Special |
| A-1 | |

iii

## TABLE OF CONTENTS

# LIST OF FIGURES

## LIST OF FIGURES (Continued)

## LIST OF TABLES

# 1.    INTRODUCTION

## 1.1    BACKGROUND

The detailed structure of the gravity field is inferred from data collected by a variety of instruments (sensors). These sensors measure different quantities and have different spectral responses and noise characteristics. Gravity estimates are obtained by combining measurements from all sources. From a practical point of view, it is of fundamental importance:

- To determine the accuracy of gravity estimates obtained from data already collected

- To determine what additional data and survey characteristics would yield a required accuracy of the estimates of gravity in a given region.

## 1.2    STUDY OBJECTIVES

The objectives of this study were to develop a methodology and a computer program for quantifying the errors in the estimates of gravity available from multisensor survey data. Survey types explicitly considered in this study consist of any combination of

- Satellite radar altimetry

- Satellite-to-satellite tracking (SST) in a high-low configuration

- Land-based/shipborne gravimetry

- Airborne gradiometry.

Other survey possibilities can be easily incorporated into the formulation.

A separate phase of this study dealt with the estimation of weapons systems' target miss induced by errors in the gravity estimates obtained from multisensor survey data. The results of this second phase of the study are presented in a separate, expanded version of this report.

## 1.3    TECHNICAL APPROACH

The approach utilizes a flat-earth approximation that furnishes algebraic frequency-domain interrelations among geodetic quantities. An extension of classical Wiener smoothing techniques (Ref. 1) permits the computation of the average power spectral density of the post-survey gravity residuals.

Since the Wiener smoother is optimal in the sense of minimizing the mean-square residuals, the results can be viewed as representing the best possible use of the survey data. Actually, there are some approximations involved in the evaluation of the spectral density of the residuals and, more fundamentally, in the use of the flat-earth formulation with its entailing loss of accuracy for wavelengths comparable to the radius of the earth. Nonetheless, since most of the energy in the gravity anomaly, deflections of the vertical, gravity disturbance vector and the gradients of gravity is contained in the frequency band where the method yields accurate results, the analysis does provide an accurate measure of the performable accuracy of the estimates of these quantities obtained from multisensor survey data.

Figure 1.3-1 presents a graphic illustration of the multisensor survey analysis methodology. The circle represents the results that are obtained through the application of the techniques discussed herein. They are the statistics of the post-survey residual gravity errors. The ovals represent the quantities that must be specified in the evaluation of the errors. These are: a statistical model for the unsurveyed anomalous field, sensor error models, and the characteristics of the survey. The box represents the operations performed on the input specifications to obtain the statistics of the residual gravity field.

R-62394a
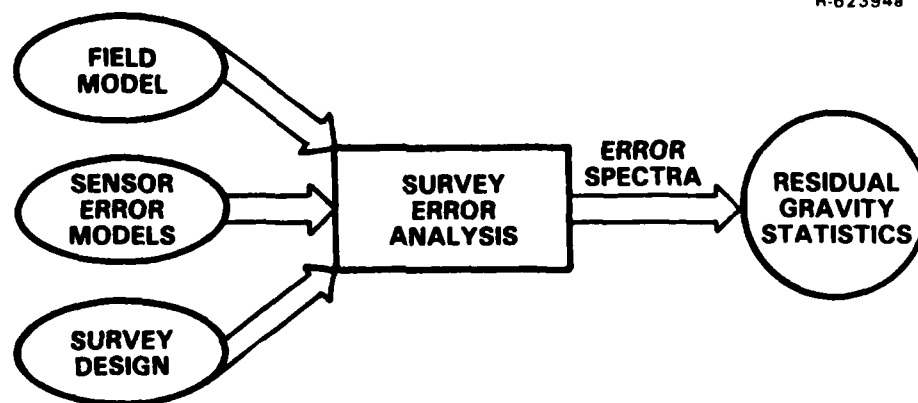


Figure 1.3-1    Multisensor Survey Analysis Methodology

The field model is the a priori power spectral density of the anomalous potential at the earth's surface. The statistics of all other field-related quantities are obtained from this power spectral density through the use of flat-earth relations (Ref. 2). The field model describes the local behavior of the gravity field in the vicinity of the region of interest (e.g., a missile launch point). Either analytical or empirical models can be used in the analysis.

A computer program was designed on the basis of the theory discussed in this report. A wide variety of survey possibilities were simulated. The results of these simulations are included and discussed in this report.

## 1.4  REPORT ORGANIZATION

The organization of this document is as follows: Chapter 2 presents an overview of the methodology for the analysis of multisensor gravity survey residual errors including error models for the various survey possibilities considered. Chapter 3 presents a collection of results obtained through the use of the techniques described in the previous chapter. Chapter 4 presents a summary of the information contained in this report and discusses several possible extensions of the analysis.

Various appendices complement this report. Appendix A presents a succinct compilation of those concepts of Fourier analysis necessary for the development of the theory of Chapter 2. Appendices B and C discuss additional technical aspects of the analysis. Appendix B gives the derivations of the flat-earth frequency-domain relations. Appendix C presents detailed derivations of the formulas for the spectral density of the post-survey residuals.

## 1.5  A NOTE ON TERMINOLOGY

It is customary to refer to functions that assume random values as random processes when these functions depend on a single variable or coordinate and as random fields when they depend on two or more variables or coordinates (see, for example, Ref. 3). To avoid confusion, the noun field is used only

in reference to the gravity field. Functions that assume random values are referred to as random processes in n-dimensional space or simply as random processes when the number of independent variables is clear from the context.

Random processes can be scalar or vector-valued depending on whether to every point in space there corresponds one or more than one real numbers. For the purpose of this report, a vector denotes any list of numbers associated with every point of the coordinate system. This list of numbers need not be a physical vector. For example, a three-dimensional vector process in two-dimensional space can consist of the undulation of the geoid, the gravity anomaly and the north component of the gravity disturbance vector over the earth's surface.

The term geodetic quantities refers to the collection consisting of the anomalous potential, the undulation of the geoid, the deflections of the vertical, the gravity anomaly, the gravity disturbance, the components of the gravity disturbance vector and the gravity gradients. Linear combinations of these quantities are referred to as field-related quantities.

2.      ANALYSIS OF MULTISENSOR GRAVIMETRIC SURVEY
                    RESIDUAL ERRORS


          This chapter presents a method for determining the
statistics of the errors in the anomalous field estimates ob-
tained from multisensor survey data.  The method, which is
based on an extension of optimal Wiener smoothing theory, per-
mits a characterization of the errors in estimates of point
and spatial averages of the gravity field in wavelengths which
are small compared to the radius of the earth.  Survey types
include any combination of satellite altimetry, satellite-to-
satellite tracking (SST), land-based/shipborne gravimetry and
airborne gradiometry.

          In the analysis, the round earth is approximated by
an infinite plane (flat-earth) which practically coincides
with the earth in the neighborhood of the region in which esti-
mates are sought.  Frequency-domain mappings (transfer func-
tions) are used to related field-related variables in a concise
algebraic manner.  The anomalous gravity field is viewed as a
realization of a stationary random process on the earth plane.
Values of the field above the earth are obtained via the flat-
earth upward continuation formula of Heiskanen and Moritz
(Ref. 2).

          Frequency-domain techniques are extensively used in
this chapter.  Appendix A contains a summary of the relevant
concepts, definitions, and results of Fourier analysis.

          This chapter is organized as follows:  Section 2.1
presents the frequency-domain relations between geodetic quan-
tities.  The expression for the average PSD of the post-survey

2-1

residuals is discussed in <u>Section 2.2</u>. Survey geometry and error models are described in <u>Section 2.3</u>.

## 2.1    FREQUENCY-DOMAIN FLAT-EARTH RELATIONS

To determine the residual gravity errors resulting from the performance of a multisensor survey, it is necessary to relate in a geophysically consistent manner the different types of gravity data collected by the survey.

Geodetic quantities are interrelated by integro-differential operators. For example, the deflections of the vertical are given in terms of the gravity anomaly by the formulas of Vening Meinesz, the gravity disturbance vector is the gradient of the anomalous potential, etc. These relations imply specific correlation structures when the gravity field is viewed as a realization of a stationary random field.

A similar observation can be made for the post-survey residual errors. Since the errors in the estimates obtained with any geophysically consistent data processing algorithm must satisfy the same mathematical constraints linking the estimated variables, the statistics of the errors will display the same correlation structure present in the original quantities.

With the use of the flat-earth approximation, the relatively complex integro-differential operators become simple algebraic relations between Fourier transforms. Ratios between Fourier transforms of geodetic quantities turn out to be rational functions of frequency denominated transfer functions[*]. In the case in which the field is seen as a realization of a

---

[*]The term "transfer function" is borrowed from an analogous concept in Systems Theory.

random process, ratios and products of transfer functions re-
late the power spectral and cross-spectral densities of all
field-related quantities.

Table 2.1-1 presents in the last column the transfer
functions from anomalous surface potential, $T_o$, to the geo-
detic quantities listed in the first column of the table. The
notation used throughout this report for all geodetic quanti-
ties is given in the second column of the table, while the
third column presents the space-domain relations between each
of the variables and the anomalous potential. The constant $g_o$
used in the table represents the mean value of gravity of the
earth ($g_o \simeq 9.798$ m/sec$^2$). The interpretation of each of the
transfer functions in Table 2.1-1 is discussed next.

Let $\hat{T}_o(\underline{s})$ be the Fourier transform of the anomalous
surface potential, i.e.,

$$\hat{T}_o(\underline{s}) = \iint\limits_{-\infty}^{\infty} T_o(\underline{x})e^{-i2\pi<\underline{x},\underline{s}>} \, dx_1 dx_2 \qquad (2.1-1)$$

In the above equation, $\underline{x} = (x_1,x_2)^T$ denotes the position of a
point on the plane with $x_1$ and $x_2$ measured in the east and
north directions, respectively, $\underline{s} = (s_1,s_2)^T$ is the vector
planar frequency with $s_1$ and $s_2$ representing frequencies meas-
ured in the east and north directions, $i = \sqrt{-1}$, and $<\underline{x},\underline{s}>$ is
the inner product of the vectors $\underline{x}$ and $\underline{s}$.

The Fourier transform of any of the quantities in the
first column of Table 2.1-1 can be obtained by multiplying
$\hat{T}_o(\underline{s})$ by the corresponding transfer function in the last column
of the table. For example, the Fourier transform of the anoma-
lous potential at height z is given by

TABLE 2.1-1

## TRANSFER FUNCTIONS FROM ANOMALOUS SURFACE POTENTIAL

| QUANTITY | SYMBOL | RELATION TO ANOMALOUS POTENTIAL | TRANSFER FUNCTION FROM ANOMALOUS SURFACE POTENTIAL[*] |
|---|---|---|---|
| Anomalous Potential at Height z | $T_z$ | $T_z$ | $e^{-2\pi s z}$ |
| Undulation of the Geoid | $N$ | $T_o/g_o$ | $1/g_o$ |
| East Deflection of the Vertical | $\eta$ | $-(\partial T_o/\partial x_1)/g_o$ | $-i2\pi s_1/g_o$ |
| North Deflection of the Vertical | $\xi$ | $-(\partial T_o/\partial x_2)/g_o$ | $-i2\pi s_2/g_o$ |
| Gravity Anomaly | $\Delta g$ | $-(\partial T_z/\partial z)\|_{z=0} - 2T_o/R$ | $2\pi s - 2/R$ |
| East Component of the Gravity Disturbance Vector at Height z | $\Gamma_{x_1}$ | $\partial T_z/\partial x_1$ | $i2\pi s_1 e^{-2\pi s z}$ |
| North Component of the Gravity Disturbance Vector at Height z | $\Gamma_{x_2}$ | $\partial T_z/\partial x_2$ | $i2\pi s_2 e^{-2\pi s z}$ |
| Vertical Component of the Gravity Disturbance Vector at Height z | $\Gamma_z$ | $\partial T_z/\partial z$ | $-2\pi s e^{-2\pi s z}$ |
| Gravity Disturbance at Height z | $\delta g$ | $-\partial T_z/\partial z$ | $2\pi s e^{-2\pi s z}$ |
| East-East Gradient at Height z | $\Gamma_{x_1 x_1}$ | $\partial^2 T_z/\partial x_1^2$ | $-4\pi^2 s_1^2 e^{-2\pi s z}$ |
| North-North Gradient at Height z | $\Gamma_{x_2 x_2}$ | $\partial^2 T_z/\partial x_2^2$ | $-4\pi^2 s_2^2 e^{-2\pi s z}$ |
| Vertical-Vertical Gradient at Height z | $\Gamma_{zz}$ | $\partial^2 T_z/\partial z^2$ | $4\pi^2 s^2 e^{-2\pi s z}$ |
| East-North Gradient at Height z | $\Gamma_{x_1 x_2}$ | $\partial^2 T_z/\partial x_1 \partial x_2$ | $-4\pi^2 s_1 s_2 e^{-2\pi s z}$ |
| East-Vertical Gradient at Height z | $\Gamma_{x_1 z}$ | $\partial^2 T_z/\partial x_1 \partial z$ | $-i4\pi^2 s_1 s e^{-2\pi s z}$ |
| North-Vertical Gradient at Height z | $\Gamma_{x_2 z}$ | $\partial^2 T_z/\partial x_2 \partial z$ | $-i4\pi^2 s_2 s e^{-2\pi s z}$ |

[*]$s = (s_1^2 + s_2^2)^{1/2}$

$$\hat{T}_z(\underline{s}) = e^{-2\pi s z}\,\hat{T}_o(\underline{s}) \qquad\qquad (2.1\text{-}2)$$

A complete derivation of the transfer functions presented in Table 2.1-1 is given in Appendix B.1. In particular, it is shown there that Eq. 2.1-2 is the frequency-domain equivalent of the flat-earth upward continuation formula of Ref. 2.

In the case in which the surface anomalous potential is seen as a realization of a stationary random process, all field-related quantities turn out to be jointly stationary. In fact, it is shown in Appendix B.2 that if $\underline{w}$ and $\underline{u}$ represent two vectors of field-related quantities with

$$\underline{w} = (w_1, w_2, \ldots, w_p)^T \qquad (2.1\text{-}3)$$

and

$$\underline{u} = (u_1, u_2, \ldots, u_q)^T \qquad (2.1\text{-}4)$$

then the cross-spectral density matrix of $\underline{w}$ and $\underline{u}$, $\Phi_{\underline{w},\underline{u}}(\underline{s})$, is given in terms of the power spectral density (PSD) of the surface anomalous potential, $\Phi_{T_o,T_o}(\underline{s})$, by[†]

$$\Phi_{\underline{w},\underline{u}} = \underline{G}\,\underline{F}^* \, \Phi_{T_o,T_o} \qquad (2.1\text{-}5)$$

where

$$\underline{G}(\underline{s}) = [G_1(\underline{s}),\ G_2(\underline{s}),\ \ldots,\ G_p(\underline{s})]^T \qquad (2.1\text{-}6)$$

and

$$\underline{F}(\underline{s}) = [F_1(\underline{s}),\ F_2(\underline{s}),\ \ldots,\ F_q(\underline{s})]^T \qquad (2.1\text{-}7)$$

are the vector transfer functions from surface anomalous potential to $\underline{w}$ and $\underline{u}$, respectively.

As an example, consider the situation where the vector $\underline{w}$ consists of three quantities: the east deflection of the vertical, the north deflection of the vertical and the undulation of the geoid so that

---

[†] A superscript asterisk denotes complex conjugate when attached to a scalar quantity and conjugate transpose when attached to a matrix or a vector.

$$\underline{w} = (\eta, \ \xi, \ N)^T \qquad (2.1\text{-}8)$$

and suppose the vector $\underline{u}$ has two components: the undulation of the geoid and the gravity disturbance at height $z$; i.e.,

$$\underline{u} = (N, \ \delta g)^T \qquad (2.1\text{-}9)$$

The vector transfer functions $\underline{G}$ and $\underline{F}$ are, from Table 2.1-1,

$$\underline{G}(\underline{s}) = (-i2\pi s_1/g_o, \ -i2\pi s_2/g_o, \ 1/g_o)^T \qquad (2.1\text{-}10)$$

and

$$\underline{F}(\underline{s}) = (1/g_o, \ 2\pi s e^{-2\pi s z})^T$$

Therefore, from Eq. 2.1-5, the cross-spectral density matrix

$$\Phi_{\underline{w},\underline{u}} = \begin{pmatrix} \Phi_{\eta,N} & \Phi_{\eta,\delta g} \\ \Phi_{\xi,N} & \Phi_{\xi,\delta g} \\ \Phi_{N,N} & \Phi_{N,\delta g} \end{pmatrix} \qquad (2.1\text{-}11)$$

is given in terms of the PSD of the anomalous surface potential, $\Phi_{T_o,T_o}$, by

$$\Phi_{\underline{w},\underline{u}}(\underline{s}) = \begin{pmatrix} -i2\pi s_1/g_o{}^2 & -i4\pi^2 s_1 s e^{-2\pi s z}/g_o \\ -i2\pi s_2/g_o{}^2 & -i4\pi^2 s_2 s e^{-2\pi s z}/g_o \\ 1/g_o{}^2 & 2\pi s e^{-2\pi s z}/g_o \end{pmatrix} \Phi_{T_o,T_o}(\underline{s})$$

$$(2.1\text{-}12)$$

## 2.2    MULTISENSOR SURVEY ERROR ANALYSIS

The frequency-domain flat-earth relations discussed in the previous section together with an extension of Wiener smoothing techniques form the basis for the analysis of the performable accuracy of the gravity estimates obtained from multisensor survey data.

The problem of determining the errors in the estimation of the gravity field from multisensor survey data can be formulated in the following manner:  it is desired to characterize the differences (estimation errors)

$$\delta \underline{w}(\underline{x}) = \underline{w}(\underline{x}) - \underline{w}^O(\underline{x}) \qquad (2.2\text{-}1)$$

between the true values of the process $\underline{w}(\underline{x})$, and the best estimates* $\underline{w}^O(\underline{x})$.  The components of $\underline{w}$ are any collection of field-related quantities.

The estimates $\underline{w}^O(\underline{x})$ are optimally obtained from n classes of measurements

$$\Gamma_\beta = \{\underline{\psi}_\beta(\underline{x}) | \underline{x} \; \epsilon \; M_\beta\}; \; \beta = 1,2,\ldots,n \qquad (2.2\text{-}2)$$

corresponding to the measurements that constitute the survey. Each class $\Gamma_\beta$ represents a collection of vector measurements, $\underline{\psi}_\beta$, in which all measurement points form a rectangular grid $M_\beta$.

The data, $\underline{\psi}_\beta$, are linear combinations of field-related quantities, $\underline{u}_\beta$, corrupted by additive noise, $\underline{E}_\beta$; i.e.,

---

*In the mean-square sense.

$$\underline{\psi}_\beta(\underline{x}) = \underline{u}_\beta(\underline{x}) + \underline{E}_\beta(\underline{x}); \quad \underline{x} \; \varepsilon \; M_\beta \tag{2.2-3}$$

In addition, the measurement errors, $\underline{E}_\beta$, $\beta = 1,2,\ldots,n$, are taken to be stationary gaussian processes independent of the gravity field.

The grid $M_\beta$ (see Fig. 2.2-1) is completely character-ized by three quantities: a rotation matrix, $\theta_\beta$, determined by the orientation of the survey tracks with respect to the east direction, a translation vector $\underline{r}_\beta$ which locates the posi-tion of the origin of the grid in the east-north frame, and a spacing matrix $J_\beta$, determined by the separation between survey tracks and between samples along a track. In terms of the quantities in Fig. 2.2-1, $\theta_\beta$, $\underline{r}_\beta$ and $J_\beta$ are defined by

$$\theta_\beta = \begin{pmatrix} \cos\theta & -\sin\theta \\ \sin\theta & \cos\theta \end{pmatrix} \tag{2.2-4}$$

$$\underline{r}_\beta = \theta_\beta \; (r_1', \; r_2')^T \tag{2.2-5}$$

and

$$J_\beta = \begin{pmatrix} \tau_1' & 0 \\ 0 & \tau_2' \end{pmatrix} \tag{2.2-6}$$

For the survey possibilities considered in this report, data can be divided into several classes, $\Gamma_\beta$. These are

- Two scalar-measurement classes for each satellite radar-altimeter mission. One class for the ascending passes and another class for the descending passes

2-8
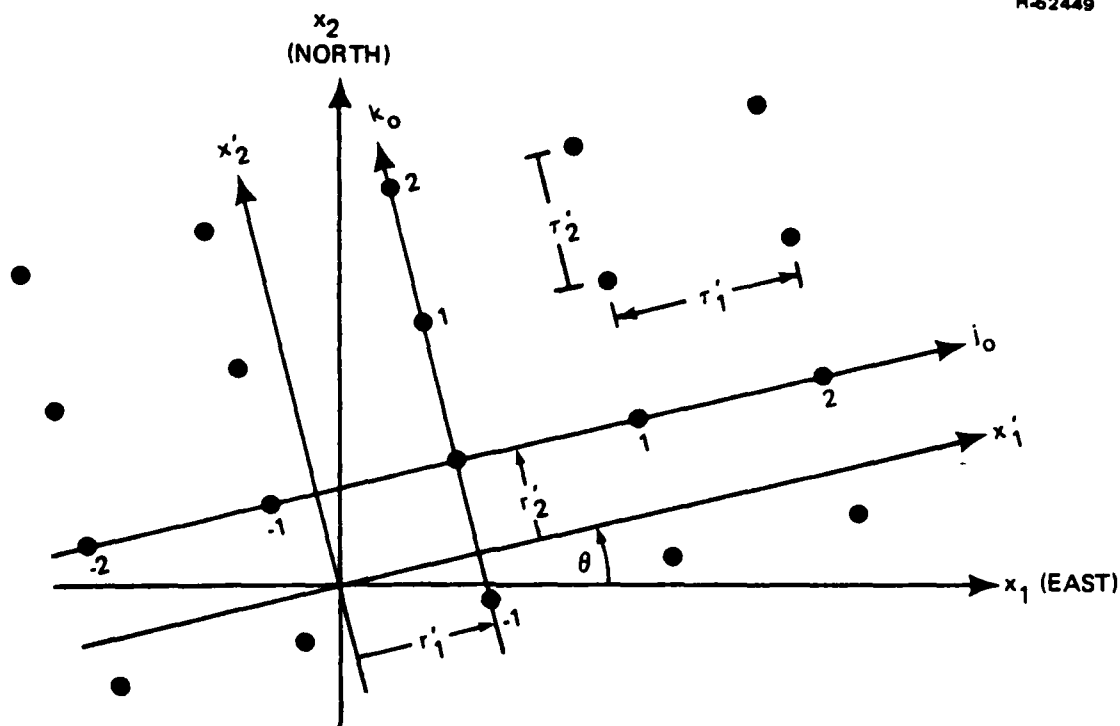
Figure 2.2-1    Definition of the Grid $M_\beta$

- Two scalar-measurement classes for a high-low satellite-to-satellite tracking mission. One class for the ascending and another for the descending passes of the low satellite

- One scalar-measurement class for a land-based or ship gravimetric survey. The differences between land-based and ship surveys are reflected in the error models

- One vector-measurement class for an airborne gradiometer survey. Each vector measurement in this class consists of six entries corresponding to the two outputs from each of the instruments in a gradiometer triad.

Appendix C presents a detailed analysis of the problem formulated above. The statistics of the post-survey residual errors at any given point are shown to depend upon the relative

position of the point with respect to the measurements. The average spectral density of the residuals is then defined by averaging over all possible relative locations with respect to the measurements. For the residual surface anomalous potential, the average spectral density is given by

$$\Phi_{\delta T_o, \delta T_o} = \cfrac{1}{\displaystyle\sum_{\beta=1}^{n} \underline{F}_\beta^* \, \Phi_{\underline{\zeta}_\beta, \underline{\zeta}_\beta}^{-1} \, \underline{F}_\beta + 1/\Phi_{T_o, T_o}} \qquad (2.2\text{-}7)$$

where $\underline{F}_\beta$ is the vector transfer function from surface anomalous potential to the quantities measured in class $\beta$, $\Phi_{\underline{\zeta}_\beta, \underline{\zeta}_\beta}$ is the spectral density matrix of the errors in class $\beta$ (see below) and $\Phi_{T_o, T_o}$ is the PSD of the unsurveyed surface anomalous potential obtained from a gravity-field model.

The spectral density matrix of the errors in class $\beta$ consists of two terms:

$$\Phi_{\underline{\zeta}_\beta, \underline{\zeta}_\beta}(\underline{s}) = \tilde{\Phi}_{\underline{E}_\beta, \underline{E}_\beta}(\underline{s}) + \Phi_{\underline{a}_\beta, \underline{a}_\beta}(\underline{s}) \qquad (2.2\text{-}8)$$

The first term, $\tilde{\Phi}_{\underline{E}_\beta, \underline{E}_\beta}$, is the unnormalized[*] spectral density of the (discrete) measurement error process $\underline{E}_\beta$ of Eq. 2.2-3. Explicit expressions for $\tilde{\Phi}_{\underline{E}_\beta, \underline{E}_\beta}$ are given in Section 2.3 for the various survey possibilities considered. The second term, $\Phi_{\underline{a}_\beta, \underline{a}_\beta}$, is the spectral density matrix of the aliasing errors in class $\beta$ computed from

$$\Phi_{\underline{a}_\beta, \underline{a}_\beta}(\underline{s}) = \sum_{\underline{\Lambda} \varepsilon Q_\beta} \underline{F}_\beta(\underline{s} + \theta_\beta J_\beta^{-1} \underline{\Lambda}) \, \underline{F}_\beta^*(\underline{s} + \theta_\beta J_\beta^{-1} \underline{\Lambda}) \, \Phi_{T_o, T_o}(\underline{s} + \theta_\beta J_\beta^{-1} \underline{\Lambda})$$

$$(2.2\text{-}9)$$

---

[*]See Appendix A.

where $\underline{\Lambda} = (\ell,m)^T$ is a vector with integer components and the set $Q_\beta$ is defined as

$$Q_\beta = \{\underline{\Lambda}|\underline{\Lambda}\neq\underline{0}, \ ||\underline{s}+\Theta_\beta J_\beta^{-1}\underline{\Lambda}|| < 2||\underline{\bar{s}}'||\} \qquad (2.2-10)$$

where

$$\underline{\bar{s}}' = (1/2\tau_1', \ 1/2\tau_2')^T \qquad (2.2-11)$$

is the vector of Nyquist frequencies associated with the grid $M_\beta$ and $||\cdot||$ denotes vector magnitude.

Equation 2.1-5 is used to determine the statistics of residuals in quantities other than the surface anomalous potential. If $\underline{w}$ is a vector whose components are arbitrary field-related quantities, the spectral density matrix of the post-survey residuals in $\underline{w}$ is obtained from

$$\Phi_{\delta\underline{w},\delta\underline{w}} = \underline{G} \ \underline{G}^* \ \Phi_{\delta T_o,\delta T_o} \qquad (2.2-12)$$

where $\underline{G}$ is the vector transfer function from surface anomalous potential to $\underline{w}$. The inverse Fourier transform of $\Phi_{\delta\underline{w},\delta\underline{w}}$ yields the covariance matrix of the residuals:

$$R_{\delta\underline{w},\delta\underline{w}}(\underline{x}) = \iint\limits_{-\infty}^{\infty} \Phi_{\delta\underline{w},\delta\underline{w}}(\underline{s})e^{i2\pi<\underline{x},\underline{s}>} \ ds_1 ds_2 \qquad (2.2-13)$$

from which root-mean-square (rms) values of the residuals in the components of $\underline{w}$ are easily obtained by taking square roots of the diagonal entries in $R_{\delta\underline{w},\delta\underline{w}}(\underline{0})$.

In many instances it is convenient to express post-survey residual gravity in terms of spatially-averaged values. Next, the formulas for the average spectral density of the

residuals are particularized to the estimation of spatially-averaged quantities.

Consider a square block with sides of length, a, parallel to the east and north directions. Let $\underline{x} = (x_1, x_2)^T$ be the center of the block. The a-mean, $\bar{y}^a$, of a field-related quantity y at the point $\underline{x}$ is the average of y on this block, i.e.,

$$\bar{y}^a(\underline{x}) = \frac{1}{a^2} \int_{x_2-a/2}^{x_2+a/2} \int_{x_1-a/2}^{x_1+a/2} y(\underline{x}') \, dx_1' dx_2' \qquad (2.2\text{-}14)$$

where $\underline{x}' = (x_1', x_2')^T$.

Now, suppose that the vector of quantities to be estimated from the survey data consists exclusively of a-means. Let $\underline{\bar{w}}^a$ be the field vector to be estimated. It is shown in Appendix C that the vector transfer function from anomalous surface potential to the estimated vector is $\hat{h} \, \underline{G}$ where $\underline{G}$ is the vector transfer function from anomalous surface potential to the vector $\underline{w}$ whose a-means are $\underline{\bar{w}}^a$ and

$$\hat{h}(\underline{s}) = \frac{\sin \pi a s_1}{\pi a s_1} \frac{\sin \pi a s_2}{\pi a s_2} \qquad (2.2\text{-}15)$$

is the transfer function associated with the a-mean averaging operation. Consequently, from Eq. 2.1-5, the average spectral density of the residuals in the a-means, $\Phi_{\delta \underline{\bar{w}}^a, \delta \underline{\bar{w}}^a}$, is

$$\Phi_{\delta \underline{\bar{w}}^a, \delta \underline{\bar{w}}^a} = \underline{G} \, \underline{G}^* \, |\hat{h}|^2 \, \Phi_{\delta T_o, \delta T_o} \qquad (2.2\text{-}16)$$

with $\Phi_{\delta T_o, \delta T_o}$ given by Eq. 2.2-7.

2-12

From Eqs. 2.2-12 and 2.2-16, the spectral density
matrix of a-mean residuals can be expressed as

$$\Phi_{\delta \bar{\underline{w}}^a, \delta \bar{\underline{w}}^a} = |\hat{h}|^2 \, \Phi_{\delta \underline{w}, \delta \underline{w}} \qquad (2.2\text{-}17)$$

Thus, to evaluate the statistics of the residuals in the a-means
it suffices to multiply the spectral density of the residuals in
(the point quantities) $\underline{w}$ by the squared magnitude of the averag-
ing transfer function $\hat{h}$ as in Eq. 2.2-17.


## 2.3    SURVEY GEOMETRY AND MEASUREMENT ERROR MODELS

This section presents the geometry and the error models
associated with the following types of survey:

- Satellite Radar Altimetry

- High-Low SST

- Land-based/Shipborne Gravimetry

- Airborne Gradiometry

in subsections 2.3.1 through 2.3.4, respectively.  Survey geom-
etry refers to the position of the measurements and the orien-
tation of the sensors with respect to the earth.  Measurement
error models refer to the enumeration and characterization of
the various error sources which affect the individual
measurements.

The geometry and type of survey determine the rotation
and spacing matrices $\Theta_\beta$ and $J_\beta$ and the transfer functions $F_\beta$
from anomalous surface potential to the quantities being meas-
ured.  These, in turn, characterize completely the aliasing
errors once a field model is specified (Eq. 2.2-9).

2-13

The measurement error models determine the spectral densities $\tilde{\Phi}_{\underline{E}_\beta, \underline{E}_\beta}$ of Eq. 2.2-8. Explicit formulas for these spectral densities are given in this section.

### 2.3.1 Satellite Radar-Altimeter Survey

The geometry of a satellite radar-altimeter survey is illustrated in Fig. 2.3-1. Satellite groundtracks are viewed as two collections of parallel equally-spaced straight-line tracks containing data at regular intervals along each track.

Two measurement classes are associated with the survey: one class, A, corresponds to the ascending tracks; the other, D, corresponds to the descending tracks. Let the grids associated

R-40095a
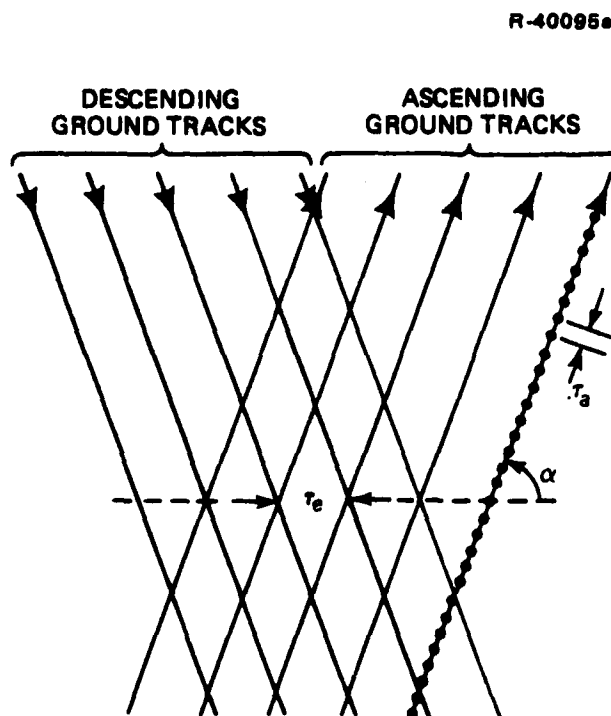


Figure 2.3-1    Satellite Altimeter Survey Geometry

with these two classes be $M_A$ and $M_D$. Contiguous parallel tracks are separated by a distance $\tau_e$ in the east direction and successive measurements along a track are separated by a distance

$$\tau_a \simeq t_a \ R \left[ \frac{Gm_e}{(R+h)^3} \right]^{1/2} \qquad (2.3\text{-}1)$$

where $t_a$ is the time interval between altimeter samples ($t_a \simeq 0.1$ sec for GEOS-3 and SEASAT-1), $Gm_e$ is the product of the gravitational constant and the mass of the earth ($Gm_e \simeq 3.986 \times 10^{14}$ m³/sec²), R is the radius of the earth ($R \simeq 6.378 \times 10^6$ m) and h is the height of the satellite over the earth's surface ($h \simeq 8.0 \times 10^5$ m) for GEOS-3 and SEASAT-1.

The angle $\alpha$ is the angle the ascending groundtracks form with the east direction at the center of the region where estimates are sought (the origin of the plane of the flat-earth approximation). This angle can be computed from

$$\tan \alpha = \frac{(\cos^2 \vartheta - \cos^2 \gamma)^{1/2}}{\cos \gamma - 0.058834 \ \cos^2 \vartheta \ (\frac{R+h}{R})^{3/2}} \qquad (2.3\text{-}2)$$

where $\vartheta$ is the latitude of the origin of the plane of the flat-earth approximation and $\gamma$ is the inclination of the satellite's orbit ($\gamma = 115°$ for GEOS-3 and $\gamma = 108°$ for SEASAT-1).

The grids $M_A$ and $M_D$ have axes parallel to those of primed reference frames (see Fig. 2.2-1) which correspond to rotation angles of $\alpha$ and $-\alpha$ with respect to the east direction. Let $\Theta_A$ and $\Theta_D$ be the rotation matrices of the grids $M_A$ and $M_D$, respectively. These matrices are given by

$$\theta_A = \begin{pmatrix} \cos \alpha & -\sin \alpha \\ \sin \alpha & \cos \alpha \end{pmatrix} \qquad (2.3\text{-}3)$$

and

$$\theta_D = \begin{pmatrix} \cos \alpha & \sin \alpha \\ -\sin \alpha & \cos \alpha \end{pmatrix} \qquad (2.3\text{-}4)$$

The spacing matrices $J_A$ and $J_D$ of the grids $M_A$ and $M_D$ coincide with each other and are given by

$$J_A = J_D = \begin{pmatrix} \tau_a & 0 \\ 0 & \tau_c \end{pmatrix} \qquad (2.3\text{-}5)$$

where $\tau_a$ is given by Eq. 2.3-1 and

$$\tau_c = \tau_e \sin \alpha \qquad (2.3\text{-}6)$$

The value of $\tau_e$ (Fig. 2.3-1) can be found from the equatorial separation of the groundtracks, $\tau_{eq}$, by the simple formula

$$\tau_e = \tau_{eq} \cos \vartheta \qquad (2.3\text{-}7)$$

Satellite radar-altimetry data furnish values of the undulation of the geoid corrupted by measurement noise. Thus, the transfer functions from anomalous surface potential to the quantities being measured in classes A and D, $F_A$ and $F_D$, are identical to each other and correspond to the transfer function from anomalous surface potential to undulation of the geoid given in Table 2.1-1; i.e.,

$$F_A(\underline{s}) = F_D(\underline{s}) = 1/g_0 \qquad (2.3\text{-}8)$$

Measurement error models are discussed next. For sym-
metry reasons, the spectral densities of the errors in classes
A and D agree with each other when they are expressed in terms
of the primed coordinate systems of their respective classes.
Thus, an expression for the spectral density of the errors,
$\tilde{\Phi}'_{E,E}(\underline{s}')$, in terms of frequencies $\underline{s}' = (s_a, s_c)^T$ measured in
the along-track $(s_a)$ and cross-track $(s_c)$ directions is derived
first. The spectral densities of the errors in classes A and
D are then obtained in terms of east and north frequencies by
suitable rotations of coordinate systems.

The Nyquist frequencies in the along-track and cross-
track directions are $1/2\tau_a$ and $1/2\tau_c$, respectively. Since the
measurement error spectral density $\tilde{\Phi}'_{E,E}(\underline{s}')$ is periodic in the
along-track and cross-track directions with a period of twice
the Nyquist frequency in each direction, it suffices to speci-
fy $\tilde{\Phi}'_{E,E}(\underline{s}')$ on the domain $-1/2\tau_a < s_a < 1/2\tau_a$ and $-1/2\tau_c < s_c < 1/2\tau_c$.

The error $E(\underline{\Omega})$ in the measurement at the point
$\underline{\Omega} = (j,k)^T$ of any one of the grids $M_A$ or $M_D$ is taken to be the
additive combination of three independent error sources:

$$E(\underline{\Omega}) = N(\underline{\Omega}) + C(\underline{\Omega}) + B(\underline{\Omega}) \qquad (2.3-9)$$

The terms N, C and B correspond respectively to

- Instrument noise and sea-state effects
  (scattering of the radar pulse by ocean
  surface waves)

- Uncorrected ocean-current dynamic height

- Post-adjustment bias-type orbit and tide-
  correction errors.

2-17

The spectral density of the measurement errors, $\tilde{\Phi}'_{E,E}$, is the sum of the spectral densities of the terms on the right-hand side of Eq. 2.3-9; i.e.,

$$\tilde{\Phi}'_{E,E} = \tilde{\Phi}'_{N,N} + \tilde{\Phi}'_{C,C} + \tilde{\Phi}'_{B,B} \qquad (2.3-10)$$

First, consider the instrument noise and sea-state errors N. These errors are independent from measurement point to measurement point and from track to track. Their covariance is

$$R_{N,N}(\underline{\Omega}) = \sigma_N^2 \, \delta(\underline{\Omega}) \qquad (2.3-11)$$

where $\sigma_N$ is the standard deviation of the error N in each measurement ($\sigma_N = 0.6$ m for GEOS-3 and 0.1 m for SEASAT-1) and where $\delta(\underline{\Omega})$ is given by

$$\delta(\underline{\Omega}) = \begin{cases} 1 & \text{if } \underline{\Omega} = \underline{0} \\ 0 & \text{otherwise} \end{cases} \qquad (2.3-12)$$

The spectral density $\tilde{\Phi}'_{N,N}$ is the finite Fourier transform of $R_{N,N}$:

$$\tilde{\Phi}'_{N,N}(\underline{s}') = \Delta(J_A) \sum_{\underline{\Omega}} R_{N,N}(\underline{\Omega}) \, e^{-i2\pi \langle J_A\underline{\Omega}, \underline{s}' \rangle} \qquad (2.3-13)$$

where $J_A = J_B$ is the spacing matrix of the grid and $\Delta(J_A) = \tau_a \tau_c$ is the determinant of $J_A$. Since $R_{N,N}(\underline{\Omega})$ vanishes for all $\underline{\Omega} \neq \underline{0}$, the spectral density $\Phi'_{N,N}$ can be easily evaluated. The result is the constant (white) spectrum

$$\tilde{\Phi}'_{N,N}(\underline{s}') = \tau_a \tau_c \sigma_N^2 \qquad (2.3-14)$$

Next, consider the uncorrected ocean-current dynamic height errors $C(\underline{\Omega})$. Reference 4 presents a statistical model

2-18

for the spatial distribution of the ocean-current induced sea-surface height over the geoid as a continuous scalar process defined in two-dimensional space, $h(\underline{x}')$. The spectral density of $h$ is that of an isotropic third-order Markov model (Ref. 5) given by

$$\Phi'_{h,h}(\underline{s}') = \frac{10\pi\sigma_h^2\beta_h^5}{[\beta_h^2+(2\pi s')^2]^{7/2}} \qquad (2.3\text{-}15)$$

where $\sigma_h$ (in m) is the standard deviation of the sea-surface height given as a function of latitude by

$$\sigma_h = 0.677 \sin\vartheta \qquad (2.3\text{-}16)$$

and where $1/\beta_h = 4.2\times10^4$m is the characteristic distance[*] of the model. In Eq. 2.3-15, $s' = ||\underline{s}'|| = (s_a^2+s_c^2)^{1/2}$.

The spectral density $\Phi'_{h,h}$ is an instantaneous model in the sense that it characterizes the spatial variability of the sea-surface height at a fixed time. Actually (Ref. 6), ocean-current induced sea-surface height does not vary substantially for time spans of the order of one day. However, after a period of one or two weeks, there is no significant correlation between the sea-surface height at the beginning and end of the period. Consequently, the sea-surface height model of Eq. 2.3-15 can be used to infer the behavior of the errors $C(\underline{\Omega})$ for a single track of data but cannot be used for relating the errors in different tracks.

---

[*]The characteristic distance $1/\beta_h$ should not be confused with the correlation distance. For a third-order Markov process the correlation distance is $2.903/\beta_h$ (Ref. 5). The correlation distance of the sea-surface height model is 122 km.

In practical situations, most pairs of parallel ground-tracks chosen arbitrarily over the region where estimates are sought correspond to satellite passes interspaced by periods of several weeks. Thus, the ocean-current induced sea-surface height errors on different tracks are modeled as being independent of one another.

The spectral density of the sea-surface height on a single groundtrack[*], $S_{h,h}(s_a)$ is obtained by integrating the two-dimensional spectral density $\Phi'_{h,h}(\underline{s}')$ in the crosstrack direction (see Appendix A, Eq. A-106):

$$S_{h,h}(s_a) = \int_{-\infty}^{\infty} \Phi'_{h,h}(\underline{s}') \, ds_c \qquad (2.3-17)$$

The result of this integration is

$$S_{h,h}(s_a) = \frac{16\sigma_h^2\beta_h^5/3}{[\beta_h^2+(2\pi s_a)^2]^3} \qquad (2.3-18)$$

This spectral density describes the behavior of the groundtrack sea-surface height as a continuous (one-dimensional) process. The spectral density of the measurement errors along a track of data, $S_{C,C}(s_a)$ correspond to the aliased version of this continuous process. In Appendix C.2, the effects of sampling a two-dimensional process are analyzed. A similar analysis for one-dimensional processes yields the following relation between the spectral density, $S_{h,h}$ and $S_{C,C}$ of the continuous and sampled versions of the process

---

[*]The uppercase letter S is used to denote one-dimensional spectral densities.

2-20

$$S_{C,C}(s_a) = \sum_{\ell=-\infty}^{\infty} S_{h,h}\ (s_a + \ell/\tau_a) \qquad (2.3\text{-}19)$$

Since sea-surface height errors in different tracks are independent, the (two-dimensional) error spectral density $\tilde{\Phi}'_{C,C}(\underline{s}')$ is white in the crosstrack direction. Thus,

$$\tilde{\Phi}'_{C,C}(\underline{s}') = \tau_c \sum_{\ell=-\infty}^{\infty} S_{h,h}(s_a + \ell/\tau_a) \qquad (2.3\text{-}20)$$

A graphical interpretation of Eq. 2.3-19 is presented in Fig. 2.3-2. The PSD of the errors along a track is obtained as the infinite superposition of translates of the PSD of the continuous process representing the sea-surface height. Consider the interval $-1/2\tau_a < s_a < 1/2\tau_a$. Except for the regions near the edges of the interval, there is negligible contribution to the sum in Eq. 2.3-19 from terms for which $\ell \neq 0$[*]. In the regions near the edges of the interval, the PSD of the errors arising from instrument noise and sea-state effects, $\tilde{\Phi}_{N,N}$, is much larger (ten orders of magnitude) than $\tilde{\Phi}'_{C,C}$. Thus, for all practical purposes, the PSD of the ocean-current induced sea-surface height errors in the interval $-1/2\tau_a < s_a < 1/2\tau_a$ can be taken as

$$\tilde{\Phi}'_{C,C}(\underline{s}') = \frac{16\tau_c\sigma_h^2\beta_h^5/3}{[\beta_h^2 + (2\pi s_a)^2]^3} \qquad (2.3\text{-}21)$$

For values of $s_a$ outside this interval, $\tilde{\Phi}'_{C,C}(\underline{s}')$ is obtained by repeating Eq. 2.3-21 periodically as indicated by the solid line in Fig. 2.3-2.

---

[*]This is because the characteristic distance $1/\beta_h$ is two orders of magnitude larger than the sampling spacing $\tau_a$.

$s_{c,c}$

$\ell = 1$    $\ell = 0$    $\ell = -1$    $\ell = -2$

$-3/2\tau_a$    $-1/\tau_a$    $-1/2\tau_a$    $1/2\tau_a$    $1/\tau_a$    $3/2\tau_a$    $s_a$
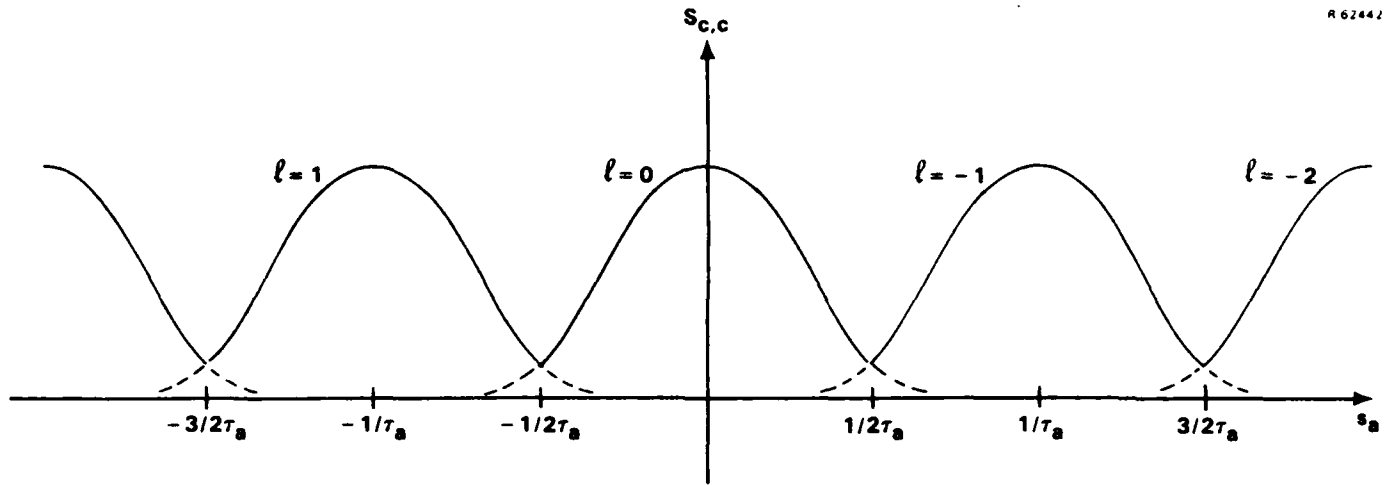
Figure 2.3-2    Graphical Interpretation of Eq. 2.3-19

Next, consider the bias-type orbit and tide correction errors, $B(\underline{\Omega})$. On any finite-length of single-track data, these errors manifest themselves as an apparent bias with a standard deviation of $\sigma_B = 0.5$ m. In the cross-track direction, the errors $B(\underline{\Omega})$ are modeled as being independent from track to track for the same reasons uncorrected ocean-current induced sea-surface height errors are taken as independent in that direction.

The spectral density of $B(\underline{\Omega})$ is modeled as being Gaussian in the along-track direction with a correlation distance equal to the radius of the earth, R, and as being white in the cross-track direction. Thus, for $-1/2\tau_a < s_a < 1/2\tau_a$

$$\tilde{\Phi}'_{B,B}(\underline{s}') = \sqrt{\pi} \; \tau_c \; R\sigma_B^2 \; e^{-\pi^2 R^2 s_a^2} \tag{2.3-22}$$

For $|s_a| > 1/2\tau_a$ the value of $\tilde{\Phi}'_{B,B}(s_a)$ is found by reproducing periodically the values on the right-hand side of Eq. 2.3-22.

The satellite radar-altimeter survey error spectrum $\tilde{\Phi}'_{E,E}(\underline{s}')$ is given by the sum of the (periodically-continued)

2-22

spectra of Eqs. 2.3-14, 2.3-21 and 2.3-22. In terms of frequencies measured in the east $(s_1)$ and north $(s_2)$ directions, the class A measurement error spectrum can be computed from

$$\tilde{\Phi}_{E,E}(\underline{s}) = \tilde{\Phi}'_{E,E}(\theta_A^* \underline{s}) \qquad (2.3-23)$$

and the measurement error spectrum of class D can be obtained from

$$\tilde{\Phi}_{E,E}(\underline{s}) = \tilde{\Phi}'_{E,E}(\theta_D^* \underline{s}) \qquad (2.3-24)$$

where $\theta_A$ and $\theta_D$ are given by Eqs. 2.3-3 and 2.3-4 and where $\underline{s} = (s_1, s_2)^T$.

### 2.3.2 High-Low SST Survey

The convention on the position of the measurements of a survey consisting of high-low SST data is shown in Fig. 2.3-3. The survey data consist of range-rate measurements from a satellite in synchronous orbit to a satellite in a lower orbit corrected for the nominal motion of the low satellite and the spurious motion of the high satellite. In other words, the data consist of noisy measurements of the line-of-sight component of the variational velocity induced on the low satellite by the gravity disturbance at height h.

As in the geometry of the satellite radar-altimeter survey, measurements on the earth plane lie at regular intervals on equally-spaced ascending and descending groundtracks. The same notation used in Subsection 2.3.1 is adopted here for convenience. Thus, Eqs. 2.3-1 through 2.3-7 which describe

2-23
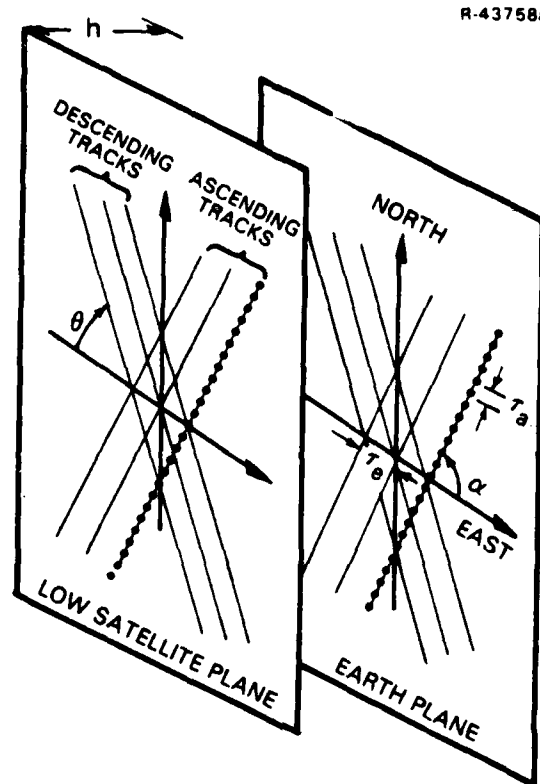
Figure 2.3-3     Convention on the Position of
                 High-Low SST Measurements

the geometry of the grids $M_A$ (ascending groundtracks) and $M_D$ (descending groundtracks) hold in this case as well.*

The transfer functions from anomalous surface potential to the measurements in classes A and D are considered next. The acceleration perturbation, $\dot{\underline{v}}$, acting on the low satellite at any point along its trajectory is the gravity disturbance vector; i.e.,

$$\dot{\underline{v}} = (\Gamma_{x_1}, \Gamma_{x_2}, \Gamma_z) \qquad (2.3-25)$$

---

*In Eq. 2.3-1, $t_a$ becomes the time interval between successive range-rate samples usually taken as $t_a = 10$ sec.

Therefore, the velocity perturbation, $\underline{v}$, is the time-integral of the gravity disturbance at height h over the satellite's groundtrack.

Let V be the speed at which the groundtrack is swept:

$$V \simeq R \left[ \frac{Gm_e}{(R+h)^3} \right]^{1/2} \qquad (2.3\text{-}26)$$

Since integration with respect to time can be replaced by integration with respect to distance in the along-track direction normalized by V, the vector transfer function from anomalous surface potential to velocity perturbation, $\underline{F}_v$, is the product of the transfer function from anomalous surface potential to gravity disturbance at height h and the transfer function associated with the operation of spatial integration in the along-track direction normalized by the constant V. It is shown in Appendix A (Eq. A-13) that the transfer function corresponding to integration in the along-track direction is $1/(i2\pi s_a)$ where $s_a$ is frequency measured in the along-track direction. Thus, from Table 2.1-1

$$\underline{F}_v = \frac{e^{-2\pi s h}}{V s_a} (s_1, s_2, is)^T \qquad (2.3\text{-}27)$$

At any point along the satellite's path, the line-of-sight component of the velocity $\underline{v}$ is the scalar product $\langle \underline{u}, \underline{v} \rangle$ where $\underline{u}$ is a unit vector in the direction from the high to the low satellite. Measurement geometry is illustrated in Fig. 2.3-4. The high satellite lies on the equatorial plane at a distance $h_s = 3.5786 \times 10^7$ m from the surface of the earth. The low satellite is at latitude $\vartheta$ and at longitude $\lambda$ measured with respect to the meridian on which the high satellite remains stationary. The unit vector in the direction from the high to

2-25
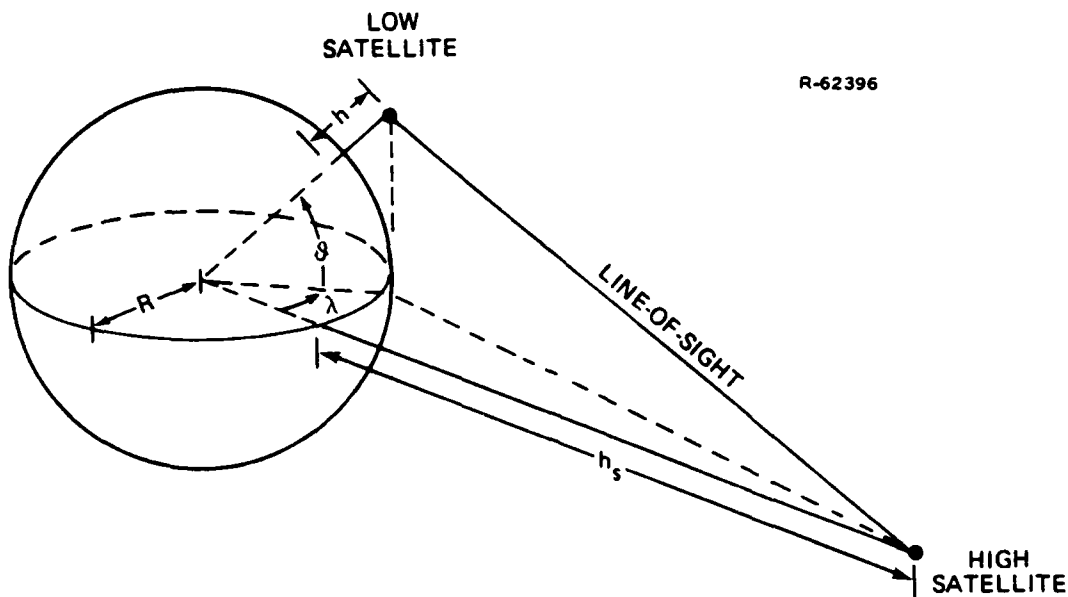
Figure 2.3-4    SST Measurement Geometry

the low satellite is given in an east-north-vertical frame at the position of the low satellite by

$$\underline{u} = \begin{pmatrix} u_1 \\ u_2 \\ u_z \end{pmatrix} = \frac{1}{\rho} \begin{pmatrix} (R+h_s)\sin\lambda \\ (R+h_s)\ \sin\vartheta\cos\lambda \\ (R+h)-(R+h_s)\cos\vartheta\cos\lambda \end{pmatrix} \qquad (2.3\text{-}28)$$

where

$$\rho = [(R+h)^2 + (R+h_s)^2 - 2(R+h)(R+h_s)\cos\vartheta\cos\lambda]^{1/2} \quad (2.3\text{-}29)$$

The unit vector, $\underline{u} = (u_1, u_2, u_z)^T$, varies as the low satellite changes its position over the earth. This implies that the measurement equations are time-varying. However, gravity estimates are sought on a small region of the earth over which the unit vector $\underline{u}$ can be approximated by a constant vector. This constant vector is chosen as that obtained from Eq. 2.3-28 when $\vartheta$ and $\lambda$ are interpreted as the coordinates of the origin of the plane of the flat-earth approximation.

2-26

The transfer function from anomalous surface potential to measured quantities is given by the scalar product $\langle \underline{u}, \underline{F}_v \rangle$. For the measurements of class A, the along-track frequency $s_a$ appearing in Eq. 2.3-27 can be expressed in terms of east ($s_1$) and north ($s_2$) frequencies as

$$s_a = s_1 \cos\alpha + s_2 \sin\alpha \qquad (2.3-30)$$

where $\alpha$ is the angle of Eq. 2.3-2. Consequently, the transfer function of class A is

$$F_A(\underline{s}) = \frac{(u_1 s_1 + u_2 s_2 + i u_z s) e^{-2\pi s h}}{V(s_1 \cos\alpha + s_2 \sin\alpha)} \qquad (2.3-31)$$

Similarly, the transfer function of class D is

$$F_D(\underline{s}) = \frac{(u_1 s_1 + u_2 s_2 + i u_z s) e^{-2\pi s h}}{V(s_1 \cos\alpha + s_2 \sin\alpha)} \qquad (2.3-32)$$

A simplified measurement error model has been used to obtain the results of Chapter 4. The errors in the measurements are modeled as being independent of one another. The spectral densities of the errors in classes A and D are identical to each other and are given by

$$\tilde{\Phi}_{E,E}(\underline{s}) = \tau_a \tau_c \sigma^2 \qquad (2.3-33)$$

where $\tau_a$ and $\tau_c$ are the measurement spacings in the along-track and cross-track directions and where $\sigma$ is the standard deviation of the error in each measurement.

### 2.3.3 Land-Based/Shipborne Gravimetric Survey

Land-based and shipborne gravimetric surveys are considered in this subsection. Shipborne gravimetric survey geometry and measurement error models are discussed first. Corresponding models for land-based surveys are then obtained by removing from the shipborne gravimetric survey models those effects which are particular to ocean surveys.

Shipborne Gravimetric Survey - The geometry of a shipborne gravimetric survey is illustrated in Fig. 2.3-5. Survey data are collected at regular intervals by a gravimeter on board a ship traveling at constant speed along parallel equally-spaced east-west tracks. Since the measurement grid is oriented with the east-north reference frame, the rotation matrix, $\theta$, is the identity, I. The spacing matrix is

R-40096
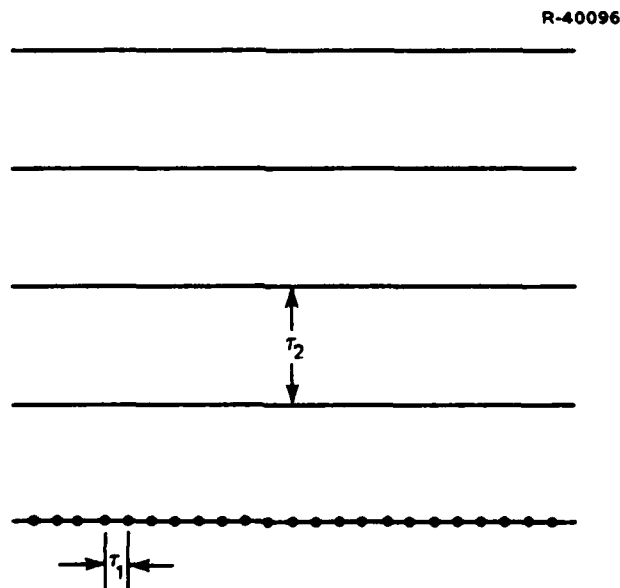


Figure 2.3-5    Shipborne Gravimetric Survey Measurement Geometry

2-28

$$J = \begin{pmatrix} \tau_1 & 0 \\ 0 & \tau_2 \end{pmatrix} \qquad (2.3\text{-}34)$$

where $\tau_2$ is the spacing between tracks and where

$$\tau_1 = V \, \Delta t \qquad (2.3\text{-}35)$$

is the spacing in the east direction given in terms of the nominal ship's speed V and the time interval between samples $\Delta t$. Typical values are assumed for $\tau_2$, V, and $\Delta t$ based on NAVOCEANO's survey patterns.

The transfer function from surface anomalous potential to the quantity being measured is discussed next. Denote by $\zeta$ the difference between the gravimeter readings and reference gravity at the points where measurements are taken. Because of the motion of the ship over the earth's surface, the quantity $\zeta$ is not the gravity anomaly. To account for the ship's motion, several corrections are applied to the acceleration $\zeta$.

Let $\underline{v} = (v_1, v_2)^T$ and $\vartheta$ be the true velocity of the survey ship with respect to the earth* and its true latitude. The gravity field includes the centrifugal acceleration due to the rotation of the earth. This acceleration is directed away from the axis of rotation and has a magnitude $R\omega^2\cos\vartheta_t$ at latitude $\vartheta_t$ ($\omega$=0.7292115147×10$^{-4}$ rad/sec). The component directed towards the center of the earth is $-R\omega^2\cos^2\vartheta_t$. The motion of the ship in the east direction causes the instantaneous angular

_____

*$E(v_1) = V$, $E(v_2) = 0$

2-29

velocity to differ from the angular velocity of the earth by an amount $\delta\omega$ given by

$$\delta\omega = \frac{v_1}{R \cos\vartheta_t} \qquad (2.3\text{-}36)$$

To first-order, the corresponding contribution to the gravimeter measurement is

$$\zeta' = -2R\omega \cos^2\vartheta_t \; \delta\omega \qquad (2.3\text{-}37)$$

or, combining Eqs. 2.3-36 and 2.3-37,

$$\zeta' = -2\omega v_1 \cos\vartheta_t \qquad (2.3\text{-}38)$$

In addition to the contribution resulting from the difference in rotation rates, there is an acceleration of

$$\zeta'' = -(v_1^2 + v_2^2)/R \qquad (2.3\text{-}39)$$

resulting from the motion of the ship over a curved surface.

If the gravimeter readings were error-free, the gravity anomaly could be computed from

$$\Delta g = \zeta - \zeta' - \zeta'' \qquad (2.3\text{-}40)$$

However, the velocity and latitude which enter into the computations in Eqs. 2.3-38 and 2.3-39 are not perfectly known. The evaluation of Eq. 2.3-40 is performed using the Inertial Navigation System (INS)-indicated velocity $\underline{v}^o = (v_1^o, v_2^o)^T$ and latitude $\vartheta^o$. Thus, shipborne gravimetric data consist of the

following combination of gravimeter readings and measurements
from an inertial navigator:

$$\psi = \zeta + 2\omega v_1^o \cos\vartheta^o + ||\underline{v}^o||^2/R \qquad (2.3-41)$$

By adding and subtracting the true correction $\zeta' + \zeta''$, Eq. 2.3-41
can be written as

$$\psi = (\zeta - \zeta' - \zeta'') + 2\omega\cos\vartheta^o \, \delta v_1 + 2\omega v_1^o \sin\vartheta^o \, \delta\vartheta$$

$$+ 2v_1^o \delta v_1/R + 2v_2^o \delta v_2/R \qquad (2.3-42)$$

where second-order terms have been neglected and where

$$\delta\underline{v} = (\delta v_1, \delta v_2)^T = (v_1^o - v_1, \, v_2^o - v_2)^T \qquad (2.3-43)$$

is the error in the velocity estimate from the INS and
$\delta\vartheta = \vartheta^o - \vartheta_t$ is the error in latitude.

When typical values of $\delta v_1$, $\delta v_2$, and $\delta\vartheta$ are considered,
the combined contribution of the last three terms in the right-
hand side of Eq. 2.3-42 is several orders of magnitude smaller
than that of the term $2\omega\cos\vartheta^o \, \delta v_1$. Therefore, the last three
terms in Eq. 2.3-42 can be neglected. On the other hand, since
the latitude $\vartheta^o$ does not vary substantially over the survey
region, the angle $\vartheta^o$ can be replaced by $\vartheta$, the latitude of the
origin of the plane of the flat-earth approximation. Thus,
for all practical purposes, Eq. 2.3-42 can be rewritten as

$$\psi = \zeta - \zeta' - \zeta'' + 2\omega\cos\vartheta \, \delta v_1 \qquad (2.3-44)$$

The term $2\omega\cos\vartheta \, \delta v_1$ is called the Eötvos correction
error. It is caused by the error in the estimate of the east
component of velocity obtained from the INS aboard the survey

ship. The east-velocity error, in turn, arises from the east
component of the gravity disturbance vector sensed by the iner-
tial navigator and from random accelerometer and gyro errors.
Consequently, if shipborne gravimetric data are viewed as grav-
ity anomaly measurements, the measurement errors are correlated
with the gravity field. This correlation must be accounted
for in data processing algorithms.

An equivalent formulation is obtained when the data
are viewed as consisting of noisy measurements of linear combi-
nations of the gravity anomaly and the east component of the
gravity disturbance vector modulated by the INS response.
This convention is adopted here. Let u and y be the INS east-
velocity errors induced by the gravity field and by random
errors in the inertial navigator instruments (accelerometer
and gyro errors), respectively. Equation 2.3-44 becomes

$$\psi = (\zeta - \zeta' - \zeta'') + (2\omega\cos\vartheta)u + (2\omega\cos\vartheta)y \qquad (2.3\text{-}45)$$

The term $(2\omega\cos\vartheta)u$ is considered part of the measured quantities.
Measurement errors include the term $(2\omega\cos\vartheta)y$. In this formu-
lation, measurement errors turn out to be independent of the
gravity field.

In order to determine the transfer function, F, from
the anomalous surface potential to the quantity being meas-
ured, it is necessary to relate the velocity errors u and the
east component of the gravity disturbance vector $\Gamma_{x_1}$. The INS
transfer function from sensed acceleration to indicated veloc-
ity is very well approximated by that of a damped second-order
system. When the input acceleration and the output velocity

are expressed as functions of time the (steady-state) transfer function[*], $\bar{G}(f)$, is given by

$$\bar{G}(f) = \frac{f/2\pi}{2\rho f_o f + i(f^2 - f_o^2)} \qquad (2.3\text{-}46)$$

where $f$ is frequency measured in Hertz, $\rho$ is the INS damping coefficient and $f_o = (g_o/R)^{1/2}/2\pi$ is the Schuler frequency ($f_o = 1.9708 \times 10^{-4}$ Hz).

The INS transfer function from sensed acceleration to indicated velocity as functions of distance in the east direction, $G(s_1)$, can be obtained by making the transformation $f = Vs_1$. Thus, $G(s_1) = \bar{G}(Vs_1)$, and from Eq. 2.3-46,

$$G(s_1) = \frac{s_1/(2\pi V)}{2\rho(f_o/V)s_1 + i[s_1^2 - (f_o/V)^2]} \qquad (2.3\text{-}47)$$

It then follows from Eqs. 2.3-40 and 2.3-45 that the shipborne gravimetric survey transfer function, $F$, is given by

$$F(\underline{s}) = [2\pi s - 2/R] + 2\omega\cos\vartheta[i2\pi s_1]G(s_1) \qquad (2.3\text{-}48)$$

where the two quantities in brackets are the transfer functions from anomalous surface potential to gravity anomaly and to the east component of the gravity disturbance vector at the surface, respectively.

Note that the relation $f = Vs_1$ used in deriving Eq. 2.3-47 is an approximation because the east velocity is

_____

[*]The integration in the definition of Fourier transform is carried out over the time domain.

not truly constant. However, its use in obtaining Eq. 2.3-47 is equivalent to neglecting second-order terms.

The shipborne survey measurement error model is discussed next. Consider first the uncorrelated Eötvos correction error, C, corresponding to the term $(2\omega\cos\vartheta)y$ in Eq. 2.3-45. These errors are modeled as arising from a white noise sensed acceleration input with a constant spectral density q. Therefore, the spectral density of the velocity errors, y, on a single track of data is

$$S_{y,y}(s_1) = q|G(s_1)|^2 \qquad (2.3-49)$$

The value of q was chosen by assuming that the velocity errors, y, have an rms value $\sigma_y$ for a typical INS, i.e.,

$$\sigma_y^2 = \int_{-\infty}^{\infty} S_{y,y}(s_1)\, ds_1 \qquad (2.3-50)$$

This results in a value of $q = 8\pi V f_o \rho \sigma_y^2$.

Velocity errors arising from accelerometer and gyro errors are modeled as independent on different tracks. Following the same reasoning used in obtaining Eq. 2.3-21 from Eq. 2.3-18, the spectral density of the uncorrelated Eötvos correction errors in the interval $-1/2\tau_1 < s_1 < 1/2\tau_1$ can be written as

$$\tilde{\Phi}_{C,C}(\underline{s}) = 4\omega^2\cos^2\vartheta\,\tau_2\, q|G(s_1)|^2 \qquad (2.3-51)$$

where $\tau_1$ and $\tau_2$ are defined in Fig. 2.3-5.

2-34

The gravimeter recordings themselves also contain various errors. _First_, there are quantization, instrument noise and improperly filtered heave motion induced errors. These are all combined into a single error term, I, modeled as being independent from point to point and track to track, and having an rms value of $\sigma_I = 1.0 \times 10^{-6}$ m/sec$^2$ (0.1 mgal). The PSD of I is

$$\Phi_{I,I}(\underline{s}) = \tau_1 \tau_2 \sigma_I^2 \qquad (2.3-52)$$

_Second_, the platform is not directly on the geoid because of tidal and ocean current dynamic sea-surface height effects. If the platform is at height h over the geoid, the gravimeter reading is in error by an amount $-2g_o h/R$ ($2g_o/R = 0.308$ mgal/m). In the open ocean, the effects on the gravimeter readings caused by tidal effects can be predicted to an accuracy of better than 0.03 mgal (Ref. 7). Consequently, these effects are neglected in the error model.

Consider the errors K induced in the gravimeter readings by ocean currents. Ocean current induced sea-surface height, h, is modeled as in Eq. 2.3-15. The spectral density of h (seen as a continuous process) is

$$\Phi_{h,h}(\underline{s}) = \frac{10\pi\sigma_h^2\beta_h^5}{[\beta_h^2 + (2\pi s)^2]^{7/2}} \qquad (2.3-53)$$

As opposed to the altimeter survey case, successive tracks are surveyed within relatively short periods of time. Thus, Eq. 2.3-53 is adopted directly as the model for sea-surface height in the survey region. The spectral density of the aliased version of h, H, is given by

$$\tilde{\phi}_{H,H}(s) - \sum_{\Lambda} \phi_{h,h}(s + J^{-1}\Lambda) \qquad (2.3\text{-}54)$$

where the summation is taken over all integer-valued vectors $\underline{\Lambda} = (j,k)^T$ and where $J$ is as in Eq. 2.3-34.

For frequencies $\underline{s}$ such that $-1/2\tau_1 < s_1 < 1/2\tau_1$ and $-1/2\tau_2 < s_2 < 1/2\tau_2$ the contribution to the sum in Eq. 2.3-54 from all terms for which $j \neq 0$ is negligible because the along-track Nyquist wavelength, $2\tau_1$, is two orders of magnitude smaller than the correlation distance of the sea-surface height model (122 km). However, in some instances, the Nyquist wavelength in the crosstrack direction, $2\tau_2$, is comparable to the correlation distance of the sea-surface height model. For $-1/2\tau_1 < s_1 < 1/2\tau_1$ and $-1/2\tau_2 < s_2 < 1/2\tau_2$, the aliased spectrum of the sea-surface height is approximated as

$$\tilde{\phi}_{H,H}(\underline{s}) = \sum_{k=-1}^{1} \phi_{h,h}\,[\underline{s} + (0, k/\tau_2)^T] \qquad (2.3\text{-}55)$$

For the same range of frequencies, the corresponding PSD of the gravimeter measurement errors, K, induced by sea-surface height is

$$\tilde{\phi}_{K,K}(\underline{s}) = \frac{4g_o^2}{R^2}\, \tilde{\phi}_{H,H}(\underline{s}) \qquad (2.3\text{-}56)$$

with $\tilde{\phi}_{H,H}$ as in Eq. 2.3-55.

In the absence of any other error sources, the spectral density of the shipborne survey measurement errors, $\tilde{\phi}_{E,E}$ is given by the sum of the spectral densities of the velocity-induced errors (Eq. 2.3-51), the quantization errors (Eq. 2.3-52) and the ocean current-induced errors (Eq. 2.3-56); i.e.,

$$\tilde{\Phi}_{E,E}(\underline{s}) = \tilde{\Phi}_{C,C}(\underline{s}) + \tilde{\Phi}_{I,I}(\underline{s}) + \tilde{\Phi}_{K,K}(\underline{s}) \qquad (2.3\text{-}57)$$

for $-1/2\tau_1 < s_1 < 1/2\tau_1$ and $-1/2\tau_2 < s_2 < 1/2\tau_2$. However, actual surveys conducted by NAVOCEANO follow the geometry of Fig. 2.3-5 on nearly rectangular blocks. An example of the characteristic block layout is presented in Fig. 2.3-6. Often, two contiguous blocks share a common region but, in some instances, there are small data gaps (islands, reefs, etc.) in the coverage. Since track spacing is chosen on the basis of high-frequency energy content in the gravity field, neighboring blocks tend to have the same track spacing but the tracks in one block are not, in general the continuation of tracks in another block.

R-62443
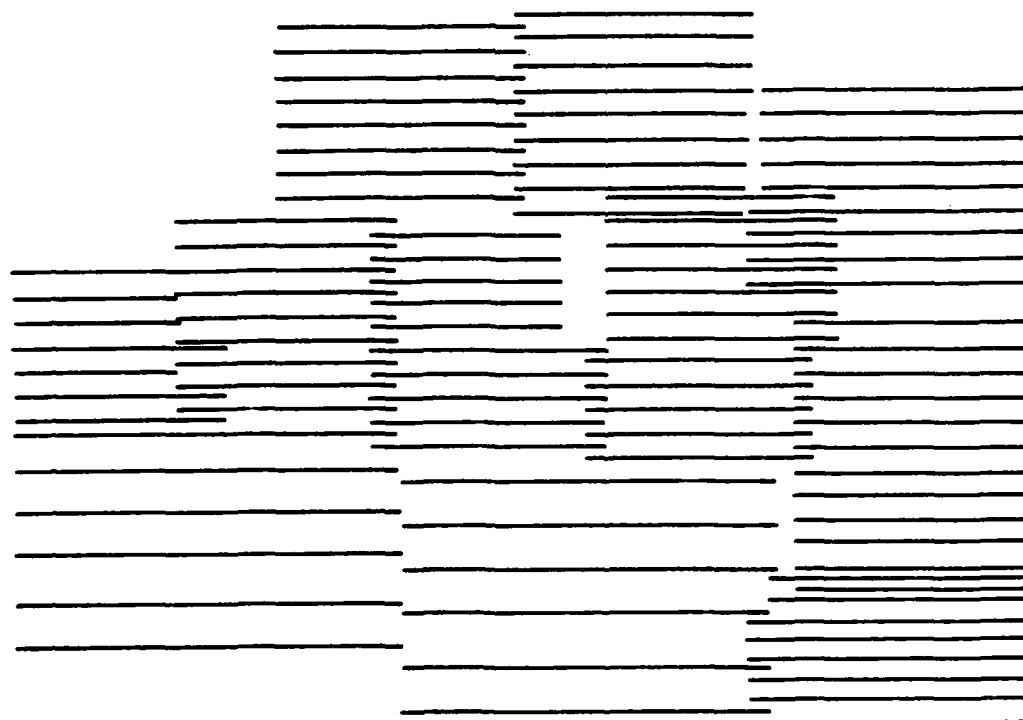


Figure 2.3-6    Characteristic Block Layout of
NAVOCEANO Surveys

A conservative approach was used to take into account these irregularities:  Only the information contained in shipborne survey data in the shorter wavelengths is used to arrive at gravity estimates.  This was modeled by setting the measurement error spectra $\tilde{\Phi}_{E,E}$ equal to infinity for longer wavelengths.  Thus, Eq. 2.3-57 was modified as

$$\tilde{\Phi}_{E,E}(\underline{s}) = \begin{cases} \tilde{\Phi}_{C,C}(\underline{s}) + \tilde{\Phi}_{I,I}(\underline{s}) + \tilde{\Phi}_{K,K}(\underline{s}) & \text{if } s > s_o \\ \infty & \text{if } s < s_o \end{cases}$$

$$(2.3-58)$$

with $s = ||\underline{s}|| = (s_1^2 + s_2^2)^{1/2}$ and $s_o$ equal to the frequency cutoff selected.  For numerical computations the number $10^{30}$ was used in place of infinity.  This number is at least 10 orders of magnitude larger than any other quantity appearing in the computations when MKS units are used.

Summarizing, for a shipborne gravimetric survey the transfer function from anomalous surface potential to the quantities being measured is given by Eq. 2.3-48 and the spectral density of the measurement errors is given by Eq. 2.3-58.

Land-Based Gravimetric Survey - The  model  for  the geometry of a land-based gravimetric survey is illustrated in Fig. 2.3-7.  Measurement points are assumed to form a grid oriented with the east and north axes.  The distances between data points in the east and north directions are $\tau_1$ and $\tau_2$, respectively.  It then follows that, as in the shipborne gravimetric survey, the rotation matrix, $\Theta$, of the measurement grid is the identity and the spacing matrix, J, is given by an expression identical to Eq. 2.3-34.  Land-based gravimetric data are thus assumed to have been gridded prior to processing. Research is currently in progress to account directly for the

R-62444
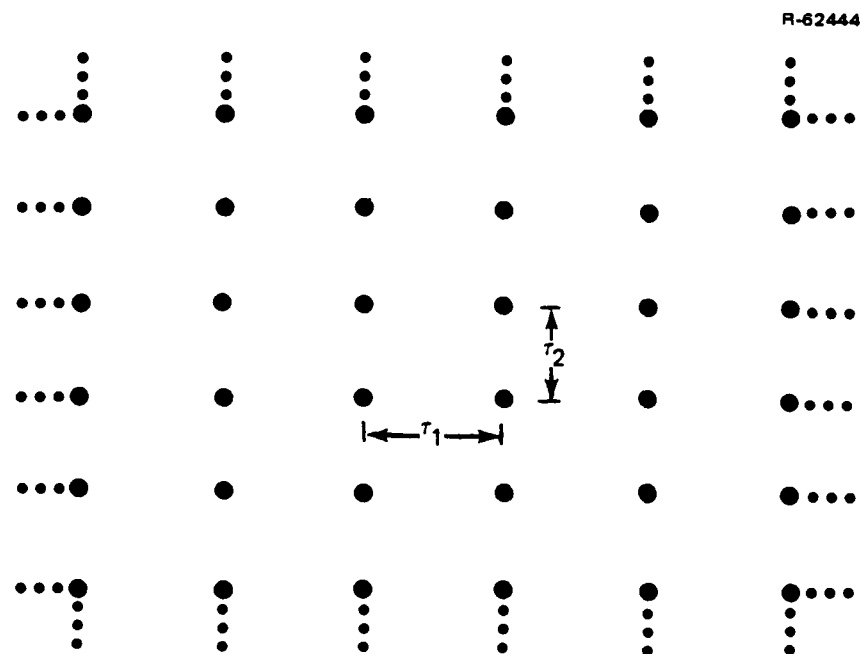
Figure 2.3-7     Land-Based Gravimetric Survey Geometry

irregular geometry associated with the collection of land-based
gravimetric data.

Data consist of measurements of gravity anomaly re-
duced to the geoid.  The transfer function from anomalous sur-
face potential to measured quantities is

$$F(\underline{s}) = 2\pi s - 2/R \qquad (2.3-59)$$

Measurement errors are modeled as being independent
from point to point with standard deviation $\sigma$.  Their spectral
density is

$$\widetilde{\Phi}_{E,E}(\underline{s}) = \tau_1 \tau_2 \sigma^2 \qquad (2.3-60)$$

Instrument errors, gridding errors, and errors in the process
of reducing the measurements to the geoid are included in

2-39

Eq. 2.3-60. For the results given in Chapter 3 of this report, $\tau_1 = \tau_2 = 1.5\times10^5$ m and $\sigma = 3\times10^{-5}$ m/sec$^2$ (3 mgal).

### 2.3.4  Airborne Gradiometer Survey

Figure 2.3-8 presents the convention on the position of the measurements of an airborne gradiometer survey. Data are collected by a triad of gradiometers aboard an aircraft flying on parallel equally spaced east-west tracks at an altitude h above the surface of the earth. The spacing in the north direction is $\tau_2$ and the spacing in the east direction is

$$\tau_1 = Vt_g \qquad (2.3-61)$$

where V is the (nominal) speed of the aircraft and $t_g$ is the time interval between successive samples. Thus, the rotation matrix of the measurement grid, $\theta$, is the identity and the spacing matrix is

$$J = \begin{pmatrix} \tau_1 & 0 \\ 0 & \tau_2 \end{pmatrix} \qquad (2.3-62)$$

R—437578
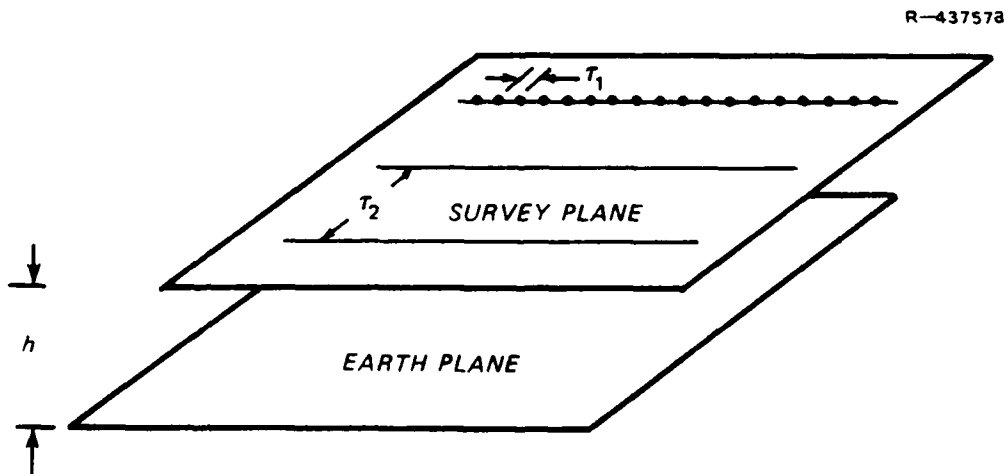


Figure 2.3-8    Airborne Gradiometer Survey
Measurement Geometry

Prototype gravity gradiometers developed by the Bell Aerospace Division of Textron, Inc. (Bell) and the Charles Stark Draper Laboratory (CSDL) were considered in the analysis. Measurement equations for airborne surveys using the Bell and CSDL gradiometers are given below.

Bell Gradiometer Survey Transfer Function - A schematic diagram of a Bell gradiometer is presented in Fig. 2.3-9. The instrument uses four matched-accelerometers mounted on a slowly rotating (0.25 Hz) table. The outputs of the accelerometers are mixed, preamplified, band-limited and demodulated at twice the rotation frequency to yield two gradient measurements, one at 0 deg phase and the other at 90 deg. Let the axes x', y' and z' be defined as in Fig. 2.3-9. One of the measurements (inline-channel), $v_i$, consists of the difference between the two inline gradients lying on the plane of rotation divided by two:

$$v_i = (\Gamma_{x'x'} - \Gamma_{y'y'})/2 \qquad (2.3-63)$$

R-28144b
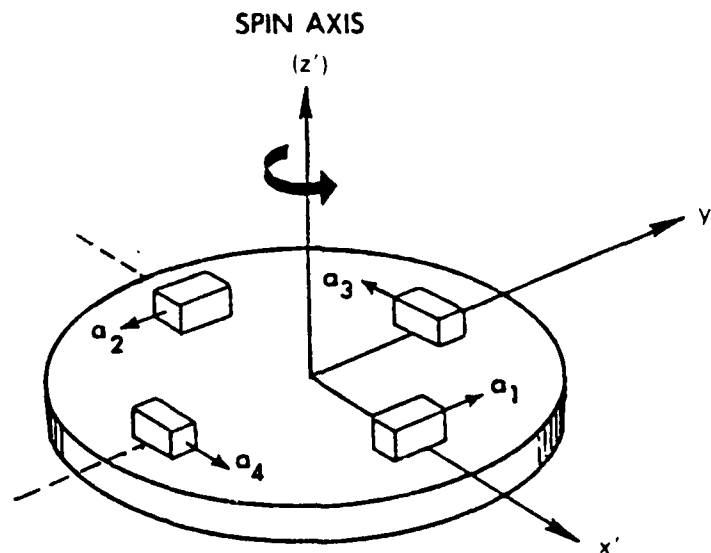


Figure 2.3-9     Bell Gradiometer Idealization

2-41

The other measurement (cross-channel), $v_c$, yields the rotation plane cross-gradient:

$$v_c = \Gamma_{x'y'} \qquad\qquad (2.3\text{-}64)$$

The geometry for the configuration of the gradiometer triad was chosen so that the instruments' spin axes coincided with the vertical (z), north ($x_2$) and east ($x_1$) directions (Fig. 2.3-10). These orientations are consistent with test data provided by Bell for their Baseline gradiometer instrument. Consequently, from Eqs. 2.3-63 and 2.3-64 it follows that the measurement equations are given by

$$
\begin{pmatrix} v_1 \\ v_2 \\ v_3 \\ v_4 \\ v_5 \\ v_6 \end{pmatrix}
=
\begin{pmatrix}
1/2 & -1/2 & 0 & 0 & 0 & 0 \\
0 & 0 & 0 & 1 & 0 & 0 \\
-1/2 & 0 & 1/2 & 0 & 0 & 0 \\
0 & 0 & 0 & 0 & 1 & 0 \\
0 & 1/2 & -1/2 & 0 & 0 & 0 \\
0 & 0 & 0 & 0 & 0 & 1
\end{pmatrix}
\begin{pmatrix} \Gamma_{x_1 x_1} \\ \Gamma_{x_2 x_2} \\ \Gamma_{zz} \\ \Gamma_{x_1 x_2} \\ \Gamma_{x_1 z} \\ \Gamma_{x_2 z} \end{pmatrix}
$$

$$(2.3\text{-}65)$$

where $v_1$, $v_3$ and $v_5$ are the inline-channel outputs and $v_2$, $v_4$ and $v_6$ the cross-channel outputs from the gradiometers whose spin axes are oriented in the vertical, north and east directions, respectively. The vector transfer function, $\underline{F}$, from anomalous surface potential to the measured quantities is easily obtained from Table 2.1-1. The result is
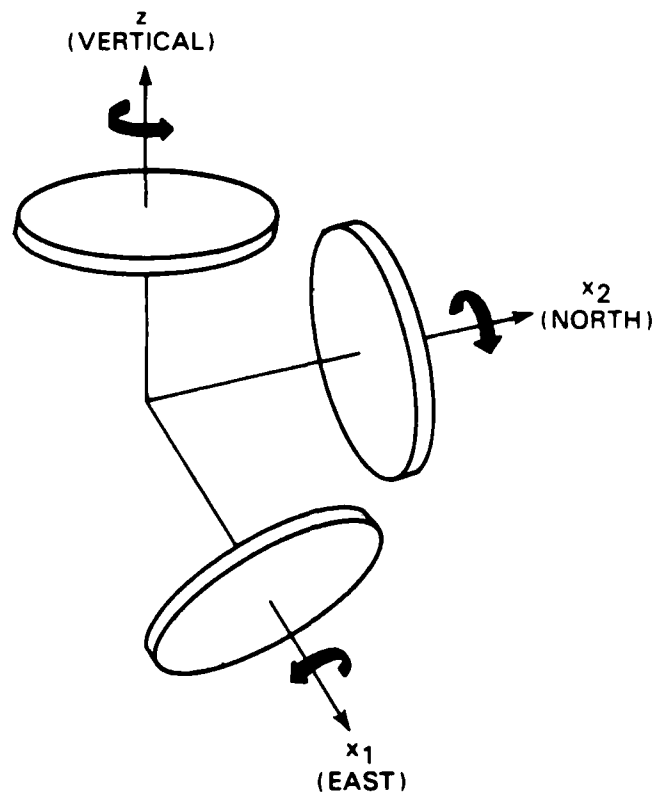
Figure 2.3-10    Bell Gradiometer Triad

$$\underline{F}(\underline{s}) = B \, \underline{H} \, (\underline{s}) \qquad (2.3\text{-}66)$$

where B is the 6×6 matrix of Eq. 2.3-65 and $\underline{H}$ is the vector

$$\underline{H}(\underline{s}) = 4\pi^2 e^{-2\pi sh} \begin{pmatrix} -s_1^2 \\ -s_2^2 \\ s^2 \\ -s_1 s_2 \\ -i s_1 s \\ -i s_2 s \end{pmatrix} \qquad (2.3\text{-}67)$$

2-43

CSDL Gradiometer Survey Transfer Function - The CSDL gradiometer (Fig. 2.3-11) employs a floated electrostatically suspended sphere with dense material packed symmetrically about two opposite poles. Gravity gradients induce a torque on the sphere that is sensed through the voltages needed to hold the sphere in its nominal attitude. Two measurements are obtained from a single gradiometer instrument. With the co-ordinates x', y' and z' defined as in Fig. 2.3-11, the measurements are

$$v_{x'} = \Gamma_{x'z'}$$

$$\text{(2.3-68)}$$

$$v_{y'} = \Gamma_{y'z'}$$

AXIS OF WEIGHTS    R-28195b

$(\dot{z})$

DENSE MATERIAL

x'

y'

DENSE MATERIAL
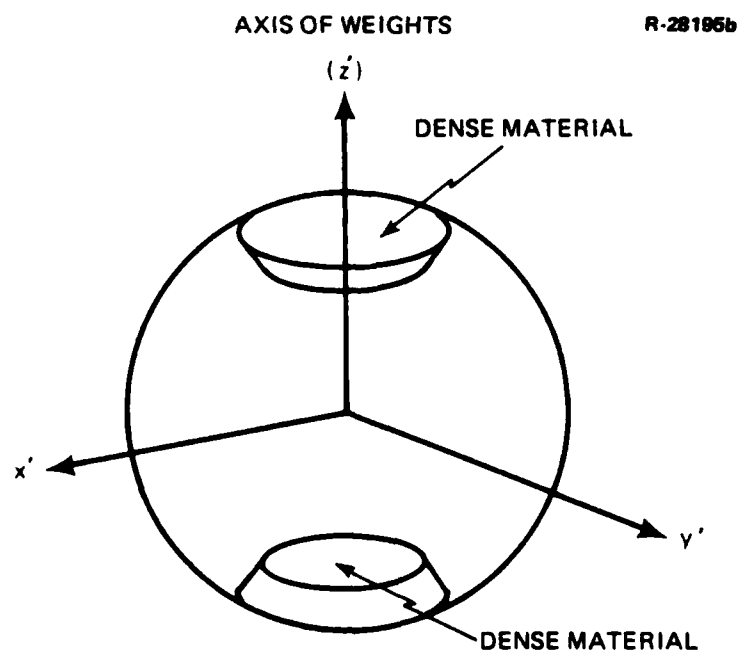
Figure 2.3-11    CSDL Gradiometer Float Element

The geometry considered for the CSDL gradiometer triad is shown in Fig. 2.3-12. The axes of weights of the three gradiometers ($z_1$, $z_2$ and $z_3$) are all oriented at an angle of 35.2644 deg with respect to the vertical. The projection of the $z_1$ axis on the horizontal plane coincides with the east direction and forms angles of 120 deg with the projections of the axes of weights of the other two gradiometers on the same plane. Let $v_1$ and $v_2$ be the measurements produced by the gradiometer whose weight axis is $z_1$, $v_3$ and $v_4$ those produced by
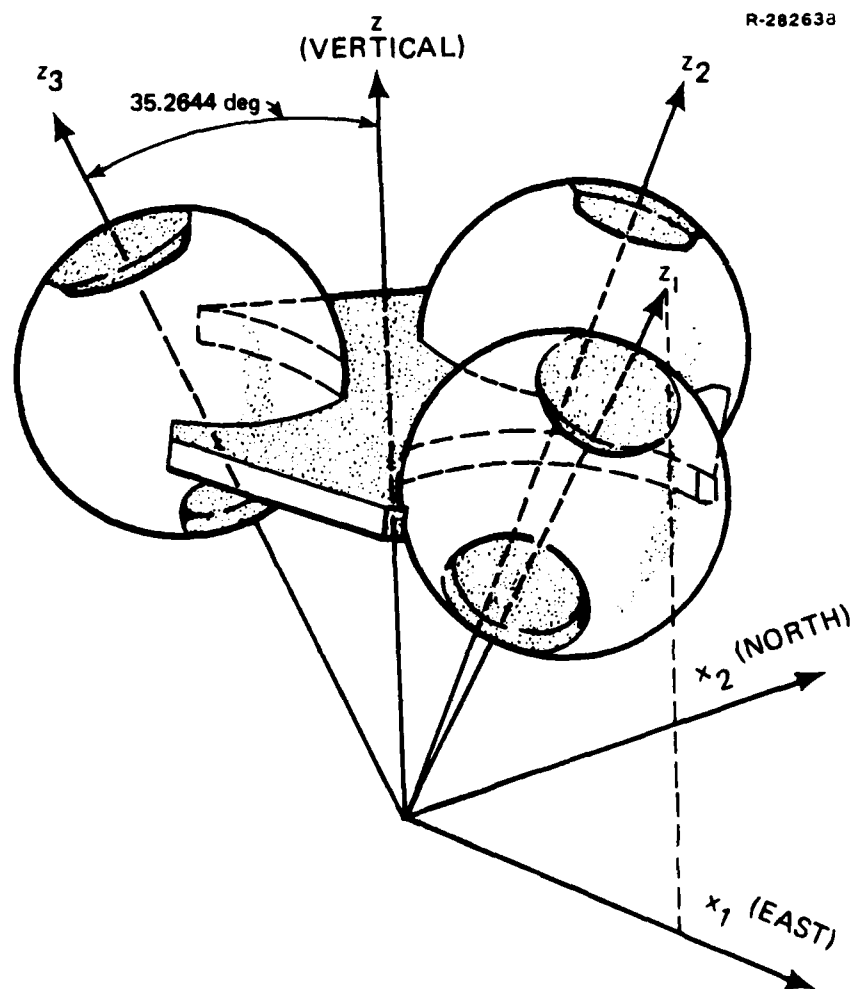


Figure 2.3-12    CSDL Gradiometer Triad (Tetrahedron Geometry)

the gradiometer with weight axis $z_2$, and $v_5$ and $v_6$ those produced by the gradiometer with weight axis $z_3$. The measurements can be expressed in terms of the gradients of the disturbance potential in the east-north-vertical frame (Ref. 8) by

$$
\begin{pmatrix} v_1 \\ v_2 \\ v_3 \\ v_4 \\ v_5 \\ v_6 \end{pmatrix} = \begin{pmatrix} 0.4714 & 0 & -0.4714 & 0 & 0.3333 & 0 \\ 0 & 0 & 0 & 0.5771 & 0 & 0.8165 \\ 0.1178 & 0.3536 & -0.4714 & -0.4082 & -0.1667 & 0.2887 \\ 0.2500 & -0.2500 & 0 & -0.2887 & -0.7071 & -0.4082 \\ 0.1178 & 0.3536 & -0.4714 & 0.4082 & -0.1667 & -0.2887 \\ -0.2500 & 0.2500 & 0 & -0.2887 & 0.7071 & -0.4082 \end{pmatrix} \begin{pmatrix} \Gamma_{x_1 x_1} \\ \Gamma_{x_2 x_2} \\ \Gamma_{zz} \\ \Gamma_{x_1 x_2} \\ \Gamma_{x_1 z} \\ \Gamma_{x_2 z} \end{pmatrix}
$$

$$(2.3\text{-}69)$$

It then follows that the vector transfer function from anomalous surface potential to measured quantities has the same form as that obtained for the Bell triad; i.e.,

$$\underline{F}(\underline{s}) = C \, \underline{H} \, (\underline{s}) \qquad (2.3\text{-}70)$$

where C is the 6×6 matrix appearing in Eq. 2.3-69 and $\underline{H}(\underline{s})$ is the vector transfer function from anomalous surface potential to the gradients of the anomalous potential at height h given by Eq. 2.3-67.

Gradiometer Survey Measurement Error Models - The following measurement error sources were considered in the simulations performed:

- Instrument noise (self-noise)

- Errors induced by the mechanical vibrations to which the gradiometers are subjected aboard an aircraft.

Spectral densities for the time variation of the self-noise of the Bell Baseline, Bell Ball-Bearing and CSDL gradiometers were derived from the manufacturers' test data in Ref. 9. The same self-noise spectra was obtained for both channels of each of the instruments considered. In addition, no significant correlation was observed between the two outputs of each instrument.

As an example of the self-noise spectra derived in Ref. 9, Fig. 2.3-13 presents the spectra of the self-noise of the Bell Baseline gradiometer with its spin axis in the vertical and horizontal positions. The shape of the spectra shown in Fig: 2.3-13 is typical of that obtained for the Bell Ball-Bearing and CSDL instruments as well. The spectrum decays at a rate of 6 db/octave (red noise) and flattens out (white noise) at high frequencies. The analytic form of such a spectral density is

$$S_{N,N}(f) = \frac{r}{f^2} + w \qquad (2.3-71)$$

where f is measured in Hz. For the Bell Baseline gradiometer the values of r and w are

$$r = 2.0 \times 10^{-6} \; E^2 \cdot Hz$$

$$\qquad (2.3-72)$$

$$w = 81 \; E^2/Hz$$
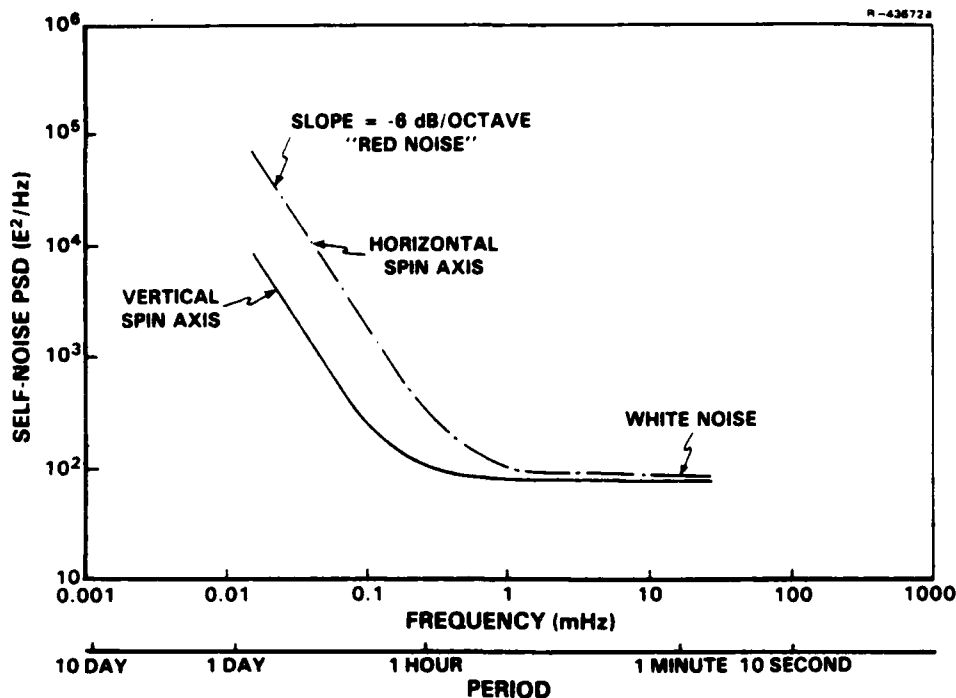
Figure 2.3-13    Self-Noise Spectra of the Bell
Baseline Gradiometer

when the spin axis is vertical, and

$$r = 16 \times 10^{-6} \ E^2 \cdot Hz$$

$$w = 86 \ E^2/Hz$$

(2.3-73)

when the spin axis is horizontal (Ref. 9).  For the Bell Ball-
Bearing gradiometer, data corresponding to an inclination of
the spin axis with respect to the vertical of 55 deg were
analyzed.   The results are

$$r = 7.7 \times 10^{-6} \ E^2 \cdot Hz$$

$$w = 290 \ E^2/Hz$$

(2.3-74)

2-48

These values were used for both horizontal and vertical spin
axes of the gradiometers. For the CSDL gradiometers, the values
of r and w were found to be

$$r = 0.2 \times 10^{-6} \ E^2 \cdot Hz$$

(2.3-75)

$$w = 2.3 \ E^2/Hz$$

The effects of translational and angular vibrations on
the gradiometer measurements are also analyzed in Ref. 9. The
net result is an increase in the power level of the white noise
floor, w, which depends on the orientation of the instrument.
Vibration data corresponding to the Bell Baseline instrument
were received from the manufacturer. The sensitivities obtained
were used in determining the modified white noise levels for the
Bell instruments. In the absence of vibration data from CSDL,
no vibrationally induced errors were included in the CSDL gra-
diometer error model.

Because of the way the instruments sense and process
the gradients of the field, there is no correlation between
vibrationally induced errors in both channels of a single gradi-
ometer. Vibrationally induced errors at the outputs of differ-
ent instruments were modeled as uncorrelated.

Other sources of error which were not included in the
analysis because their magnitude is very small compared to the
self-noise and vibrationally induced errors are:

- Thermally induced errors. Temperature
  sensitivity data for the Bell gradiometers
  (Refs. 10, 11 and 12) indicate that, other
  than the red noise discussed in the fore-
  going, these errors can be neglected.

2-49

- Motion correction errors. Airborne gradiometer measurements must be corrected to account for the fact that the instruments are not stationary in inertial space. The corrections are on the order of 4 Eötvos. Errors in the corrections amount to a few hundredths of an Eötvos.

- Errors due to uncertainty in the aircraft's altimeter readings. These errors are of the same order of magnitude as the motion correction errors.

In addition, the gradiometers are naturally susceptible to time-varying gravity gradient fields caused by relative motions of nearby masses such as gimbals in the inertial platform. Corrections can be applied to the gradiometer output signals to compensate for the gradient fields caused by disturbing masses whose positions can be monitored. Errors in these corrections are unaccounted for in the results given in Chapter 3.

The spectral density of the survey measurement errors was taken to coincide on a single data track with the spectral density given by Eq. 2.3-71 (with suitable choices for the parameters r and w) after transforming time frequencies into spatial frequencies through the mapping

$$f = V\, s_1 \qquad\qquad (2.3\text{-}76)$$

where V is the aircraft's speed. On different data tracks, measurement errors were taken to be independent. The measurement error spectral density matrix, $\tilde{\Phi}_{\underline{E},\underline{E}}(\underline{s})$, is diagonal with entries along the diagonal given by

$$\tilde{\Phi}_{E_m,E_m}(\underline{s}) = \tau_2 V \left[ \frac{r_m/V^2}{s_1^2} + w_m \right] \qquad\qquad (2.3\text{-}77)$$

for $-1/2\tau_1 < s_1 < 1/2\tau_1$ and $m = 1, 2, \ldots, 6$. The values of $r_m$ and $w_m$ for the Bell and CSDL triads are given in Tables 2.3-1 and 2.3-2.

TABLE 2.3-1

RED NOISE PARAMETERS

| | BELL BASELINE | BELL BALL-BEARING | CSDL |
|---|---|---|---|
| $r_1$ $(E^2 \cdot Hz)$ | $2.0 \times 10^{-6}$ | $7.7 \times 10^{-6}$ | $2.0 \times 10^{-7}$ |
| $r_2$ $(E^2 \cdot Hz)$ | $2.0 \times 10^{-6}$ | $7.7 \times 10^{-6}$ | $2.0 \times 10^{-7}$ |
| $r_3$ $(E^2 \cdot Hz)$ | $16 \times 10^{-6}$ | $7.7 \times 10^{-6}$ | $2.0 \times 10^{-7}$ |
| $r_4$ $(E^2 \cdot Hz)$ | $16 \times 10^{-6}$ | $7.7 \times 10^{-6}$ | $2.0 \times 10^{-7}$ |
| $r_5$ $(E^2 \cdot Hz)$ | $16 \times 10^{-6}$ | $7.7 \times 10^{-6}$ | $2.0 \times 10^{-7}$ |
| $r_6$ $(E^2 \cdot Hz)$ | $16 \times 10^{-6}$ | $7.7 \times 10^{-6}$ | $2.0 \times 10^{-7}$ |

TABLE 2.3-2

WHITE NOISE PARAMETERS

| | BELL BASELINE | BELL BALL-BEARING | CSDL |
|---|---|---|---|
| $w_1$ $(E^2/Hz)$ | 440 | 650 | 2.3 |
| $w_2$ $(E^2/Hz)$ | 440 | 650 | 2.3 |
| $w_3$ $(E^2/Hz)$ | 97 | 300 | 2.3 |
| $w_4$ $(E^2/Hz)$ | 97 | 300 | 2.3 |
| $w_5$ $(E^2/Hz)$ | 97 | 300 | 2.3 |
| $w_6$ $(E^2/Hz)$ | 97 | 300 | 2.3 |

## 3.                    SIMULATION RESULTS

A large variety of simulation results were obtained with the techniques of Chapter 2. The results consist of gravity residuals in the form of point values and 5 $\widehat{\text{min}}$, 15 $\widehat{\text{min}}$, 1 deg and 5 deg means.

In order to examine the sensitivity of the results to the local characteristics of the gravity field, three different field models were used in the simulations:

- Attentuated White Noise (AWN) gravity model

- Baseline gravity model

- Active gravity model.

These models are discussed in Section 3.1.

The simulation results are given in Sections 3.2 through 3.5. Section 3.2 presents results for nine different survey possibilities. Sections 3.3, 3.4 and 3.5 examine the sensitivity of specific survey alternatives to variations in survey parameters.

## 3.1    GRAVITY FIELD MODELS

A stationary gravity field model is completely specified by the spectral density of the anomalous surface potential, spectral densities, covariances and cross-correlations

3-1

of all other geodetic quantities are easily derived from $\Phi_{T_o,T_o}$ through the frequency-domain approach given in Section 2.1. The three models used in the simulations are discussed below.

A single shell of the Attenuated White Noise model (Ref. 13) contributes a surface potential with a spectral density of the form

$$\Phi^{(k)}(\underline{s}) = 8\pi D_k^2 \sigma_k^2 \, e^{-4\pi D_k s} \qquad (3.1-1)$$

This spectral density can be viewed as arising from a spherical shell at depth $D_k$ below the surface of the earth on which the potential is white (hence the name Attenuated White Noise) and such that the surface potential has variance $\sigma_k^2$. The complete AWN model consists of five independent shells; i.e.,

$$\Phi_{T_o,T_o}(\underline{s}) = \sum_{k=1}^{5} \Phi^{(k)}(\underline{s}) \qquad (3.1-2)$$

Global data were used to fit the ten parameters of the model in Ref. 13. The resulting values of the parameters are given in Table 3.1-1.

TABLE 3.1-1

AWN MODEL PARAMETERS

| SHELL (k) | $D_K$ (km) | $\sigma_K$ ($m^2/sec^2$) |
|---|---|---|
| 1 | 10 | 0.721 |
| 2 | 76 | 23.03 |
| 3 | 376 | 53.50 |
| 4 | 1055 | 55.36 |
| 5 | 2189 | 278.3 |

The Baseline and Active field models are members of the same class of models. They are both sums of two third-order Markov models (Ref. 14). A single third-order Markov model has a surface potential with a spectral density of the form

$$\phi^{(k)}(\underline{s}) = \frac{10\pi\sigma_k^2\beta_k^5}{[\beta_k^2 + (2\pi s)^2]^{7/2}} \tag{3.1-3}$$

where $1/\beta_k$ is called the characteristic distance and $\sigma_k^2$ is the variance of the surface potential. For the Baseline and Active models

$$\Phi_{T_o,T_o}(\underline{s}) = \sum_{k=1}^{2} \phi^{(k)}(\underline{s}) \tag{3.1-4}$$

with $\phi^{(k)}$ as in Eq. 3.1-3. The four parameters of the Baseline and Active models were obtained by fitting to data in the North Atlantic and in the Bonin Trench, respectively. Their values are given in Tables 3.1-2 and 3.1-3.

· TABLE 3.1-2

BASELINE MODEL PARAMETERS

| K | $1/\beta_k$ (km) | $\sigma_k$ $(m^2/sec^2)$ |
|---|---|---|
| 1 | 27.78 | 16.00 |
| 2 | 370.4 | 91.43 |

3-3

TABLE 3.1-3

ACTIVE MODEL PARAMETERS

| K | $1/\beta_k$ (km) | $\sigma_k$ ($m^2/sec^2$) |
|---|---|---|
| 1 | 22.22 | 29.98 |
| 2 | 350.03 | 103.68 |

Since the spectral densities given in Eqs. 3.1-1 and 3.1-3 are functions of the frequency magnitude s, the three models are isotropic*. Graphs of the spectral densities of the anomalous surface potential for the AWN, Baseline and Active models as functions of s are given in Fig. 3.1-1. The AWN model
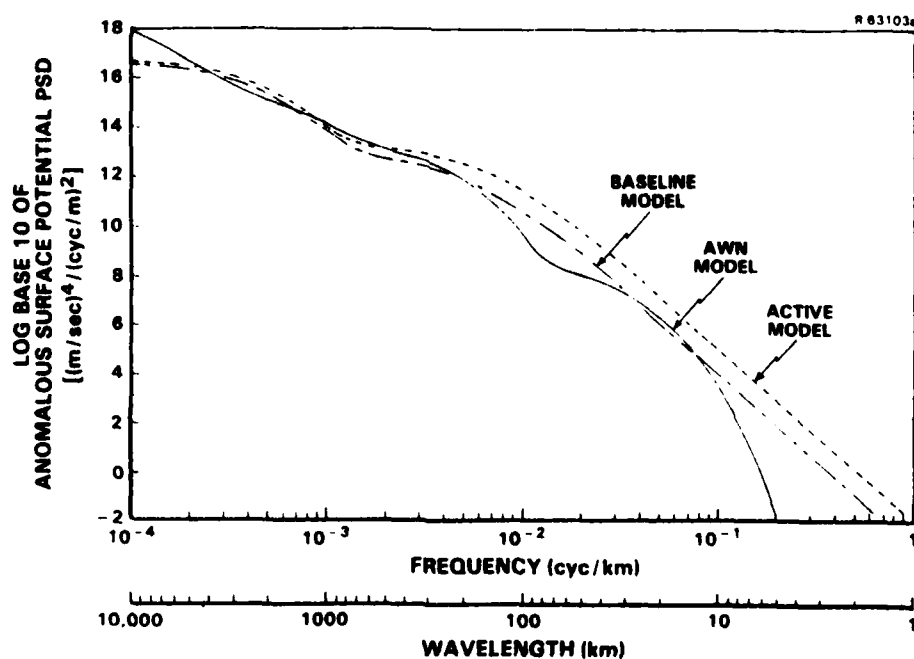


Figure 3.1-1    Spectral Densities of the Anomalous Surface Potential for the AWN, Baseline, and Active Models

---

*The methodology of Chapter 2 is applicable to non-isotropic models as well.

3-4

has very little energy at high frequencies; it represents a smooth slowly varying local gravity field. On the other hand, the Active model contains a substantial amount of high-frequency energy since, as its name indicates, it represents a very active local gravity field. The Baseline model corresponds to an intermediate case.

For reference purposes, Table 3.1-4 presents the rms values of the gravity anomaly, the deflections of the vertical and gradients of the anomalous potential at the surface for the three models. Shown in parentheses are the 1 deg means.

TABLE 3.1-4

RMS VALUES OF MODEL QUANTITIES[*]

| QUANTITY | AWN MODEL | BASELINE MODEL | ACTIVE MODEL |
|---|---|---|---|
| Gravity Anomaly (mgal) | 42.7 (36.2) | 51.1 (29.8) | 112.5 (48.1) |
| East Deflection of the Vertical ($\widehat{sec}$) | 6.8 (5.4) | 7.6 (4.4) | 16.8 (7.2) |
| North Deflection of the Vertical ($\widehat{sec}$) | 6.8 (5.4) | 7.6 (4.4) | 16.8 (7.2) |
| East-East Gradient (E) | 13.8 (3.5) | 20.7 (3.8) | 60.6 (8.1) |
| North-North Gradient (E) | 13.8 (3.5) | 20.7 (3.8) | 60.6 (8.1) |
| Vertical-Vertical Gradient (E) | 22.6 (5.7) | 33.8 (6.2) | 99.0 (13.0) |
| East-North Gradient (E) | 8.0 (2.0) | 12.0 (2.2) | 35.0 (4.4) |
| East-Vertical Gradient (E) | 16.0 (4.0) | 23.9 (4.4) | 70.0 (9.2) |
| North-Vertical Gradient (E) | 16.0 (4.0) | 23.9 (4.4) | 70.0 (9.2) |

*1 deg means shown in parentheses.

3-5

## 3.2    COMPARISON OF SURVEY ALTERNATIVES

To illustrate the versatility of the methodology de-
scribed in Chapter 2, nine survey possibilities were simulated
using the three field models introduced in the previous section.
Post-survey rms residuals in the deflections of the vertical and
the gravity anomaly are presented in Tables 3.2-1, 3.2-2, and
3.2-3 for the AWN, Baseline, and Active models, respectively.
All results correspond to a survey in an equatorial region.

Each table contains 10 columns. The first column,
labeled NONE, corresponds to the unsurveyed field. The acro-
nyms ALT, SST, SHIP, GRAV and GRAD, used in the remaining nine
columns, represent satellite radar altimetry, satellite-to-
satellite tracking, ship gravimetry, land-based gravimetry and
airborne gradiometry, respectively. Each column corresponds
to the survey combination indicated by the acronyms in its
header. A description of the survey parameters is given next.

Satellite Radar-Altimeter Survey - The GEOS-3 geometry
and parameters were used. The equatorial separation of GEOS-3
groundtracks was taken as 30 nm.

Satellite-to-Satellite Tracking - The low satellite's
altitude is 150 km. Its orbit inclination is 94 deg. Measure-
ments of line-of-sight range-rate are taken every 10 sec and
the noise level has a standard deviation of 1 µm/sec per meas-
urement. The separation of the groundtracks of the low satel-
lite is 30 nm at the equator. The high satellite is directly
above the region where estimates are sought.

Shipborne Gravimetry - Spacings between contiguous
survey tracks were selected following NAVOCEANO's methodology.
The remaining parameters are defined in Subsection 2.3.3.

TABLE 3.2-1

AWN MODEL SIMULATION RESULTS

| | SURVEY TYPE | | | | | | | | | |
|---|---|---|---|---|---|---|---|---|---|---|
| | NONE | SST | ALT | SST ALT | GRAV GRAD | ALT SHIP | SST GRAD | ALT GRAD | SST ALT GRAD | ALT GRAD SHIP |
| RMS North Deflection of the Vertical* (sec) | 6.8 (5.4) | 2.1 (0.5) | 1.4 (0.4) | 1.3 (0.1) | 0.8 | 0.7 | 0.5 | 0.5 | 0.4 | 0.4 |
| RMS East Deflection of the Vertical* (sec) | 6.8 (5.4) | 1.9 (0.5) | 1.5 (0.5) | 1.4 (0.1) | 0.5 | 0.6 | 0.4 | 0.4 | 0.4 | 0.3 |
| RMS Gravity Anomaly* (mgal) | 42.7 (36.2) | 13.2 (3.2) | 9.6 (2.8) | 9.1 (0.7) | 4.6 | 4.3 | 3.0 | 3.0 | 2.8 | 2.4 |

*1 deg means shown in parenthesis.

TABLE 3.2-2

BASELINE MODEL SIMULATION RESULTS

| | SURVEY TYPE | | | | | | | | | |
|---|---|---|---|---|---|---|---|---|---|---|
| | NONE | SST | ALT | SST ALT | GRAV GRAD | ALT SHIP | SST GRAD | ALT GRAD | SST ALT GRAD | ALT GRAD SHIP |
| RMS North Deflection of the Vertical* (sec) | 7.6 (4.4) | 4.5 (0.5) | 2.2 (0.4) | 2.1 (0.2) | 1.0 | 0.6 | 0.6 | 0.5 | 0.5 | 0.4 |
| RMS East Deflection of the Vertical* (sec) | 7.6 (4.4) | 4.2 (0.4) | 2.8 (0.5) | 2.8 (0.3) | 0.6 | 0.6 | 0.4 | 0.4 | 0.4 | 0.3 |
| RMS Gravity Anomaly* (mgal) | 51.1 (29.8) | 29.2 (3.0) | 16.9 (3.2) | 16.7 (1.7) | 5.2 | 4.2 | 3.4 | 3.2 | 3.0 | 2.5 |

*1 deg means shown in parenthesis.

TABLE 3.2-3

ACTIVE MODEL SIMULATION RESULTS

| | SURVEY TYPE | | | | | | | | | |
|---|---|---|---|---|---|---|---|---|---|---|
| | NONE | SST | ALT | SST ALT | GRAV GRAD | ALT SHIP | SST GRAD | ALT GRAD | SST ALT GRAD | ALT GRAD SHIP |
| RMS North Deflection of the Vertical* (sec) | 16.8 (7.2) | 12.5 (1.6) | 5.4 (0.6) | 5.4 (0.4) | 1.7 | 0.7 | 1.2 | 0.9 | 0.9 | 0.6 |
| RMS East Deflection of the Vertical* (sec) | 16.8 (7.2) | 11.4 (1.6) | 8.0 (1.0) | 7.9 (0.8) | 1.1 | 0.6 | 0.8 | 0.8 | 0.8 | 0.4 |
| RMS Gravity Anomaly* (mgal) | 112.5 (48.1) | 80.2 (10.5) | 46.0 (5.5) | 45.7 (4.4) | 9.4 | 4.6 | 6.7 | 5.9 | 5.7 | 3.3 |

*1 deg means shown in parenthesis.

Land-Based Gravimetry - All parameters are as described in Subsection 2.3.3.

Airborne Gradiometry - Data are assumed to be collected with the Bell Baseline gradiometer triad aboard an aircraft flying at a speed of 300 kt at an altitude of 20,000 ft. Measurements are taken every 10 seconds on parallel tracks spaced 10 km apart.

Three of the five sensors considered provide information on the long-wavelength content of the gravity field. They are SST, ALT, and GRAV. The other two sensors, GRAD and SHIP, recover the short wavelengths of the gravity field. In the case of the gravimetric surveys (GRAV and SHIP), this difference is primarily a function of the density of coverage. For the other sensors (SST, ALT, and GRAD), the bandwidth of recovery is inherent in the physical characteristics of the sensor.

In Tables 3.2-1, 3.2-2, and 3.2-3 all columns contain-
ing ALT or SHIP in the header correspond to ocean surveys.
The column headed by GRAV/GRAD represents a land survey. The
two columns SST and SST/GRAD apply to ocean and to overland
surveys.

The three tables present the point value rms residuals
in the north deflection of the vertical, the east deflection
of the vertical, and the gravity anomaly. The numbers in paren-
thesis are the rms values of the residual 1 deg means. These
are given only for those surveys in which long-wavelength sen-
sors are used exclusively.

The results given in Tables 3.2-1, 3.2-2, and 3.2-3
are discussed in detail below. First, consider the order of
the columns in the tables. Note that the various columns in
the three tables are ordered in the same sequence. This order
corresponds to decreasing rms values for the residual point
gravity anomaly in the Baseline and AWN models. In the case
of the Active gravity model, the gravity anomaly residual for
the combination ALT/SHIP appears out of sequence. The reason
is that the rms residuals shown in the tables correspond to
the actual ship survey that NAVOCEANO would conduct. The cri-
terion used by NAVOCEANO to select the spacing between con-
tiguous ship tracks would choose the same spacing for the AWN
and Baseline models, but it would choose a denser collection
of tracks for a region described by the Active gravity model.
If the same ship track spacing is used for all models, the
results for the Active model appear in the same order as those
of the other two models.

For most surveys, the rms values of the residuals in
the north and in the east deflections of the vertical are not
the same. This illustrates the fact that the post-survey gravi-
ty residuals are not isotropic. Even though the three models

3-9

used in the simulations are isotropic, the gravity residuals
turn out to be anisotropic for all surveys. The primary reason
for the anisotropy is the geometry of the surveys. For example,
for an airborne gradiometer survey the survey tracks are east-
west and samples along a track are spaced approximately 1.5 km
apart, while in the cross-track direction (north-south) the
distance between samples is 10 km. In the case of the SST
survey, the rms of the residual east deflection of the verti-
cal is smaller than that of the north deflection of the verti-
cal because the 10 sec range-rate sampling implies a larger
spacing between consecutive samples on a groundtrack (roughly
north-south) than the spacing between continuous groundtracks
(east-west).

The advantages of multisensor surveys are clear from
the tables. The smallest residuals are obtained when a combi-
nation of sensors is used to cover the entire range of fre-
quencies. This involves at least one long-wavelength sensor
and one short-wavelength sensor. Little is gained by combin-
ing two long-wavelength sensors, as can be seen by comparing
the columns SST and ALT with the column headed by SST/ALT in
each of the tables. The best two-sensor results are obtained
with the ALT/GRAD sensor combination in the cases of the AWN
and the Baseline gravity models. For the Active model, the
ALT/SHIP sensor combination provides the best recovery using
only two sensors. In each case, the best two-sensor result is
not very much improved when a third sensor is added.


3.3     SATELLITE ALTIMETRY - SENSITIVITY TO TRACK SPACING

This section presents a study of the sensitivity of the
gravity recovery to satellite altimeter track spacing. Both
GEOS-3 and SEASAT-1 altimeters are considered. Some important
implications of the survey geometry are discerned and discussed.

Figures 3.3-1, 3.3-2, and 3.3-3, respectively, show
the variation with equatorial track spacing of the residual
rms gravity anomaly, east deflection of the vertical, and north
deflection of the vertical. Results for the AWN and Active
models for recovery at the equator are given in these figures.
The horizontal axes correspond to the equatorial separation
between contiguous tracks.

At first, the results appear surprising. The SEASAT-1
altimeter is of better quality than the GEOS-3 altimeter. In
addition, SEASAT-1 has a larger orbit inclination than GEOS-3.
Consequently, it is expected that the gravity anomaly and the
north deflection of the vertical are better recovered by SEASAT-1
than by GEOS-3 at all track spacings[*]. However, Figs. 3.3-1
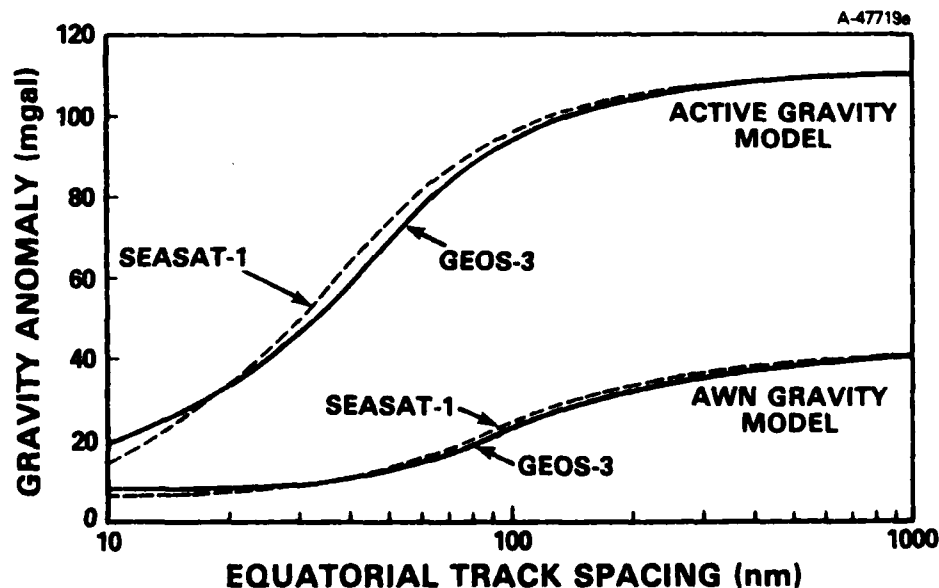


Figure 3.3-1     Sensitivity of Residual Gravity Anomaly
to Altimeter Survey Track Spacing

---

[*]For the east deflection of the vertical (Fig. 3.3-2) the results
are expected because of the difference in orbit inclination be-
tween the two satellites.

Figure 3.3-2    Sensitivity of Residual East Deflection of the
                Vertical to Altimeter Survey Track Spacing
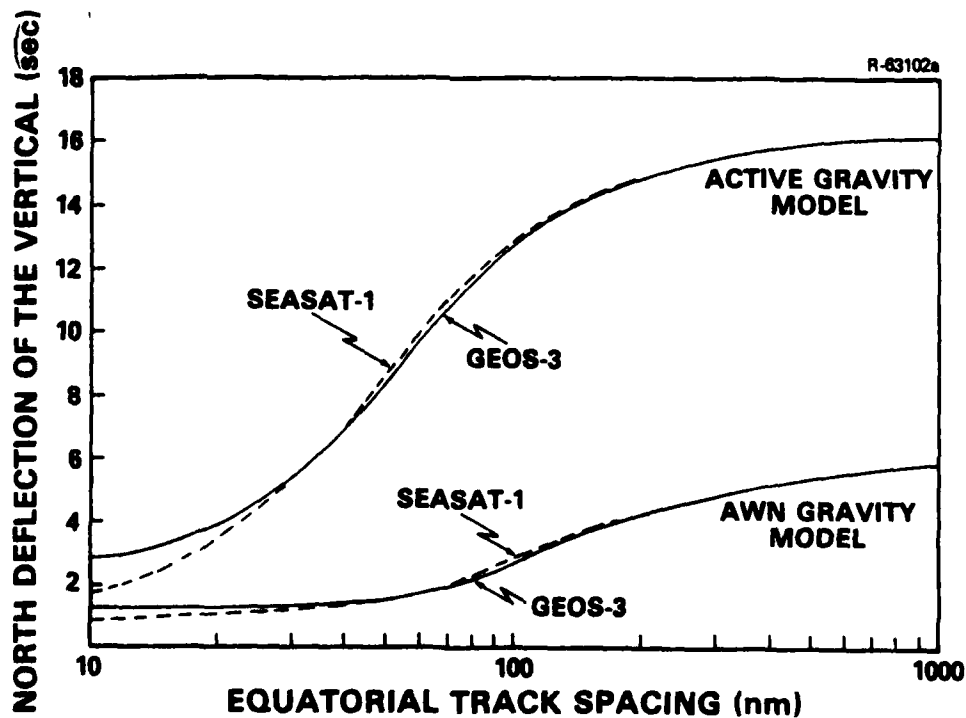


Figure 3.3-3    Sensitivity of Residual North Deflection of the
                Vertical to Altimeter Survey Track Spacing

and 3.3-3 indicate that for a wide range of track spacings the residuals in the gravity anomaly and the north deflection of the vertical are larger for SEASAT-1 than for GEOS-3. Only for very short track spacings do SEASAT-1 results show an improvement over GEOS-3.

The origin of this surprising behavior is in the geometry of the survey. Figure 3.3-4 illustrates the geometric differences between SEASAT-1 and GEOS-3 surveys. For the same equatorial separation, any two parallel SEASAT-1 tracks are separated by a larger distance in the north direction than two GEOS-3 tracks. More fundamentally, as Fig. 3.3-5 illustrates, for the same equatorial separation there are more data per unit area in a GEOS-3 survey than in a SEASAT-1 survey. Thus, the results reflect a trade-off between data quality and data quantity.

R—47720
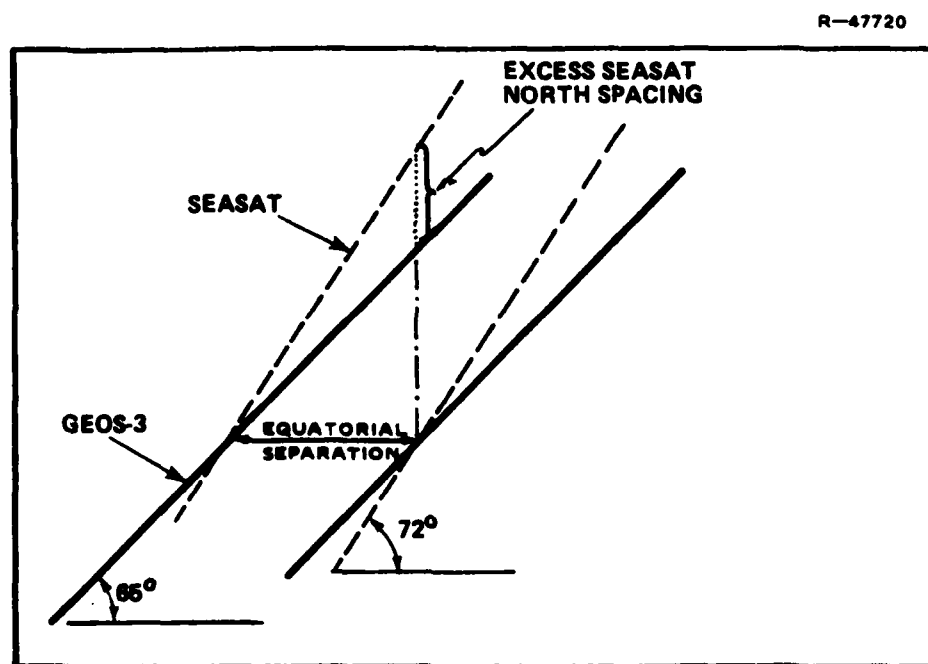


Figure 3.3-4     Geometric Differences Between SEASAT-1 and GEOS-3 Surveys

3-13

GEOS-3
AREA = 0.92H$^2$
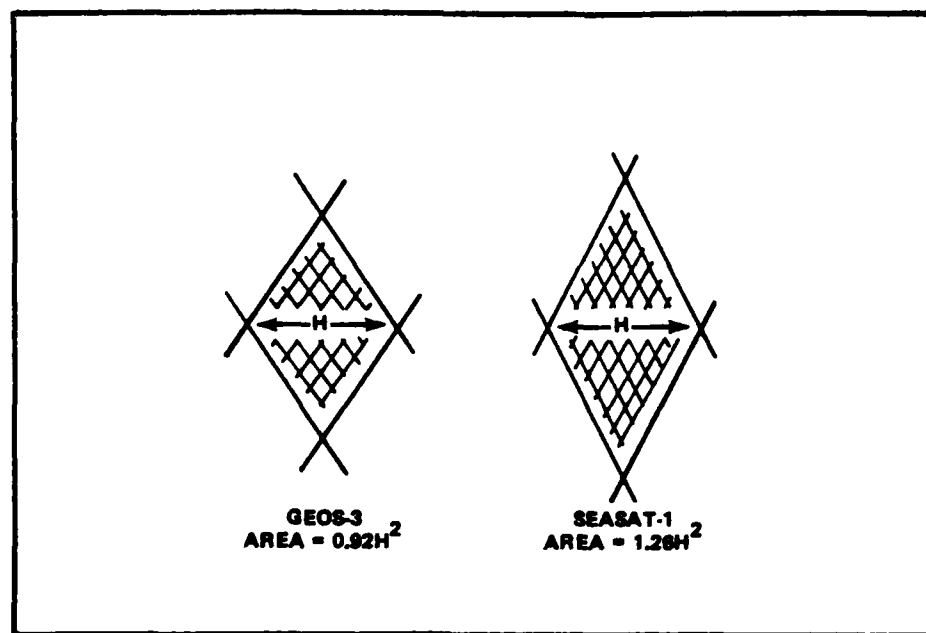
SEASAT-1
AREA = 1.28H$^2$

Figure 3.3-5    Differences in Density of Coverage
Between SEASAT-1 and GEOS-3 Surveys

When a SEASAT-1 quality altimeter is used in a satel-
lite at the same orbit of GEOS-3, the results of Figs. 3.3-6,
3.3-7 and 3.3-8 are obtained. For ease in referencing, this
case has been labeled SEASAT-1-A. It can be seen from
Figs. 3.3-6, 3.3-7 and 3.3-8 that, as expected, SEASAT-1-A
yields consistently better recovery than GEOS-3 but the im-
provement is evident only for track spacings shorter than
40 nm.

Residual 5 $\widehat{min}$, 15 $\widehat{min}$, 1 deg, and 5 deg means of the
gravity anomaly are presented in Figs. 3.3-9 through 3.3-12.
The effects of the geometric differences between the surveys
are clearly seen in these figures. The effects of the differ-
ences between the quality of the altimeters corresponding to
the GEOS-3 and SEASAT surveys are only noticeable in the re-
covery of the 5 and 15 $\widehat{min}$ means. The values of the 5 $\widehat{min}$,

3-14
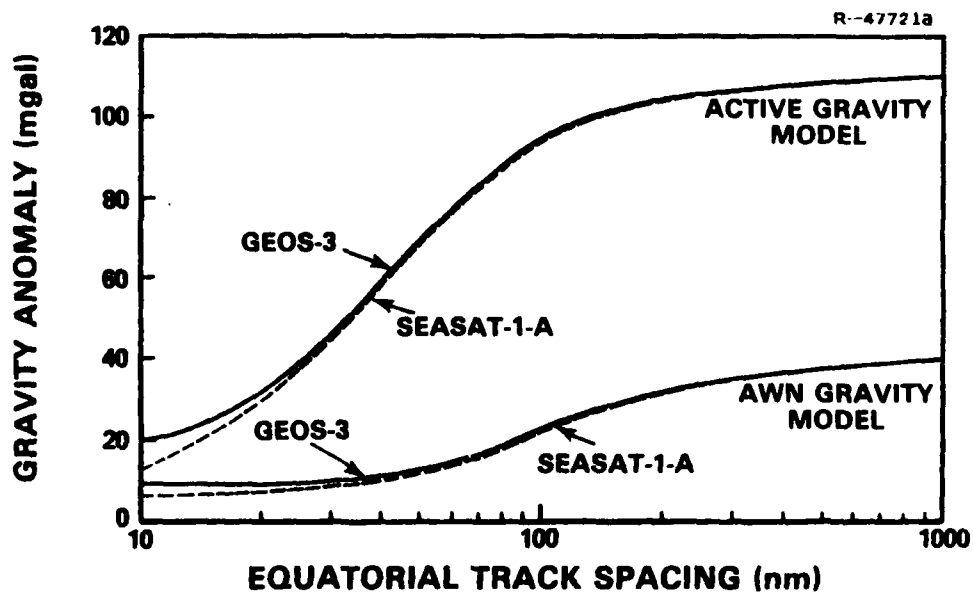
Figure 3.3-6    Sensitivity of Residual Gravity Anomaly to
                Altimeter Survey Track Spacing
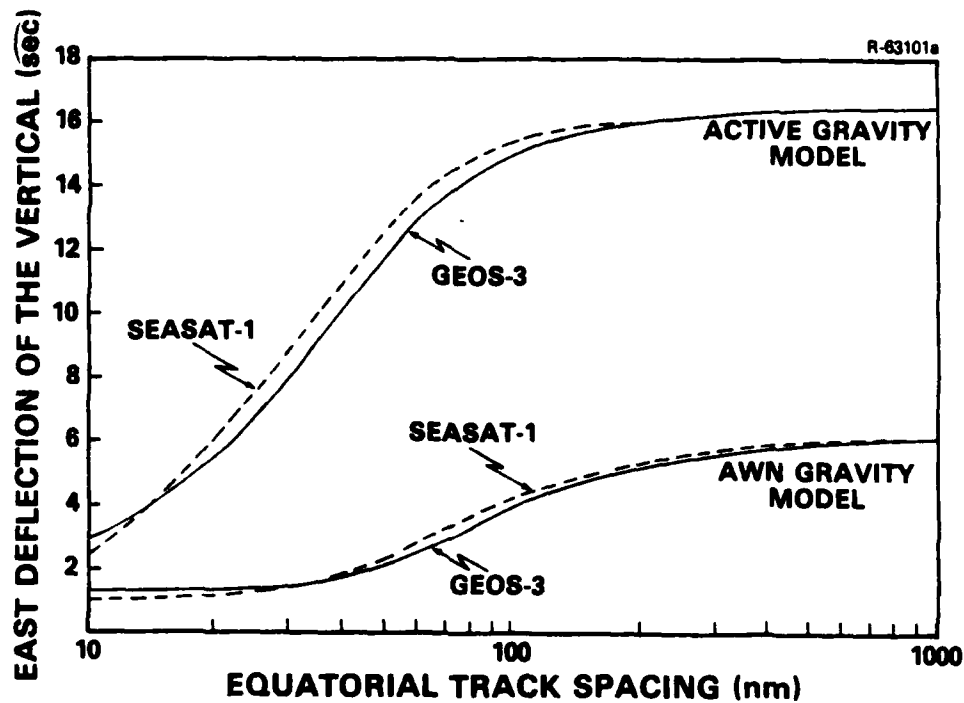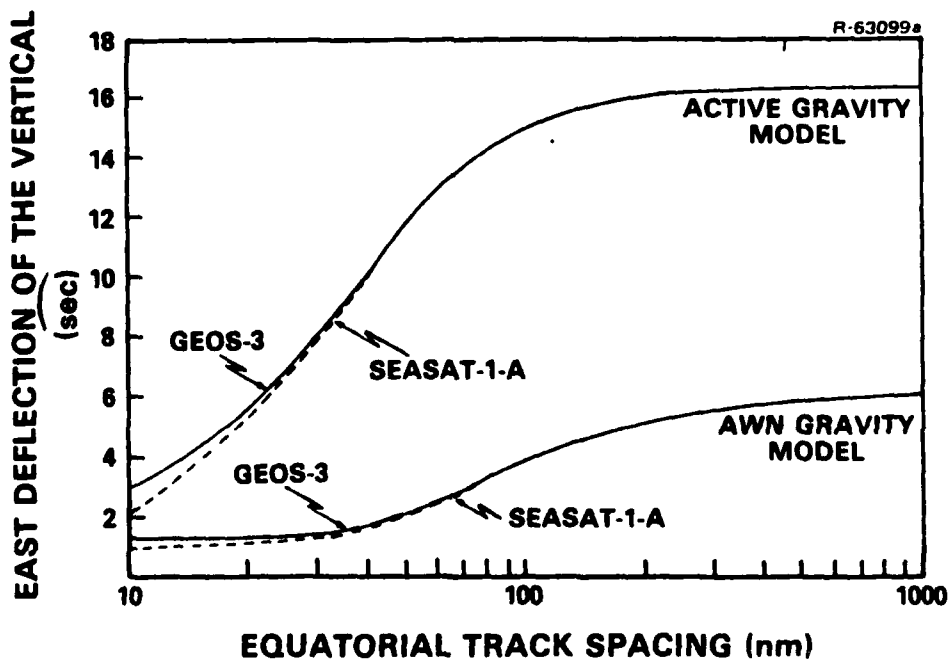


Figure 3.3-7    Sensitivity of Residual East Deflection of the
                Vertical to Altimeter Survey Track Spacing

3-15
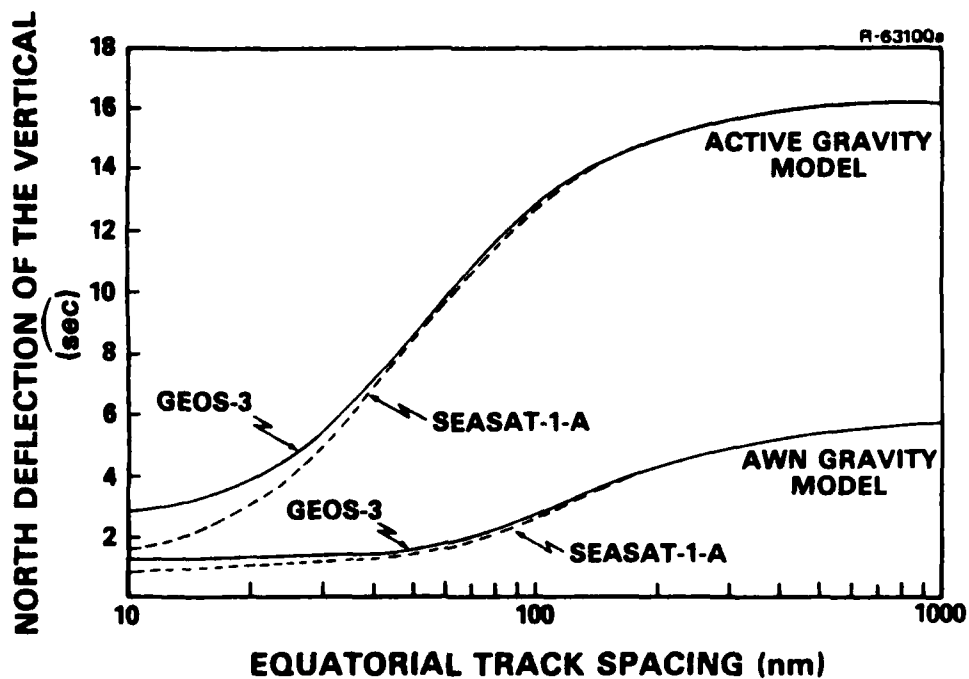
Figure 3.3-8        Sensitivity of Residual North Deflection of the
                    Vertical to Altimeter Survey Track Spacing
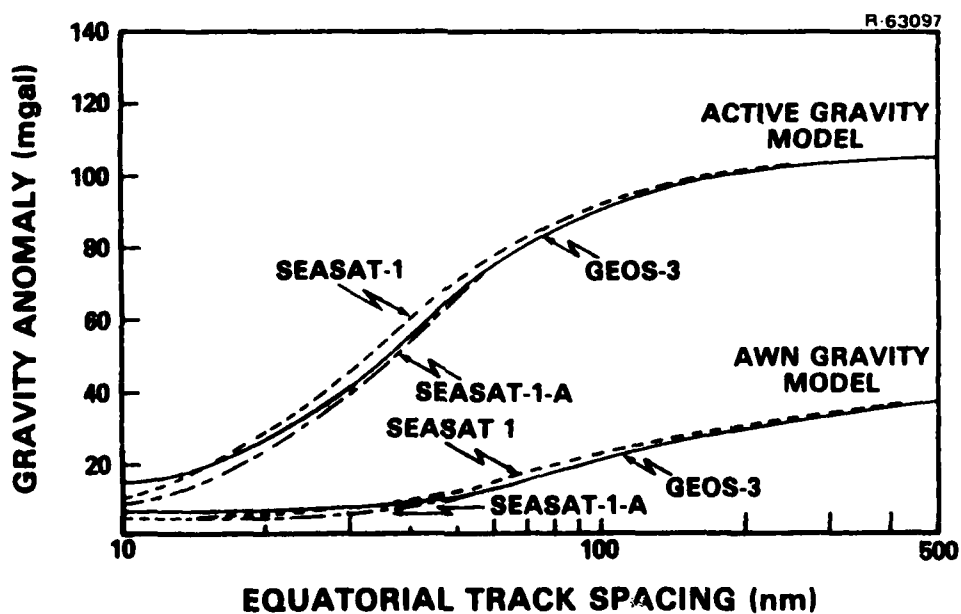


Figure 3.3-9        Satellite Altimeter Survey Residual
                    5 min Means

3-16
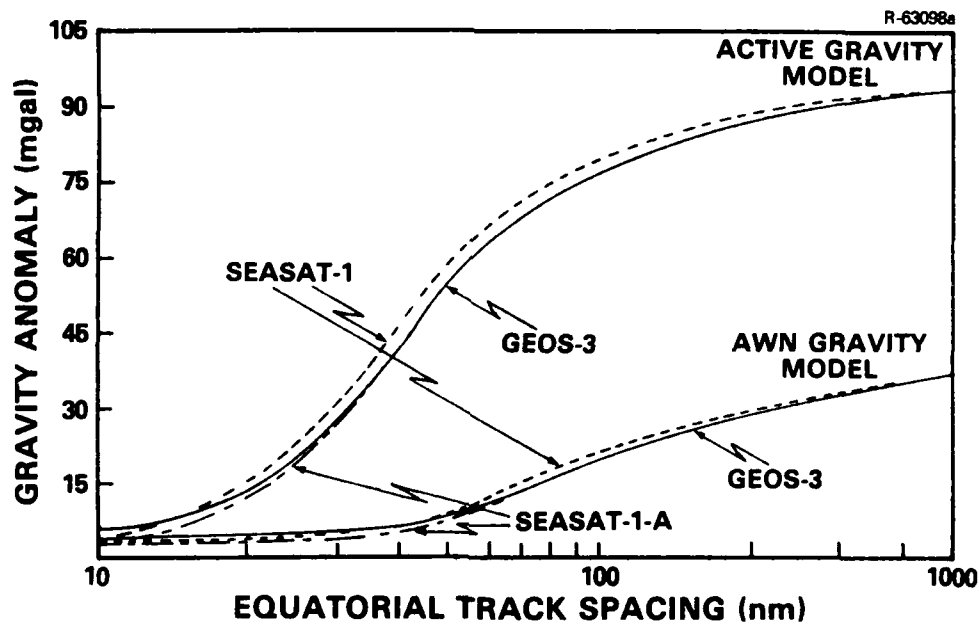
Figure 3.3-10    Satellite Altimeter Survey Residual
15 min Means
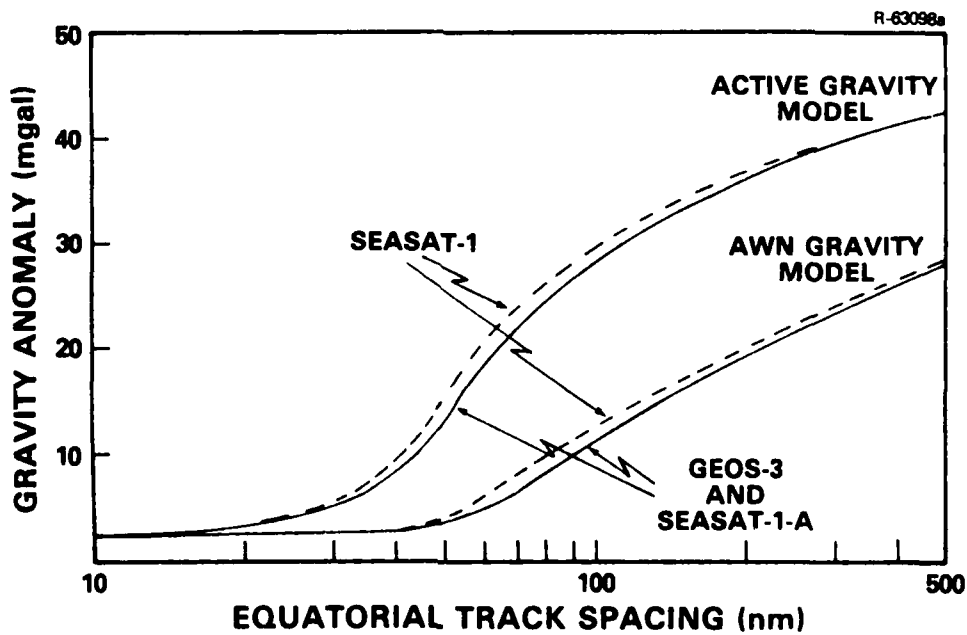


Figure 3.3-11    Satellite Altimeter Survey Residual
1 deg Means
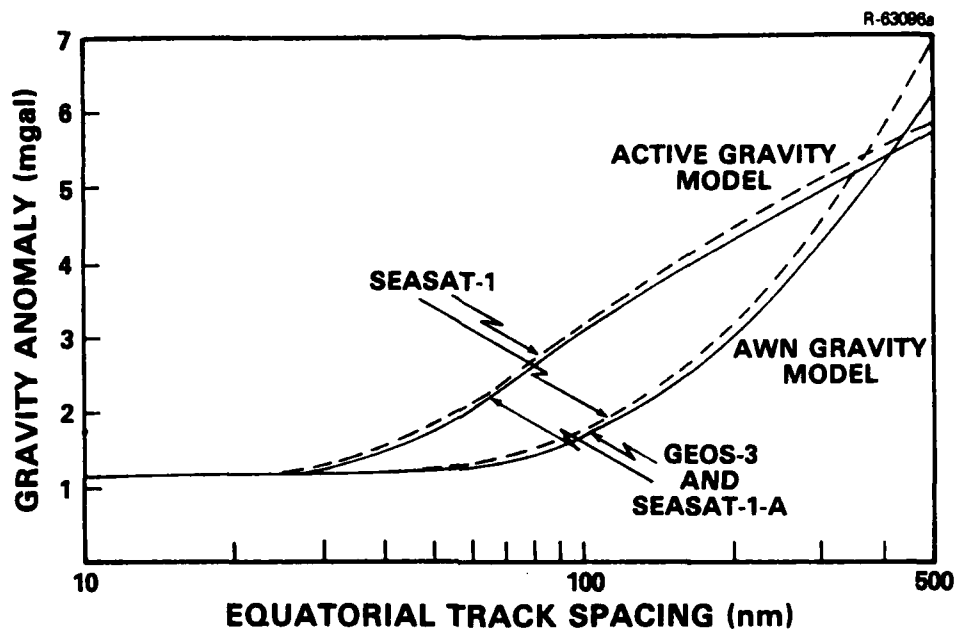
Figure 3.3-12     Satellite Altimeter Survey Residual
                  5 deg Means

15 $\widehat{min}$, 1 deg, and 5 deg means for the unsurveyed AWN and Active
fields are given as a reference in Table 3.3-1. Note that the
5 deg means of the unsurveyed field are larger for the AWN
model than for the Active model because the AWN model has more
power in the long wavelength portion of the spectrum than the
Active model (see Fig. 3.1-1). This explains why the graphs
of Fig. 3.3-12 cross for sparse surveys.

TABLE 3.3-1

SPATIALLY AVERAGED UNSURVEYED GRAVITY ANOMALY

| | 5 $\widehat{min}$ (mgal) | 15 $\widehat{min}$ (mgal) | 1 deg (mgal) | 5 deg (mgal) |
|---|---|---|---|---|
| AWN | 41.6 | 40.2 | 36.2 | 26.1 |
| Active | 110.0 | 97.7 | 48.1 | 20.1 |

Figures 3.3-11 and 3.3-12 indicate that there are fundamental lower bounds on the recovery of the 1 deg and 5 deg means of the gravity anomaly from satellite altimetry data. These bounds (approximately 2.6 mgal for the 1 deg means and 1.2 mgal for the 5 deg means) are independent of the gravity field model used in the analysis and are also independent of the survey geometry and the quality of the altimeter used.

## 3.4    SST - SENSITIVITY TO LOW SATELLITE'S ALTITUDE

A study was conducted of the sensitivity of SST survey residual gravity errors with respect to the height of the low satellite. Measurements of line-of-sight range-rate were considered to be taken every 10 sec and to have an uncertainty with a standard deviation of 1 μm/sec. The inclination of the orbit of the low satellite was taken as 94 deg and the equatorial separation between neighboring groundtracks was kept constant at 30 nm. The altitude of the low satellite over the earth's surface was allowed to vary between 100 km and 800 km.

Results for gravity recovery from an equatorial region directly under the high satellite were obtained for the AWN and Active models. The point residuals in the gravity anomaly are presented in Fig. 3.4-1. Figures 3.4-2 through 3.4-5 show the 5 $\widehat{min}$, 15 $\widehat{min}$, 1 deg, and 5 deg means of the residuals in the gravity anomaly.

As the height of the low satellite decreases, the spacing between consecutive samples along a groundtrack increases according to Eq. 2.3-1[*]. On the other hand, the closer

---

*Along-track sample spacing for altitudes of 100 km and 800 km are 66.2 km and 77.2 km, respectively.
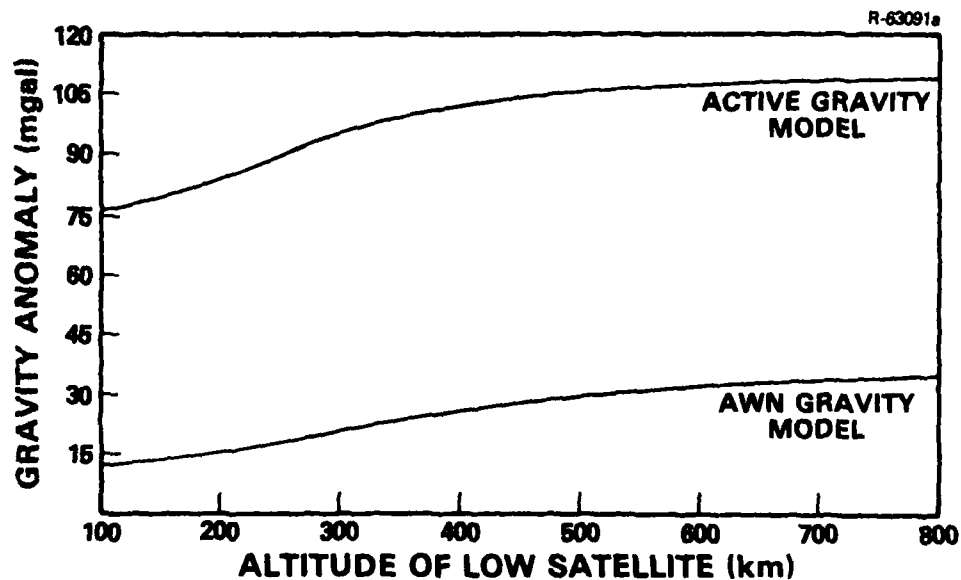
Figure 3.4-1    SST Survey RMS Residual Point
                Gravity Anomaly
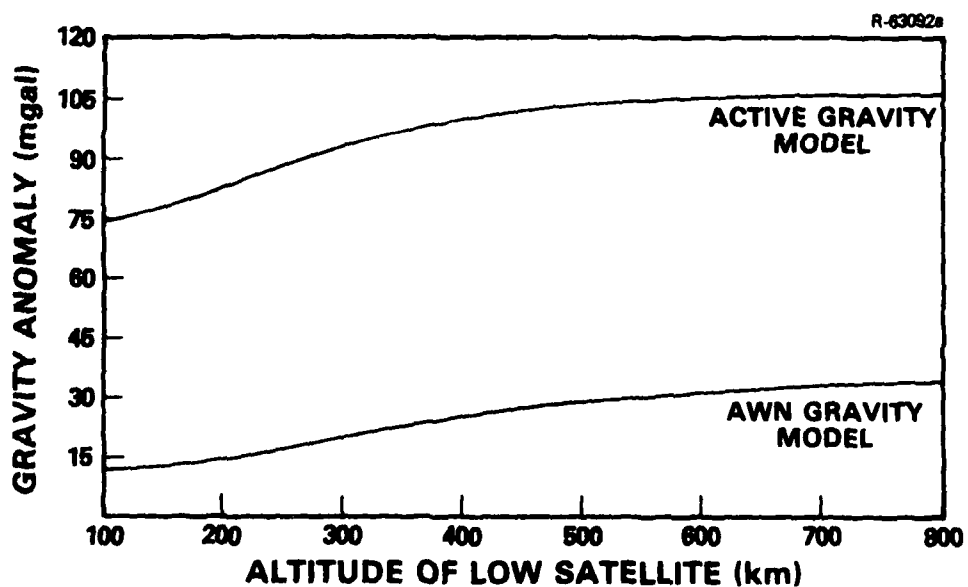


Figure 3.4-2    SST Survey Gravity Anomaly Residual
                5 min Means
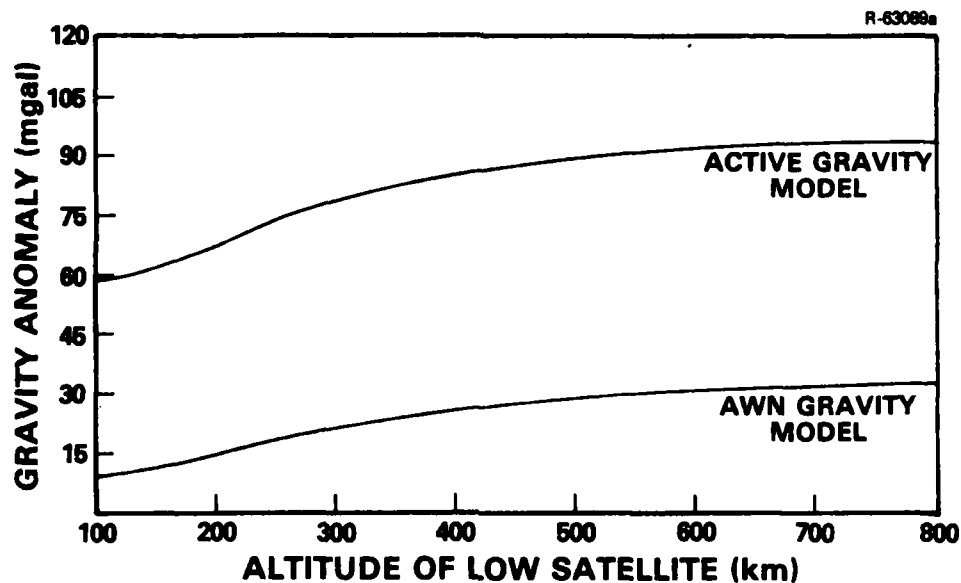
Figure 3.4-3     SST Survey Gravity Anomaly Residual
15 min Means
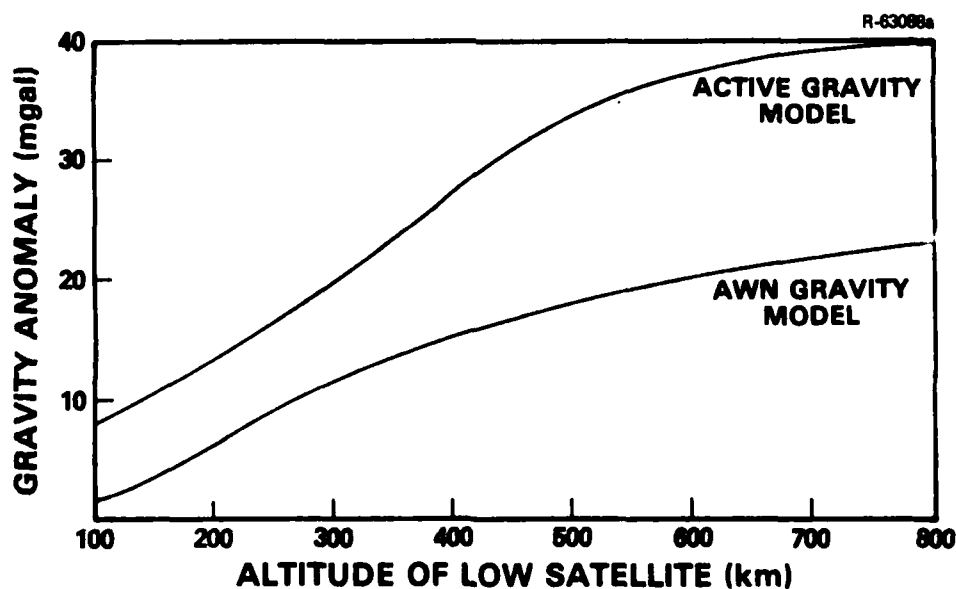


Figure 3.4-4     SST Survey Gravity Anomaly Residual
1 deg Means
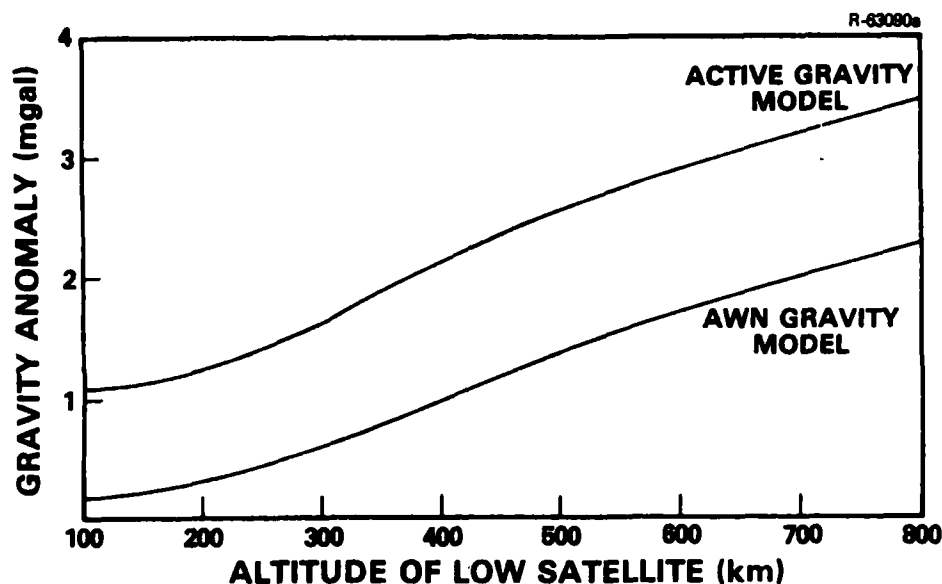
Figure 3.4-5    SST Survey Gravity Anomaly Residual
                5 deg Means

the low satellite is to the earth's surface, the stronger the
anomalous gravity field and the better the signal-to-noise
ratio of the measurements.  By far, the dominant effect is the
quality of the data.  Thus, even though the data become sparser
as the height of the low satellite decreases, residual gravity
errors are reduced.

Table 3.4-1 gives the residual 5 min, 15 min, 1 deg,
and 5 deg means of the gravity anomaly as fractions of the
corresponding unsurveyed field values for low satellite's alti-
tudes of 100 km and 800 km.  The fractions have been rounded-
off to the nearest 1/100.  The 5 deg means are very well re-
covered from SST data.  In general, the fractional recovery of
the gravity anomaly is better for the AWN model than for the
Active model because most of the energy in the field repre-
sented by the AWN model is contained in the long-wavelength
portion of the spectrum while in the case of the Active model
there is a large amount of energy at high frequencies which is
unobservable in the data.

TABLE 3.4-1

RESIDUAL GRAVITY ANOMALY AS A FRACTION OF
THE UNSURVEYED FIELD VALUES

| HEIGHT OF LOW SATELLITE | MODEL | 5 m̂in MEAN | 15 m̂in MEAN | 1 deg MEAN | 5 deg MEAN |
|---|---|---|---|---|---|
| 100 km | AWN | 0.28 | 0.22 | 0.04 | 0.01 |
| 100 km | Active | 0.68 | 0.60 | 0.17 | 0.05 |
| 800 km | AWN | 0.85 | 0.84 | 0.64 | 0.09 |
| 800 km | Active | 0.97 | 0.96 | 0.83 | 0.17 |

## 3.5    AIRBORNE GRADIOMETRY - SENSITIVITY TO TRACK SPACING

This section presents results on the sensitivity of residual gravity errors from a combined SST/Airborne gradiometric survey. The gradiometer instruments considered are the Bell Ball-Bearing and the CSDL triads discussed in Subsection 2.3.4.

For the SST survey, the low satellite's altitude above the earth's surface was taken as 120 km. The rest of the parameters were the same as those used in obtaining the results of the previous section. The gradiometer survey was assumed to be conducted at an altitude of 20,000 ft and at a speed of 300 kt. The interval between successive gradiometer samples was taken as 10 sec. Track spacing was allowed to vary between 10 km and 100 km.

The results for the rms of the residual gravity anomaly are presented in Fig. 3.5-1. Note that the differences in gravity recovery between the Bell and CSDL instruments are exaggerated in Fig. 3.5-1 because, as noted in Subsection 2.3.4,

3-23
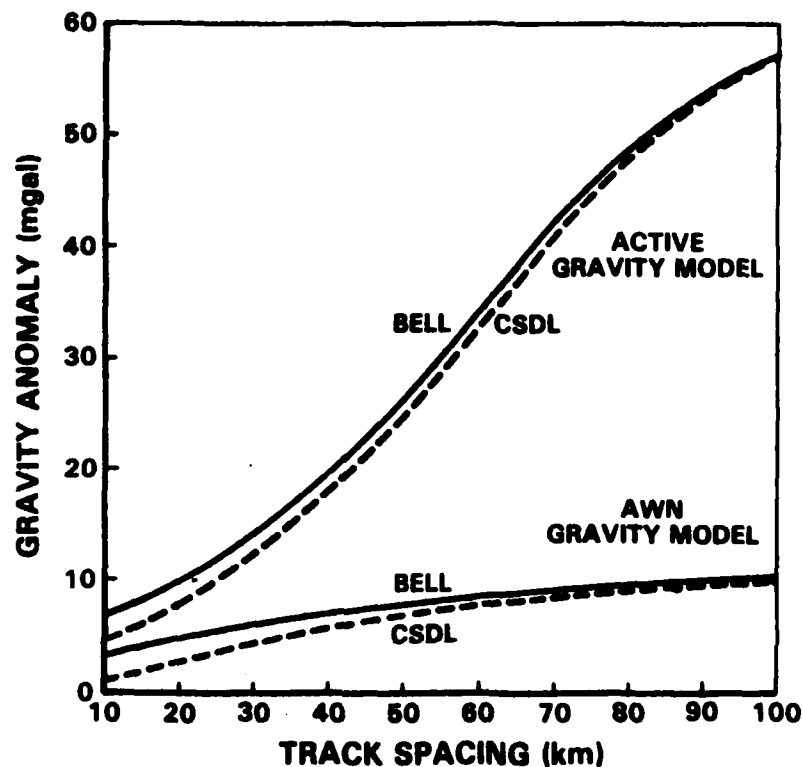
Figure 3.5-1    Sensitivity of SST/Airborne Gradiometer Survey
                Residual Gravity Anomaly to Gradiometer Survey
                Track Spacing

the error model for the CSDL instrument does not include the
effects of translational and rotational vibrations, while the
Bell Ball-Bearing instrument error model does include these
effects.

There are three possibilities to further decrease the
residual gravity anomaly. First, the slope of the residual
gravity anomaly curve at the lower end of the track spacing
scale in Fig. 3.5-1 indicates that the full benefit of an air-
borne gradiometer survey has not been attained at a track spac-
ing of 10 km. Second, residual gravity anomaly can be reduced
by lowering the height of the gradiometer survey (20,000 ft).

<u>Third</u>, the east-west gradiometer survey could be complemented with a north-south gradiometer survey to provide short-wavelength recovery over the frequency-domain region where the red noise in the east-west gradiometer survey significantly corrupts the measurements.

# 4. CONCLUSIONS AND RECOMMENDATIONS

## 4.1 CONCLUSIONS

A new method and a computer program have been developed for the analysis of multisensor surveys of the gravity field. The method is ideally suited for the design of multisensor surveys to achieve a desired level of gravity recovery accuracy.

The approach, which utilizes a flat-earth approximation in the survey region, is based on an extension of optimal Wiener smoothing theory. The Fourier transformation permits the efficient evaluation of the statistics of the post-survey residuals in the form of their average spectral density. Root-mean-square (rms) values, covariances and crosscovariances of point and spatial averages of the residuals are readily computed from their average spectral density through numerical integration.

Survey error models and gravity recovery simulation results were given for a variety of combinations of

- Satellite radar altimeters

- Satellite-to-satellite tracking in a high-low configuration

- Land-based/shipborne gravimetry

- Airborne gradiometry.

The examples given illustrate the versatility of the methodology.

4-1

## 4.2 RECOMMENDATIONS

There are several important areas of investigation for future extensions of the methodology:

- Effects of survey irregularities - The effects of gaps in satellite data and the seemingly random measurement pattern associated with land-based gravimetric surveys would be incorporated in the analysis.

- Additional sensors - Other survey possibilities such as satellite-to-satellite tracking in a low-low configuration or inertial gravimetry can be included in the formulation.

# APPENDIX A

## THE FOURIER TRANSFORMATION

This appendix presents a compilation of those defini-
tions and results of Fourier analysis employed in this report.
This appendix is not intended as a treatise on the subject of
Fourier analysis. The material is presented as an aid in under-
standing the application of the concepts rather than as an
investigation of the mathematical properties of the concepts
themselves. The reader interested in a more complete presen-
tation is referred to various excellent books on the subject
such as Refs. 3, 15, 16, and 17.

## A.1    DEFINITIONS OF FOURIER TRANSFORMS

Let $g(\underline{x})$ be a real-valued function defined for all
points $\underline{x} = (x_1, x_2)^T$ of a cartesian coordinate system. The
Fourier transform of $g$, $\hat{g}$, is a complex-valued function defined
by

$$\hat{g}(\underline{s}) = \iint\limits_{-\infty}^{\infty} g(\underline{x}) e^{-i2\pi \langle \underline{x}, \underline{s} \rangle} \, dx_1 dx_2 \qquad (A-1)$$

where $i = \sqrt{-1}$, $\underline{s} = (s_1, s_2)^T$, and where $\langle \underline{x}, \underline{s} \rangle$ is the scalar
product of the vectors $\underline{x}$ and $\underline{s}$ given by

$$\langle \underline{x}, \underline{s} \rangle = \underline{x}^T \underline{s} = x_1 s_1 + x_2 s_2 \qquad (A-2)$$

The vector $\underline{s}$ is referred to as planar frequency. Its com-
ponents, $s_1$ and $s_2$, are real numbers which, as shown below,
correspond to physical frequencies measured in the directions

A-1

of the axes of the coordinate system. The fact that $\hat{g}$ is complex-valued is solely due to the appearance of the factor i in the exponential of the integrand in Eq. A-1. Note that since $g(\underline{x})$ is real-valued,[†]

$$\hat{g}(\underline{s}) = [\hat{g}(-\underline{s})]^*  \qquad (A-3)$$

The inverse Fourier transformation permits the recovery of $g(\underline{x})$ from $\hat{g}(\underline{s})$:

$$g(\underline{x}) = \iint\limits_{-\infty}^{\infty} \hat{g}(\underline{s}) e^{i2\pi\langle\underline{x},\underline{s}\rangle} \, ds_1 ds_2 \qquad (A-4)$$

The formulas for the Fourier transform and the inverse Fourier transform are completely symmetric except for a change of sign in the exponential. The functions g and $\hat{g}$ are called a Fourier transform pair. Given any one of them, the other is uniquely determined within an equivalence class (Ref. 16).

In order to give a physical interpretation of the Fourier transformation, it is convenient to decompose $\hat{g}(\underline{s})$ into its real and imaginary parts. Let

$$\hat{g}(\underline{s}) = \hat{g}_r(\underline{s}) + i\hat{g}_i(\underline{s}) \qquad (A-5)$$

where $\hat{g}_r$ and $\hat{g}_i$ are real. From Eq. A-3 it follows that

$$\hat{g}_r(\underline{s}) = \hat{g}_r(-\underline{s}) \qquad (A-6)$$

and

$$\hat{g}_i(\underline{s}) = -\hat{g}_i(-\underline{s}) \qquad (A-7)$$

---

[†]A superscript asterisk denotes complex conjugation when attached to a scalar and conjugate transpose when attached to a matrix or a vector.

Using the identity

$$e^{i2\pi<\underline{x},\underline{s}>} = \cos 2\pi<\underline{x},\underline{s}> + i \sin 2\pi<\underline{x},\underline{s}> \qquad (A-8)$$

and Eq. A-5, the inverse Fourier transformation can be written as

$$g(\underline{x}) = \iint\limits_{-\infty}^{\infty} [\hat{g}_r(\underline{s}) \cos 2\pi<\underline{x},\underline{s}> - \hat{g}_i(\underline{s}) \sin 2\pi<\underline{x},\underline{s}>] ds_1 ds_2$$

$$+ i \iint\limits_{-\infty}^{\infty} [\hat{g}_r(\underline{s}) \sin 2\pi<\underline{x},\underline{s}> + \hat{g}_i(\underline{s}) \cos 2\pi<\underline{x},\underline{s}>] ds_1 ds_2$$

$$(A-9)$$

From Eqs. A-2, A-6 and A-7 it follows that the second integral in the right-hand side of Eq. A-9 vanishes and that

$$g(\underline{x}) = \int\limits_0^{\infty} \int\limits_0^{\infty} A_{11}(s_1,s_2) \cos 2\pi s_1 x_1 \cos 2\pi s_2 x_2 \, ds_1 ds_2$$

$$+ \int\limits_0^{\infty} \int\limits_0^{\infty} A_{22}(s_1,s_2) \sin 2\pi s_1 x_1 \sin 2\pi s_2 x_2 \, ds_1 ds_2$$

$$+ \int\limits_0^{\infty} \int\limits_0^{\infty} A_{12}(s_1,s_2) \cos 2\pi s_1 x_1 \sin 2\pi s_2 x_2 \, ds_1 ds_2$$

$$+ \int\limits_0^{\infty} \int\limits_0^{\infty} A_{21}(s_1,s_2) \sin 2\pi s_1 x_1 \cos 2\pi s_2 x_2 \, ds_1 ds_2$$

$$(A-10)$$

A-3

where

$$A_{11}(s_1,s_2) = 2[\hat{g}_r(s_1,s_2) + \hat{g}_r(s_1,-s_2)]$$

$$A_{22}(s_1,s_2) = 2[-\hat{g}_r(s_1,s_2) + \hat{g}_r(s_1,-s_2)]$$

$$A_{12}(s_1,s_2) = 2[-\hat{g}_i(s_1,s_2) + \hat{g}_i(s_1,-s_2)]$$

$$A_{21}(s_1,s_2) = 2[-\hat{g}_i(s_1,s_2) - \hat{g}_i(s_1,-s_2)]$$

(A-11)

Equation A-10 is a representation of $g(\underline{x})$ as a sum over frequency of products of trigonometric functions for the four possible phase combinations. Only positive frequencies appear in Eq. A-10. The Fourier transform $\hat{g}(\underline{s})$ associates with each pair of positive frequencies $(s_1,s_2)$ eight real numbers corresponding to the real and imaginary parts of $\hat{g}(\underline{s})$ for the four vector planar frequencies $\underline{s} = (s_1,s_2)^T$, $\underline{s} = (s_1,-s_2)^T$, $\underline{s} = (-s_1,s_2)$ and $\underline{s} = (-s_1,-s_2)^T$. Of these eight numbers only four are independent (Eq. A-3) and the relation between these numbers and the coefficients of the expansion A-10 is given by A-11. The definition of the Fourier transform (Eq. A-1) as a complex-valued function of positive and negative frequencies is a compact mathematically convenient way of representing the four amplitudes of the trigonometric expansion A-10. The inversion formula (Eq. A-4) is entirely equivalent to the expansion A-10.

Classically, the most important application of the Fourier transformation has been to the solution of differential equations. This application is a consequence of the following property of Fourier transforms: Consider the n-th partial derivative of $g(\underline{x})$ with respect to $x_k$ (k=1,2). From the formula for the inverse Fourier transform (Eq. A-4) $\partial^n g(\underline{x})/\partial x_k^n$ can be written as

END

FILMED

DTIC
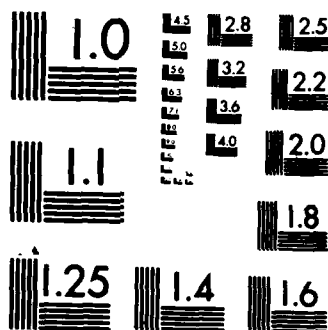
MICROCOPY RESOLUTION TEST CHART

NATIONAL BUREAU OF STANDARDS-1963-A

$$\frac{\partial^n}{\partial x_k^n} g(\underline{x}) = \iint\limits_{-\infty}^{\infty} \frac{\partial^n}{\partial x_k^n} [\hat{g}(\underline{s}) \, e^{i\langle\underline{x},\underline{s}\rangle}] \, ds_1 ds_2 \qquad (A-12)$$

With the help of Eq. A-2, the partial derivative of the integrand can be evaluated to yield

$$\frac{\partial^n}{\partial x_k^n} g(\underline{x}) = \iint\limits_{-\infty}^{\infty} [(i2\pi s_k)^n \, \hat{g}(\underline{s})] \, e^{i\langle\underline{x},\underline{s}\rangle} \, ds_1 ds_2 \qquad (A-13)$$

from which it follows that the Fourier transform of $\partial^n g(\underline{x})/\partial x_k^n$ is the Fourier transform of $g$ multiplied by $(i2\pi s_k)^n$.

As an example of the application of this property of the Fourier transformation, consider the solution of Laplace's equation with a boundary condition on a plane. Let $T_z(\underline{x})$ be the potential at height $z$ above the point $\underline{x} = (x_1, x_2)^T$. At $z=0$, the potential is known and is given by $T_o(\underline{x})$. For $z \geq 0$, $T_z(\underline{x})$ satisfies

$$\frac{\partial^2}{\partial x_1^2} T_z(\underline{x}) + \frac{\partial^2}{\partial x_2^2} T_z(\underline{x}) + \frac{\partial^2}{\partial z^2} T_z(\underline{x}) = 0 \qquad (A-14)$$

In addition, it is required that $T_z(\underline{x})$ remain bounded as $z \to \infty$.

Let $\hat{T}_z(\underline{s})$ be the Fourier transform of the potential on the plane at height $z$. Applying the Fourier transformation to Eq. A-14 results in

$$-4\pi^2 s_1^2 \hat{T}_z(\underline{s}) - 4\pi^2 s_2^2 \hat{T}_z(\underline{s}) + \frac{\partial^2}{\partial z^2} \hat{T}_z(\underline{s}) = 0 \qquad (A-15)$$

from which it follows that

$$\frac{\partial^2}{\partial z^2} \hat{T}_z(\underline{s}) = 4\pi^2 s^2 \hat{T}_z(\underline{s}) \qquad (A-16)$$

where

$$s = (s_1^2 + s_2^2)^{1/2} \qquad (A-17)$$

Equation A-16 is an ordinary differential equation for each value of $\underline{s}$. Its solution is of the form

$$\hat{T}_z(\underline{s}) = A\, e^{-2\pi sz} + B\, e^{+2\pi sz} \qquad (A-18)$$

where A and B are to be determined. From the condition that the potential must be bounded as $z \to \infty$ it follows that B=0. The value of A is obtained by setting z=0 to yield $A = \hat{T}_o(\underline{s})$. Thus, the solution to Eq. A-16 is

$$\hat{T}_z(\underline{s}) = e^{-2\pi sz}\, \hat{T}_o(\underline{s}) \qquad (A-19)$$

This equation states that the Fourier transforms of the potential at height z and at height 0 are simply related by the attenuation factor $e^{-2\pi sz}$. In the space domain, the solution is obtained by using the inverse Fourier transform; i.e.,

$$T_z(\underline{x}) = \iint\limits_{-\infty}^{\infty} \hat{T}_o(\underline{s})\, e^{-2\pi sz}\, e^{i2\pi \langle \underline{x}, \underline{s} \rangle}\, ds_1 ds_2 \qquad (A-20)$$

In the discrete case the Fourier transform is called the finite Fourier transform and is defined in a manner analogous to Eq. A-1. Let M be an orthogonal grid of points on the plane as in Fig. A-1. The normalized finite Fourier transform

A-6

R-63327
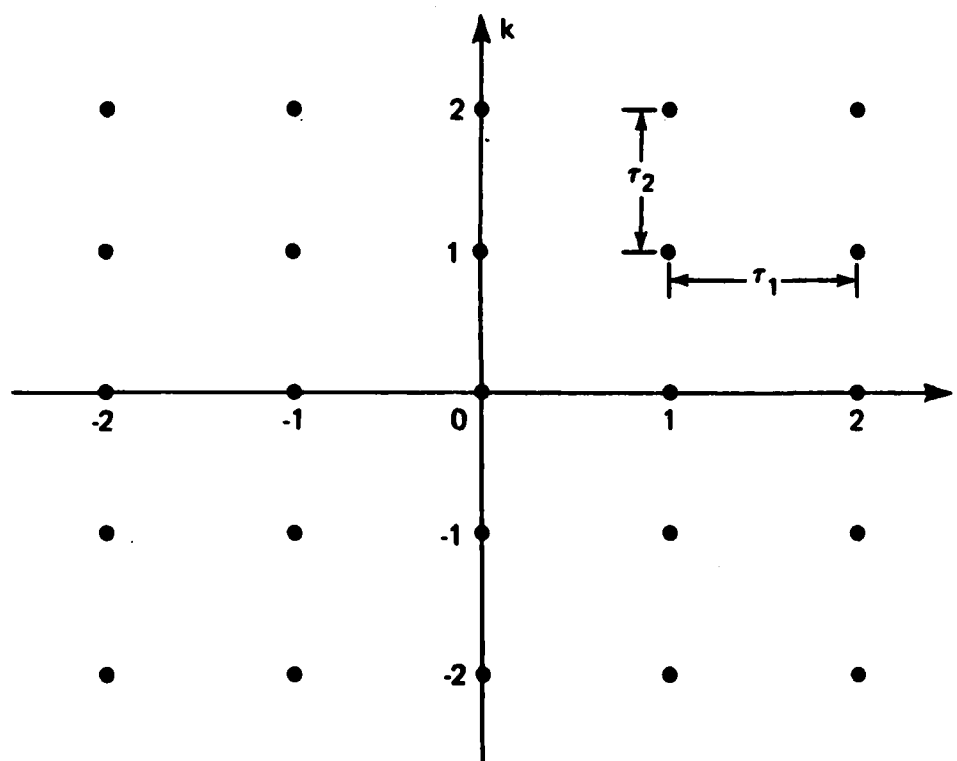


Figure A-1   Grid M

of a function $G(\underline{\Omega})$ with $\underline{\Omega} = (j,k)$ denoting the position of a point on the grid is defined as*

$$\hat{G}(\underline{p}) = \sum_{\underline{\Omega}} G(\underline{\Omega}) \, e^{-i2\pi<\underline{\Omega},\underline{p}>} \tag{A-21}$$

where $\underline{p} = (p_1, p_2)^T$, with $p_1$ and $p_2$ real numbers, is the vector of normalized frequencies in the directions of the grid axes (see below). Since $\underline{\Omega}$ is a vector of integers, the normalized finite Fourier transform is a periodic function of $p_1$ and $p_2$

---

*The symbol $\sum_{\underline{\Omega}}$ denotes summation over all possible values of the integer components of $\underline{\Omega}$.

with period 1 in each direction; i.e., if $\underline{\Lambda}=(\ell,m)^T$ is a vector
with arbitrary integer-valued entries then

$$\hat{g}(\underline{p}+\underline{\Lambda}) = \sum_{\underline{\Omega}} G(\underline{\Omega})\ e^{-i2\pi<\underline{\Omega},\underline{p}+\underline{\Lambda}>} \qquad \text{A-22)}$$

$$= \hat{G}(\underline{p})$$

because

$$e^{-i2\pi<\underline{\Omega},\underline{p}+\underline{\Lambda}>} = e^{-i2\pi<\underline{\Omega},\underline{p}>} \cdot e^{-i2\pi<\underline{\Omega},\underline{\Lambda}>} \qquad \text{(A-23)}$$

and

$$e^{-i2\pi<\underline{\Omega},\underline{\Lambda}>} = e^{-i2\pi(j\ell+km)} = 1 \qquad \text{(A-24)}$$

for all possible values of j, $\ell$, k and m.

The inverse of the normalized finite Fourier trans-
form is given by

$$G(\underline{\Omega}) = \int_{-\frac{1}{2}}^{\frac{1}{2}} \int_{-\frac{1}{2}}^{\frac{1}{2}} \hat{G}(\underline{p})\ e^{i2\pi<\underline{\Omega},\underline{p}>}\ dp_1\ dp_2 \qquad \text{(A-25)}$$

The limits of integration in Eq. A-25 can be modified as long
as they span a full period of $\hat{G}(\underline{p})$ in each dimension.

The vector $\underline{p} = (p_1,p_2)^T$ in Eqs. A-21 and A-25 is called
normalized planar frequency because it does not carry any infor-
mation as to the physical wavelengths implied by $p_1$ and $p_2$.
The reason is that the function G has been viewed as being
defined on the integer coordinates of the grid and the spacing
between consecutive points in each direction is one unit ir-
respective of the physical distance involved.

A-8

The physical position $\underline{x} = (x_1, x_2)^T$ of the point $\underline{\Omega} = (j,k)^T$ is

$$\underline{x} = J \underline{\Omega} \qquad (A-26)$$

where

$$J = \begin{pmatrix} \tau_1 & 0 \\ 0 & \tau_2 \end{pmatrix}$$

is called the grid spacing matrix (see Fig. A-1). It then follows that the normalized frequencies $p_1$ and $p_2$ can be identified with the physical frequencies $s_1 = p_1/\tau_1$ and $s_2 = p_2/\tau_2$. Letting $\underline{s} = (s_1, s_2)^T = J^{-1}\underline{p}$, Eqs. A-21 and A-25 become, respectively,

$$\hat{G}(J\underline{s}) = \sum_{\underline{\Omega}} G(\underline{\Omega}) e^{-i2\pi <J\underline{\Omega}, \underline{s}>} \qquad (A-27)$$

and

$$G(\underline{\Omega}) = \tau_1 \tau_2 \int_{-\bar{s}_2}^{\bar{s}_2} \int_{-\bar{s}_1}^{\bar{s}_1} \hat{G}(J\underline{s}) e^{i2\pi <J\underline{\Omega}, \underline{s}>} \, ds_1 ds_2 \qquad (A-28)$$

where the factor $\tau_1 \tau_2$ in Eq. A-28 arises from the change in integration variables. The quantities $\bar{s}_1 = 1/2\tau_1$ and $\bar{s}_2 = 1/2\tau_2$ are called the Nyquist frequencies of the grid.

For purposes of compatibility with the definition of the Fourier transform in the continuous case (Eqs. A-1 and A-4), it is convenient to define the unnormalized finite Fourier transform (or, simply, finite Fourier transform) as[*]

─────────────────────────

[*]With this definition the physical units of $\hat{g}$ and $\hat{G}$ coincide when G is a sampled version of g.

A-9

$$\hat{\hat{G}}(\underline{s}) = \tau_1 \tau_2 \, \hat{G}(J\underline{s}) \qquad\qquad (A-29)$$

Thus, from Eqs. A-27 and A-28, the finite Fourier transform is given by

$$\hat{\hat{G}}(\underline{s}) = \Delta(J) \sum_{\underline{\Omega}} G(\underline{\Omega}) \, e^{-i2\pi<J\underline{\Omega},\underline{s}>} \qquad\qquad (A-30)$$

and the inverse finite Fourier transform is

$$G(\underline{\Omega}) = \int_{-\bar{s}_2}^{\bar{s}_2} \int_{-\bar{s}_1}^{\bar{s}_1} \hat{\hat{G}}(\underline{s}) \, e^{i2\pi<J\underline{\Omega},\underline{s}>} \, ds_1 ds_2 \qquad\qquad (A-31)$$

where in Eq. A-30, $\Delta(J) = \tau_1 \tau_2$ is the determinant of the spacing matrix.

## A.2 CONVOLUTION

Let g and f be two functions defined for all $\underline{x}=(x_1,x_2)^T$. The convolution of g and f is a third function, h, given by

$$h(\underline{x}) = \iint_{-\infty}^{\infty} g(\underline{x}') \, f(\underline{x}-\underline{x}') \, dx_1' dx_2' \qquad\qquad (A-32)$$

In the discrete case, the convolution of G and F is defined as

$$H(\underline{\Omega}) = \sum_{\underline{\Omega}'} G(\underline{\Omega}') \, F(\underline{\Omega}-\underline{\Omega}') \qquad\qquad (A-33)$$

A-10

By changing integration variables in Eq. A-32 and summation indices in Eq. A-33 it can be verified that the roles of g and f and those of G and F are interchangeable in the definitions.

A convolution integral becomes a simple algebraic product under the Fourier transformation. To see this, consider Eq. A-32. Taking Fourier transforms on both sides of the equality, Eq. A-32 becomes

$$\hat{h}(\underline{s}) = \iint\limits_{-\infty}^{\infty} \iint\limits_{-\infty}^{\infty} g(\underline{x}') \ f(\underline{x}-\underline{x}') \ e^{-i2\pi<\underline{x},\underline{s}>} \ dx_1' dx_2' dx_1 dx_2$$

(A-34)

Changing the variables of integration $x_1$ and $x_2$ through the definition $\underline{x}''=\underline{x}-\underline{x}'$, Eq. A-34 transforms into

$$\hat{h}(\underline{s}) = \iint\limits_{-\infty}^{\infty} \iint\limits_{-\infty}^{\infty} g(\underline{x}') \ f(\underline{x}'') \ e^{-i2\pi<\underline{x}'+\underline{x}'',\underline{s}>} \ dx_1' dx_2' dx_1'' dx_2''$$

(A-35)

which can be written as

$$\hat{h}(\underline{s}) = \left[ \iint\limits_{-\infty}^{\infty} g(\underline{x}') e^{-i2\pi<\underline{x}',\underline{s}>} \ dx_1' dx_2' \right] \left[ \iint\limits_{-\infty}^{\infty} f(\underline{x}'') e^{-i2\pi<\underline{x}'',\underline{s}>} dx_1'' dx_2'' \right]$$

(A-36)

Thus,

$$\hat{h}(\underline{s}) = \hat{g}(\underline{s}) \ \hat{f}(\underline{s}) \qquad\qquad (A-37)$$

Similarly, in the discrete case the normalized finite Fourier transform of H is given by

$$\hat{H}(\underline{p}) = \hat{G}(\underline{p}) \, \hat{F}(\underline{p}) \qquad \text{(A-38)}$$

For the (unnormalized) finite Fourier transform the relation is

$$\hat{\hat{H}}(\underline{s}) = \frac{1}{\Delta(J)} \, \hat{\hat{G}}(\underline{s}) \, \hat{\hat{F}}(\underline{s}) \qquad \text{(A-39)}$$

As an example of a convolution integral, consider the flat-earth upward continuation formula of Ref. 2. The potential at height z over the point $\underline{x}$, $T_z(\underline{x})$ is related to the surface potential $T_o(\underline{x})$ through the formula

$$T_z(\underline{x}) = \frac{z}{2\pi} \iint\limits_{-\infty}^{\infty} \frac{1}{[||\underline{x}'-\underline{x}||^2+z^2]^{3/2}} \, T_o(\underline{x}') \, dx_1' dx_2' \qquad \text{(A-40)}$$

where $||\underline{x}||^2 = \langle \underline{x},\underline{x} \rangle$ is the square-magnitude of the vector $\underline{x}$. This integral can be recognized as the convolution of $T_o$ and the function $U(\underline{x})$ defined by

$$U(\underline{x}) = \frac{z/2\pi}{(||\underline{x}||^2+z^2)^{3/2}} \qquad \text{(A-41)}$$

Therefore, from Eq. A-37

$$\hat{T}_z(\underline{s}) = \hat{U}(\underline{s}) \, \hat{T}_o(\underline{s}) \qquad \text{(A-42)}$$

It is instructive to evaluate $\hat{U}(\underline{s})$. More generally, suppose that it is desired to evaluate the Fourier transform of a function $r(||\underline{x}||)$ which only depends on the magnitude of the position vector $\underline{x}$. Thr Fourier transform $\hat{r}(\underline{s})$ is given by

$$\hat{r}(\underline{s}) = \iint\limits_{-\infty}^{\infty} r(||\underline{x}||) \, e^{-i2\pi\langle\underline{x},\underline{s}\rangle} \, dx_1 dx_2 \qquad \text{(A-43)}$$

or expanding the scalar product in the exponent

$$\hat{r}(\underline{s}) = \iint\limits_{-\infty}^{\infty} r(||\underline{x}||) \; e^{-i2\pi(s_1 x_1 + s_2 x_2)} \; dx_1 dx_2 \qquad (A\text{-}44)$$

The dependence of r on the magnitude of $\underline{x}$ suggests the use of polar coordinates. Setting

$$\begin{aligned} x_1 &= \rho \cos \theta \\ x_2 &= \rho \sin \theta \end{aligned} \qquad (A\text{-}45)$$

Eq. A-44 becomes

$$\hat{r}(\underline{s}) = \int_0^\infty \rho r(\rho) \left[ \int_{-\pi}^{\pi} e^{i2\pi\rho(s_1\cos\theta + s_2\sin\theta)} \; d\theta \right] d\rho \qquad (A\text{-}46)$$

but (Ref. 18)

$$\int_{-\pi}^{\pi} e^{i2\pi\rho(s_1\cos\theta + s_2\sin\theta)} \; d\theta = 2\pi \; J_0(2\pi s\rho) \qquad (A\text{-}47)$$

where $J_0$ is the Bessel function of the first kind of order zero and

$$s = ||\underline{s}|| \qquad (A\text{-}48)$$

Thus,

$$\hat{r}(\underline{s}) = 2\pi \int_0^\infty \rho J_0 (2\pi s\rho) \; r(\rho) \; d\rho \qquad (A\text{-}49)$$

from which it follows that $\hat{r}(\underline{s})$ is only a function of the frequency magnitude s.*

The integral in Eq. A-48 is known in the mathematical literature as the zero-order Hankel transform of the function r. From a table of Hankel transforms (Ref. 19), it follows that the Fourier transform of U as given by Eq. A-41 is

$$\hat{U}(\underline{s}) = e^{-2\pi s z} \qquad \text{(A-50)}$$

Therefore, Eq. A-42 becomes

$$\hat{T}_z(\underline{s}) = e^{-2\pi s z} \, \hat{T}_o(\underline{s}) \qquad \text{(A-51)}$$

which is identical to Eq. A-19.

A.3    SPECTRAL AND CROSS-SPECTRAL DENSITIES - DEFINITIONS

Let $y_1$ and $y_2$ be two zero-mean stochastic processes defined for all points in the plane. The process $y_\ell (\ell=1,2)$ is said to be stationary if its covariance is only a function of the coordinate differences; i.e.,

$$R_{y_\ell, y_\ell} \, (\underline{x}' - \underline{x}'') = E[y_\ell(\underline{x}') \, y_\ell(\underline{x}'')] \qquad \text{(A-52)}$$

where E denotes the mathematical expectation operator. Since the roles of $\underline{x}'$ and $\underline{x}''$ are interchangeable on the right-hand side of the above equation,

---

*The converse can also be shown to be true: If $\hat{r}(\underline{s})$ is only a function of $||\underline{s}||$, the inverse Fourier transform, r($\underline{x}$) is only a function of $||\underline{x}||$.

A-14

$$R_{y_\ell, y_\ell}(\underline{x}) = R_{y_\ell, y_\ell}(-\underline{x}) \qquad \text{(A-53)}$$

The processes $y_1$ and $y_2$ are said to be jointly stationary if each of them is stationary and their crosscovariance is only a function of the coordinate differences:

$$R_{y_1, y_2}(\underline{x}' - \underline{x}'') = E[y_1(\underline{x}') \, y_2(\underline{x}'')] \qquad \text{(A-54)}$$

From Eq. A-54 it follows that

$$R_{y_2, y_1}(\underline{x}) = R_{y_1, y_2}(-\underline{x}) \qquad \text{(A-55)}$$

The power spectral density (PSD) of $y_\ell$, $\Phi_{y_\ell, y_\ell}$, is defined as the Fourier transform of its autocovariance function

$$\Phi_{y_\ell, y_\ell}(\underline{s}) = \iint_{-\infty}^{\infty} R_{y_\ell, y_\ell}(\underline{x}) \, e^{-i2\pi \langle \underline{x}, \underline{s} \rangle} \, dx_1 dx_2 \qquad \text{(A-56)}$$

It is shown in Ref. 15 that

$$\Phi_{y_\ell, y_\ell}(\underline{s}) \geq 0 \qquad \text{(A-57)}$$

The cross-spectral density of $y_1$ and $y_2$, $\Phi_{y_1, y_2}$, is similarly defined as

$$\Phi_{y_1, y_2}(\underline{s}) = \iint_{-\infty}^{\infty} R_{y_1, y_2}(\underline{x}) \, e^{-i2\pi \langle \underline{x}, \underline{s} \rangle} \, dx_1 dx_2 \qquad \text{(A-58)}$$

From Eq. A-55,

$$\Phi_{y_2, y_1}(\underline{s}) = \Phi_{y_1, y_2}^{*}(\underline{s}) \qquad \text{(A-59)}$$

A-15

Analogous definitions apply to discrete processes. Let $Y_1$ and $Y_2$ be two discrete zero-mean processes defined for the integer coordinates $\underline{\Omega} = (j,k)$. The process $Y_\ell$ is stationary if

$$R_{Y_\ell,Y_\ell}(\underline{\Omega}'-\underline{\Omega}'') = E[Y_\ell(\underline{\Omega}')Y_\ell(\underline{\Omega}'')] \qquad (A-60)$$

and $Y_1$ and $Y_2$ are jointly stationary if

$$R_{Y_1,Y_2}(\underline{\Omega}'-\underline{\Omega}'') = E[Y_1(\underline{\Omega}')Y_2(\underline{\Omega}'')] \qquad (A-61)$$

Their normalized spectral densities are defined by

$$\Phi_{Y_\ell,Y_m}(\underline{p}) = \sum_{\underline{\Omega}} R_{Y_\ell,Y_m}(\underline{\Omega})\, e^{-i2\pi<\underline{\Omega},\underline{p}>} \qquad (A-62)$$

for $\ell=1,2$ and $m=1,2$. The (unnormalized) spectral densities are

$$\tilde{\Phi}_{Y_\ell,Y_m}(\underline{s}) = \Delta(J) \sum_{\underline{\Omega}} R_{Y_\ell,Y_m}(\underline{\Omega})e^{-i2\pi<J\underline{\Omega},\underline{s}>} \qquad (A-63)$$

## A.3.1  Spectral Densities and Convolution

Suppose that the process $y_2$ can be obtained by convolving the stationary process $y_1$ with a known deterministic function f

$$y_2(\underline{x}') = \iint_{-\infty}^{\infty} f(\underline{w}')\, y_1(\underline{x}'-\underline{w}')\, dw_1'dw_2' \qquad (A-64)$$

First it will be shown that the covariance of $y_2$, $E[y_2(\underline{x}')y_2(\underline{x}'')]$ is only a function of the coordinate shift $\underline{x}'-\underline{x}''$.

From Eq. A-64,

$$E[y_2(\underline{x}')y_2(\underline{x}'')] = \iint\limits_{-\infty}^{\infty} \iint\limits_{-\infty}^{\infty} f(\underline{\omega}')f(\underline{\omega}'')E[y_1(\underline{x}'-\underline{\omega}')y_1(\underline{x}''-\underline{\omega}'')] \; d\omega_1' d\omega_2' d\omega_1'' d\omega_2''$$

(A-65)

But since $y_1$ is stationary,

$$E[y_1(\underline{x}'-\underline{\omega}')y_1(\underline{x}''-\underline{\omega}'')] = R_{y_1,y_1}[(\underline{x}'-\underline{x}'')-(\omega'-\omega'')] \quad \text{(A-66)}$$

Thus

$$E[y_2(\underline{x}')y_2(\underline{x}'')] = \iint\limits_{-\infty}^{\infty} \iint\limits_{-\infty}^{\infty} f(\underline{\omega}')f(\underline{\omega}'')R_{y_1,y_1}[(\underline{x}'-\underline{x}'')-(\underline{\omega}'-\underline{\omega}'')] \; d\omega_1' d\omega_2' d\omega_1'' d\omega_2''$$

(A-67)

This equation shows that the covariance of $y_2$ is a function of $\underline{x}'-\underline{x}''$. Therefore, $y_2$ is also a stationary process and its covariance is

$$R_{y_2,y_2}(\underline{x}) = \iint\limits_{-\infty}^{\infty} \iint\limits_{-\infty}^{\infty} f(\underline{\omega}')f(\underline{\omega}'') \; R_{y_1,y_1}[\underline{x}-(\underline{\omega}'-\underline{\omega}'')] \; d\omega_1' d\omega_2' d\omega_1'' d\omega_2''$$

(A-68)

A formula for the spectral density of $y_2$ in terms of that of $y_1$ is derived next. From Eq. A-68,

$$\Phi_{y_2,y_2}(\underline{s}) = \iint\limits_{-\infty}^{\infty} \iint\limits_{-\infty}^{\infty} \iint\limits_{-\infty}^{\infty} f(\underline{\omega}')f(\underline{\omega}'') \; R_{y_1,y_1}[\underline{x}-(\underline{\omega}'-\underline{\omega}'')]$$

$$\times \; e^{-i2\pi\langle\underline{x},\underline{s}\rangle} \; d\omega_1' d\omega_2' \; d\omega_1'' d\omega_2'' \; dx_1 dx_2 \qquad \text{(A-69)}$$

A-17

Replacing the integration variables $x_1$ and $x_2$ by $\xi_1$ and $\xi_2$ with $\underline{\xi} = \underline{x} - (\underline{\omega}' - \underline{\omega}'')$ and noting that

$$e^{-i2\pi<\underline{x},\underline{s}>} = e^{-i2\pi<\underline{\omega}',\underline{s}>} \, e^{+i2\pi<\underline{\omega}'',\underline{s}>} \, e^{-i2\pi<\underline{\xi},\underline{s}>} \qquad \text{(A-70)}$$

Eq. A-69 becomes

$$\Phi_{y_2,y_2}(\underline{s}) = \iint_{-\infty}^{\infty} f(\underline{\omega}') \, e^{-i2\pi<\underline{\omega}',\underline{s}>} \, d\omega_1' d\omega_2''$$

$$\times \iint_{-\infty}^{\infty} f(\underline{\omega}'') \, e^{+i2\pi<\underline{\omega}'',\underline{s}>} \, d\omega_1'' d\omega_2''$$

$$\times \iint_{-\infty}^{\infty} R_{y_1,y_1}(\underline{\xi}) \, e^{-i2\pi<\underline{\xi},\underline{s}>} \, d\xi_1 d\xi_2$$

$$\text{(A-71)}$$

from which

$$\Phi_{y_2,y_2}(\underline{s}) = \hat{f}(\underline{s}) \, \hat{f}^*(\underline{s}) \, \Phi_{y_1,y_1}(\underline{s}) \qquad \text{(A-72)}$$

or

$$\Phi_{y_2,y_2}(\underline{s}) = |\hat{f}(\underline{s})|^2 \, \Phi_{y_1,y_1}(\underline{s}) \qquad \text{(A-73)}$$

which is the desired relation.

Next, it is shown that $y_1$ and $y_2$ are jointly stationary. From Eq. A-64, the crosscovariance $E[y_2(\underline{x}')y_1(\underline{x}'')]$ can be written as

$$E[y_2(\underline{x}')y_1(\underline{x}'')] = \iint_{-\infty}^{\infty} f(\underline{\omega}) \, E[y_1(\underline{x}'-\underline{\omega})y_1(\underline{x}'')] d\omega_1 d\omega_2$$

$$\text{(A-74)}$$

A-18

and, because of the stationarity of $y_1$,

$$E[y_2(\underline{x}')y_1(\underline{x}'')] = \iint\limits_{-\infty}^{\infty} f(\underline{\omega}) \ R_{y_1,y_1}(\underline{x}-\underline{\omega}) \ d\omega_1 d\omega_2 \qquad \text{(A-75)}$$

Therefore, the crosscovariance of $y_2$ and $y_1$ only depends on the coordinate difference $\underline{x}$. Thus, $y_1$ and $y_2$ are jointly stationary and the crosscovariance $R_{y_2,y_1}(\underline{x})$, given by Eq. A-75, is the convolution of $f$ and $R_{y_1,y_1}$. It then also follows from Eqs. A-37 and A-75 that the cross-spectral density $\Phi_{y_2,y_1}$ is given by

$$\Phi_{y_2,y_1}(\underline{s}) = \hat{f}(\underline{s}) \ \Phi_{y_1,y_1}(\underline{s}) \qquad \text{(A-76)}$$

Similar results apply to discrete processes. If the process $Y_2$ is defined in terms of $Y_1$ through a convolution

$$Y_2(\underline{\Omega}) = \sum_{\underline{\Omega}'} F(\underline{\Omega}') \ Y_1(\underline{\Omega}-\underline{\Omega}') \qquad \text{(A-77)}$$

then the normalized spectral and cross-spectral densities of $Y_1$ and $Y_2$ are related by

$$\Phi_{Y_2,Y_2}(\underline{p}) = |\hat{F}(\underline{p})|^2 \ \Phi_{Y_1,Y_1}(\underline{p}) \qquad \text{(A-78)}$$

$$\Phi_{Y_2,Y_1}(\underline{p}) = \hat{F}(\underline{p}) \ \Phi_{Y_1,Y_1}(\underline{p}) \qquad \text{(A-79)}$$

and the (unnormalized) densities are related by

$$\tilde{\Phi}_{Y_2,Y_2}(\underline{s}) = \frac{1}{\Delta^2(J)} \ |\hat{\tilde{F}}(\underline{s})|^2 \ \tilde{\Phi}_{Y_1,Y_1}(\underline{s}) \qquad \text{(A-80)}$$

A-19

$$\tilde{\Phi}_{Y_2, Y_1}(\underline{s}) = \frac{1}{\Delta(J)} \hat{\tilde{F}}(\underline{s}) \, \tilde{\Phi}_{Y_1, Y_1}(\underline{s}) \qquad\qquad (A-81)$$

## A.3.2 <u>Spectral Densities of Isotropic Processes</u>

Consider a stationary process, y, defined for all points on the plane. It is of interest to investigate the behavior of the covariance and spectral density of y under rotations of the reference frame.

Let the primed coordinates be defined as in Fig. A-2 so that

$$\underline{x} = \theta \, \underline{x}' \qquad\qquad (A-82)$$

where

$$\theta = \begin{pmatrix} \cos\theta & -\sin\theta \\ \sin\theta & \cos\theta \end{pmatrix} \qquad\qquad (A-83)$$

R-63322
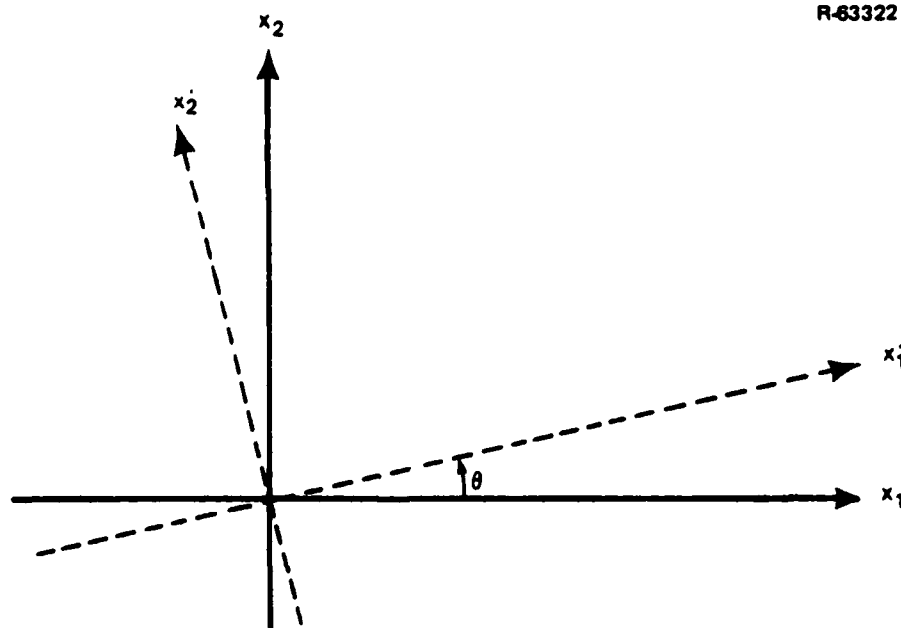


Figure A-2    Definition of Primed Reference Frame

A-20

Denoting the covariance functions in the primed and unprimed frames by $R'_{y,y}$ and $R_{y,y}$, respectively, it can be seen that

$$R'_{y',y'}(\underline{x}') = R_{y,y}(\theta\underline{x}') \qquad (A-84)$$

The spectral density of y expressed in terms of frequencies measured in the directions of the primed axes is

$$\phi'_{y',y'}(\underline{s}') = \iint\limits_{-\infty}^{\infty} R'_{y',y}(\underline{x}')\, e^{-i2\pi<\underline{x}',\underline{s}'>}\, dx'_1 dx'_2 \qquad (A-85)$$

From Eq. A-84,

$$\phi'_{y',y'}(\underline{s}') = \iint\limits_{-\infty}^{\infty} R_{y,y}(\theta\underline{x}')\, e^{-i2\pi<\underline{x}',\underline{s}'>}\, dx'_1 dx'_2 \qquad (A-86)$$

Since $\theta^{-1} = \theta^T$, it follows that $<\underline{x}',\underline{s}'> = <\theta\underline{x}',\theta\underline{s}'>$. Thus, changing variables of integration in Eq. A-86 according to the transformation A-82,

$$\phi'_{y',y'}(\underline{s}') = \iint\limits_{-\infty}^{\infty} R_{y,y}(\underline{x})\, e^{-i2\pi<\underline{x},\theta\underline{s}'>}\, dx_1 dx_2 \qquad (A-87)$$

or

$$\phi'_{y',y'}(\underline{s}') = \phi_{y,y}(\theta\underline{s}') \qquad (A-88)$$

Equations A-84 and A-88 show that, in general, the covariance function and the PSD of y depend upon the specific directions in which the coordinate differences are measured. A stationary process whose statistical behavior is the same in all directions is said to be isotropic. If the process y is isotropic, the functional form of its covariance and PSD must be independent of the orientation of the cartesian frame in

A-21

which they are expressed. From Eqs. A-84 and A-88 it follows that y is isotropic if for all possible rotation matrices

$$R_{y,y}(\underline{x}) = R_{y,y}(\theta\underline{x}) \qquad (A-89)$$

and

$$\Phi_{y,y}(\underline{s}) = \Phi_{y,y}(\theta\underline{s}) \qquad (A-90)$$

By changing to polar coordinates, it can be shown that Eqs. A-89 and A-90 are possible only if $R_{y,y}$ and $\Phi_{y,y}$ are functions of $||\underline{x}||$ and $s = ||\underline{s}||$, respectively[*].

An example of the covariance of an isotropic process is

$$R_{y,y}(\underline{x}) = \sigma^2 e^{-\beta||\underline{x}||}(1 + \beta||\underline{x}|| + \frac{1}{3}\beta^2||\underline{x}||) \qquad (A-91)$$

which is called an isotropic third-order Markov model with variance $\sigma^2$ and characteristic distance $1/\beta$ (Ref. 14). Using Eq. A-49 and a table of Hankel transforms, it is straightforward to show that

$$\Phi_{y,y}(\underline{s}) = \frac{10\pi\sigma^2\beta^5}{[\beta^2 + (2\pi s)^2]^{7/2}} \qquad (A-92)$$

Another example is furnished by the Attenuated White Noise model (Ref. 13). The covariance is given by

$$R_{y,y}(\underline{x}) = \frac{8D^3\sigma^6}{[||\underline{x}||^2 + 4D^2]^{3/2}} \qquad (A-93)$$

---

[*]That these two conditions are compatible (in fact one implies the other) is shown by the derivation of Eq. A-49 from Eq. A-43.

where $\sigma^2$ is the variance and D is called the shell depth. The PSD corresponding to Eq. A-93 is

$$\Phi_{y,y}(\underline{s}) = 8\pi D^2 \sigma^2 \ e^{-4\pi Ds} \qquad (A-94)$$

### A.3.3 Along-track Spectral Densities

The Fourier transform of a function of a single variable, g(t), is defined in a manner analogous to Eq. A-1:

$$\hat{g}(f) = \int_{-\infty}^{\infty} g(t) \ e^{-i2\pi tf} \ dt \qquad (A-95)$$

The inverse one-dimensional Fourier transform is

$$g(t) = \int_{-\infty}^{\infty} \hat{g}(f) \ e^{i2\pi tf} \ df \qquad (A-96)$$

In Eqs. A-95 and A-96, f is interpreted as frequency. The units of f are the inverse of the units of t.

Spectral densities of one-dimensional processes are denoted by the letter S and covariances by the letter C. If z(t) is a one-dimensional process, its power spectral density is

$$S_{z,z}(f) = \int_{-\infty}^{\infty} C_{z,z}(t) \ e^{-i2\pi tf} \ dt \qquad (A-97)$$

The (one-dimensional) covariance $C_{z,z}(t)$ can be recovered from the PSD $S_{z,z}(t)$ by the inverse Fourier transform (Eq. A-96).

Let $y(\underline{x})$ be a stationary process on the plane with covariance $R_{y,y}(\underline{x})$ and PSD $\phi_{y,y}(\underline{s})$. Suppose an observer is traveling on the plane at constant velocity V on a straight-line track parallel to the $x_1'$ axis of Fig. A-2 and is continuously recording (without errors) the values of the process y as a function of time. Denote by $z(t)$ the recorded data. It is desired to relate the covariance function and the PSD of $z(t)$ to the covariance and PSD of the two-dimensional process $y(\underline{x})$.

First, consider the covariance $C_{z,z}(t)$. When the observer records an interval of time t, the two points on the plane corresponding to the times at the beginning and at the end of the time interval are separated by a vector difference

$$\underline{x} = \begin{pmatrix} x_1 \\ x_2 \end{pmatrix} = \begin{pmatrix} Vt \cos\theta \\ Vt \sin\theta \end{pmatrix} \qquad \text{(A-98)}$$

In the primed coordinate system this difference is

$$\underline{x}' = \begin{pmatrix} x_1' \\ x_2' \end{pmatrix} = \begin{pmatrix} Vt \\ 0 \end{pmatrix} \qquad \text{(A-99)}$$

Therefore $C_{z,z}(t)$ can be expressed as

$$C_{z,z}(t) = R_{y,y}' \left[ (Vt,0)^T \right] \qquad \text{(A-100)}$$

Next, consider the PSD $S_{z,z}(t)$. Since from Eq. A-85

$$R_{y,y}'(\underline{x}') = \iint\limits_{-\infty}^{\infty} \phi_{y,y}'(\underline{s}') \, e^{i2\pi<\underline{x}',\underline{s}'>} \, ds_1' ds_2' \qquad \text{(A-101)}$$

Setting $\underline{x}' = (Vt,0)^T$, it follows from Eq. A-100 that

$$C_{z,z}(t) = \iint_{-\infty}^{\infty} \Phi'_{y,y}(\underline{s}') \, e^{i2\pi Vts'_1} \, ds'_1 ds'_2 \qquad (A-102)$$

where $s'_1$ is measured in the direction of the $x'_1$ axis. Substituting integration with respect to $s'_1$ by integration with respect to $f=Vs'_1$, Eq. A-102 becomes

$$C_{z,z}(t) = \int_{-\infty}^{\infty} \left\{ \frac{1}{V} \int_{-\infty}^{\infty} \Phi'_{y,y}[(f/V,s'_2)] \, ds'_2 \right\} e^{i2\pi tf} \, df$$

$$(A-103)$$

The right-hand side of Eq. A-103 is readily recognized as the inverse (one-dimensional) Fourier transform of the quantity in braces. Therefore,

$$S_{z,z}(t) = \frac{1}{V} \int_{-\infty}^{\infty} \Phi'_{y,y}(f/V,s'_2) \, ds'_2 \qquad (A-104)$$

which is the desired relation.

If the observer records the data as a function of distance rather than time, the covariance, $C_{y,y}(x'_1)$, and the PSD, $S_{y,y}(s'_1)$, of the resulting record are called along-track covariance and PSD of the process $y$. Formulas for these quantities can be obtained by setting $V = 1$, $t = x'_1$ and $f = s'_1$ in Eqs. A-100 and A-104:

$$C_{y,y}(x'_1) = R'_{y,y}[(x'_1,0)^T] \qquad (A-105)$$

$$S_{y,y}(s_1') = \int_{-\infty}^{\infty} \Phi_{y,y}'(\underline{s}') \, ds_2' \qquad \text{(A-106)}$$

In words, the along-track covariance is the two-dimensional covariance with the shift in the cross-track direction set equal to zero, and the along-track PSD is the integral of the two-dimensional PSD over the cross-track frequencies. Note that the time-covariance and PSD are related to the along-track covariance and PSD through the simple relations

$$C_{z,z}(t) = C_{y,y}(Vt) \qquad \text{(A-107)}$$

$$S_{z,z}(t) = \frac{1}{V} S_{y,y}(f/V) \qquad \text{(A-108)}$$

In general, $C_{y,y}$ and $S_{y,y}$ depend upon the direction of the track. However, if the process y is isotropic, Eqs. A-89 and A-90 imply that the functional forms of the along-track covariance and PSD are independent of the direction of the track.

## APPENDIX B
## FLAT-EARTH FREQUENCY-DOMAIN RELATIONS

This appendix presents detailed derivations of the flat-earth frequency-domain relations introduced in Chapter 2. Relations between geodetic quantities and between their statistics are analyzed in Sections B.1 and B.2 of this appendix, respectively.

### B.1    GEODETIC RELATIONS

The anomalous potential is a harmonic function at all points external to the earth's surface.  If the earth is taken to be a sphere of radius R, the anomalous potential, $T(\underline{P})$, at a point $\underline{P}$ located at a distance $r > R$ from the center of the earth is given in terms of the potential at the earth's surface, $T_o$, by Poisson's integral formula

$$T(\underline{P}) = \frac{1}{4\pi R} \int_S \frac{(r^2-R^2)}{\ell^3} T_o \, d\sigma \qquad (B-1)$$

where the integration is taken over the surface of the earth and where $\ell$ represents the distance from the point $\underline{P}$ to the surface element $d\sigma$.

The flat-earth upward continuation formula (Ref. 2) is an approximation to Eq. B-1 which corresponds to the solution of Laplace's equation with a boundary condition on a plane. The potential $T_z$ at height $z = r-R$ over the point $\underline{x}$ on the plane is given by

$$T_z(\underline{x}) = \frac{z}{2\pi} \iint\limits_{-\infty}^{\infty} \frac{T_0(\underline{x}')}{[||\underline{x}'-\underline{x}||^2 + z^2]^{3/2}} \, dx_1' dx_2' \qquad \text{(B-2)}$$

where $\underline{x} = (x_1, x_2)^T$, $\underline{x}' = (x_1', x_2')^T$ and

$$||\underline{x}'-\underline{x}|| = [(x_1'-x_1)^2 + (x_2'-x_2)^2]^{1/2} \qquad \text{(B-3)}$$

The approximation is valid for $z \ll R$ and $||\underline{x}|| \ll R$. For reasons that will become clear in the sequel, it is convenient to identify the directions of the $x_1$ and $x_2$ axes with the east and north directions, respectively, at the point corresponding to the origin of the plane of the flat-earth approximation.

The usefulness of the approximation lies in the fact that the integral in Eq. B-2 is a two-dimensional convolution. The potential at height z, $T_z$, is the convolution of the potential at the surface, $T_0$, and the function $U_z$ defined by

$$U_z(\underline{x}) = \frac{z/2\pi}{(||\underline{x}||^2 + z^2)^{3/2}} \qquad \text{(B-4)}$$

The Fourier transform of a convolution integral is equal to the product of the Fourier transforms of the functions being convolved (see Appendix A, Eq. A-36). Denoting Fourier transforms by a superscript circumflex, the frequency-domain relation corresponding to Eq. B-2 can be written as

$$\hat{T}_z(\underline{s}) = \hat{U}_z(\underline{s})\hat{T}_0(\underline{s}) \qquad \text{(B-5)}$$

where $\underline{s} = (s_1, s_2)^T$ and $s_1$ and $s_2$ are spatial frequencies measured in the east and north directions, respectively.

The Fourier transform of $U_z$ is given by

$$\hat{U}_z(\underline{s}) = \iint_{-\infty}^{\infty} U_z(\underline{x}) \, e^{i2\pi<\underline{x},\underline{s}>} \, dx_1 dx_2 \qquad \text{(B-6)}$$

where

$$<\underline{x},\underline{s}> = x_1 s_1 + x_2 s_2 \qquad \text{(B-7)}$$

is the scalar product of the vectors $\underline{x}$ and $\underline{s}$. This integral is evaluated in closed form in Appendix A. The result is

$$\hat{U}_z(\underline{s}) = e^{-2\pi s z} \qquad \text{(B-8)}$$

where $s = ||\underline{s}||$. Consequently, from Eq. B-5, the Fourier transform of the potential at height z is related to that at the surface by the simple formula

$$\hat{T}_z(\underline{s}) = e^{-2\pi s z} \, \hat{T}_0(\underline{s}) \qquad \text{(B-9)}$$

The function $e^{-2\pi s z}$ is called the transfer function from potential at the surface to potential at height z. Note that this transfer function is a simple attenuation factor whose value decreases exponentially with frequency and height.

It is shown in Appendix A that Fourier transforms of partial derivatives of a function with respect to the east and north coordinates can be obtained by multiplying the Fourier transform of the function by the factors $i2\pi s_1$ and $i2\pi s_2$, respectively. Thus, for example, the Fourier transform of the east and north components of the gravity disturbance vector at height z, $\Gamma_{x_1}$ and $\Gamma_{x_2}$, are given by the formulas

B-3

$$\hat{\Gamma}_{x_1}(\underline{s}) = i2\pi s_1 \, \hat{T}_z(\underline{s}) \qquad (B-10)$$

$$\hat{\Gamma}_{x_2}(\underline{s}) = i2\pi s_2 \, \hat{T}_z(\underline{s}) \qquad (B-11)$$

Fourier transforms of partial derivatives of the potential with respect to height can be related to the Fourier transform of the potential through equally simple formulas. For example, consider the vertical component of the gravity disturbance vector, $\Gamma_z$. Its Fourier transform is defined by

$$\hat{\Gamma}_z(\underline{s}) = \iint\limits_{-\infty}^{\infty} \Gamma_z(\underline{x}) \, e^{-i2\pi<\underline{x},\underline{s}>} \, dx_1 dx_2 \qquad (B-12)$$

Thus,

$$\hat{\Gamma}_z(\underline{s}) = \iint\limits_{-\infty}^{\infty} \frac{\partial}{\partial z} T_z(\underline{x}) \, e^{-i2\pi<\underline{x},\underline{s}>} \, dx_1 dx_2$$

$$= \frac{\partial}{\partial z} \iint\limits_{-\infty}^{\infty} T_z(\underline{x}) \, e^{-i2\pi<\underline{x},\underline{s}>} \, dx_1 dx_2$$

$$= \frac{\partial}{\partial z} \hat{T}_z(\underline{s}) \qquad (B-13)$$

Therefore, from Eq. B-9, it follows that

$$\hat{\Gamma}_z(\underline{s}) = -2\pi s \, \hat{T}_z(\underline{s}) \qquad (B-14)$$

Using Eq. B-9 it is possible to express $\hat{\Gamma}_{x_1}$, $\hat{\Gamma}_{x_2}$ and $\hat{\Gamma}_z$ in terms of the Fourier transform of the anomalous surface potential as

$$\hat{\Gamma}_{x_1}(\underline{s}) = i2\pi s_1 e^{-2\pi sz} \hat{T}_o(\underline{s}) \tag{B-15}$$

$$\hat{\Gamma}_{x_2}(\underline{s}) = i2\pi s_2 e^{-2\pi sz} \hat{T}_o(\underline{s}) \tag{B-16}$$

$$\hat{\Gamma}_{z}(\underline{s}) = -2\pi s e^{-2\pi sz} \hat{T}_o(\underline{s}) \tag{B-17}$$

The functions multiplying $\hat{T}_o$ in Eqs. B-15, B-16, and B-17 are called transfer functions from anomalous surface potential to the east, north, and vertical components of the gravity disturbance vector at height z, respectively.

Table B-1 presents the transfer functions from anomalous surface potential to all other quantities of interest in this report. This table is identical to Table 2.1-1 and is repeated here for convenience. To obtain the Fourier transform of any of the quantities in the first column of the table, the Fourier transform of the anomalous potential at the surface is multiplied by the transfer function given in the last column of the table. All transfer functions in Table B-1 are obtained by replacing the upward continuation operation and partial derivatives with respect to the east, north, and vertical coordinates by products of $e^{-2\pi sz}$, $i2\pi s_1$, $i2\pi s_2$ and $-2\pi s$, respectively.

Table B-1 can also be used to relate any pair of quantities listed in the first column. For example, the frequency-domain relation equivalent to the formula of Vening Meinesz expressing the north component of the deflection of the vertical in terms of the gravity anomaly is obtained by combining the transfer functions in the third and fourth rows of the table to yield

## TABLE B-1

### TRANSFER FUNCTIONS FROM ANOMALOUS SURFACE POTENTIAL

| QUANTITY | SYMBOL | RELATION TO ANOMALOUS POTENTIAL | TRANSFER FUNCTION FROM ANOMALOUS SURFACE POTENTIAL* |
|---|---|---|---|
| Anomalous Potential at Height z | $T_z$ | $T_z$ | $e^{-2\pi sz}$ |
| Undulation of the Geoid | N | $T_o/g_o$ | $1/g_o$ |
| East Deflection of the Vertical | $\eta$ | $-(\partial T_o/\partial x_1)/g_o$ | $-i2\pi s_1/g_o$ |
| North Deflection of the Vertical | $\xi$ | $-(\partial T_o/\partial x_2)/g_o$ | $-i2\pi s_2/g_o$ |
| Gravity Anomaly | $\Delta g$ | $-(\partial T_z/\partial z)|_{z=0} - 2T_o/R$ | $2\pi s - 2/R$ |
| East Component of the Gravity Disturbance Vector at Height z | $\Gamma_{x_1}$ | $\partial T_z/\partial x_1$ | $i2\pi s_1 e^{-2\pi sz}$ |
| North Component of the Gravity Disturbance Vector at Height z | $\Gamma_{x_2}$ | $\partial T_z/\partial x_2$ | $i2\pi s_2 e^{-2\pi sz}$ |
| Vertical Component of the Gravity Disturbance Vector at Height z | $\Gamma_z$ | $\partial T_z/\partial z$ | $-2\pi s e^{-2\pi sz}$ |
| Gravity Disturbance at Height z | $\delta g$ | $-\partial T_z/\partial z$ | $2\pi s e^{-2\pi sz}$ |
| East-East Gradient at Height z | $\Gamma_{x_1 x_1}$ | $\partial^2 T_z/\partial x_1^2$ | $-4\pi^2 s_1^2 e^{-2\pi sz}$ |
| North-North Gradient at Height z | $\Gamma_{x_2 x_2}$ | $\partial^2 T_z/\partial x_2^2$ | $-4\pi^2 s_2^2 e^{-2\pi sz}$ |
| Vertical-Vertical Gradient at Height z | $\Gamma_{zz}$ | $\partial^2 T_z/\partial z^2$ | $4\pi^2 s^2 e^{-2\pi sz}$ |
| East-North Gradient at Height z | $\Gamma_{x_1 x_2}$ | $\partial^2 T_z/\partial x_1 \partial x_2$ | $-4\pi^2 s_1 s_2 e^{-2\pi sz}$ |
| East-Vertical Gradient at Height z | $\Gamma_{x_1 z}$ | $\partial^2 T_z/\partial x_1 \partial z$ | $-i4\pi^2 s_1 s e^{-2\pi sz}$ |
| North-Vertical Gradient at Height z | $\Gamma_{x_2 z}$ | $\partial^2 T_z/\partial x_2 \partial z$ | $-i4\pi^2 s_2 s e^{-2\pi sz}$ |

$*s = (s_1^2 + s_2^2)^{1/2}$

$$\hat{\xi}(\underline{s}) = \frac{-i2\pi s_2/g_o}{2\pi s - 2/R} \Delta g(\underline{s}) \qquad (B-18)$$

where $g_o$ is the mean value of gravity over the earth ($g_o \simeq$ 9.798 m/sec$^2$).

## B.2    STATISTICAL RELATIONS

A zero-mean vector random process defined on the plane, $\underline{w}(\underline{x}) = [w_1(\underline{x}),\ldots, w_p(\underline{x})]^T$, is said to be stationary if its covariance matrix, $R_{\underline{w},\underline{w}}$, does not depend on the specific values of the coordinates but, instead, is a function of the differences between coordinates; i.e.,[*]

$$R_{\underline{w},\underline{w}} (\underline{x}'-\underline{x}'') = E[\underline{w}(\underline{x}') \; \underline{w}^T(\underline{x}'')] \qquad \text{(B-19)}$$

The k-th diagonal element of $R_{\underline{w},\underline{w}}$ is called the auto-covariance of the (scalar) random process corresponding to the k-th component of $\underline{w}$. The (k,j) element of $R_{\underline{w},\underline{w}}$, with $k{\neq}j$, is called the crosscovariance between the k-th and the j-th components of $\underline{w}$. Autocovariances are real, even and positive semi-definite functions (Ref. 3). Crosscovariances are real functions but, in general, they are neither even nor positive semidefinite. The (k,j) and (j,k) crosscovariances are identical except for a sign difference in their arguments.

Similarly, let $\underline{u}(\underline{x}) = [u_1(\underline{x}),\ldots, u_q(\underline{x})]^T$ be another stationary vector random process on the plane. The processes $\underline{w}$ and $\underline{u}$ are said to be jointly stationary if their covariance matrix, $R_{\underline{w},\underline{u}}$, is a function of the coordinate differences; i.e.,

$$R_{\underline{w},\underline{u}} (\underline{x}'-\underline{x}'') = E[\underline{w}(\underline{x}') \; \underline{u}^T(\underline{x}'')] \qquad \text{(B-20)}$$

The Fourier transform of $R_{\underline{w},\underline{w}}$ is the spectral density matrix of the process $\underline{w}$. It is customary to denote spectral densities by the Greek letter $\Phi$. Thus, $\Phi_{\underline{w},\underline{w}} = \hat{R}_{\underline{w},\underline{w}}$ and

---

[*]E stands for the mathematical expectation operator.

B-7

$$\Phi_{\underline{w},\underline{w}}(\underline{s}) = \iint\limits_{-\infty}^{\infty} R_{\underline{w},\underline{w}}(\underline{x})e^{-i2\pi<\underline{x},\underline{s}>} dx_1 dx_2 \qquad (B-21)$$

The diagonal and off-diagonal elements of $\Phi_{\underline{w},\underline{w}}$ are called power spectral and cross-spectral densities, respectively. A power spectral density (PSD) is the average density of the random measure corresponding to the spectral representation of a process (Ref. 3). Physically, a PSD can be interpreted as the average distribution of the energy density in a process as a function of frequency. Power spectral densities are real and non-negative functions. A cross-spectral density is a complex-valued function that indicates the magnitude and phase of the correlation between the spectral representations of two processes. The (k,j) and (j,k) cross-spectral densities are complex conjugates of one another.

The cross-spectral density matrix of two jointly stationary processes $\underline{w}$ and $\underline{u}$, $\Phi_{\underline{w},\underline{u}}$, is defined in a similar fashion. It is the Fourier transform of their covariance, i.e.,

$$\Phi_{\underline{w},\underline{u}}(\underline{s}) = \iint\limits_{-\infty}^{\infty} R_{\underline{w},\underline{u}}(\underline{x})e^{-i2\pi<\underline{x},\underline{s}>} dx_1 dx_2 \qquad (B-22)$$

Let $y_1(\underline{x})$ be a stationary scalar random process. It is shown in Appendix A that if $y_2(\underline{x})$ is related to $y_1(\underline{x})$ by a transfer function $Q(\underline{s})$ in the form

$$\hat{y}_2(s) = Q(\underline{s})\ \hat{y}_1(\underline{s}) \qquad (B-23)$$

then the processes $y_1$ and $y_2$ are jointly stationary. Moreover, their power spectral densities are related by

$$\Phi_{y_2,y_2} = |Q|^2 \, \Phi_{y_1,y_1} \qquad (B\text{-}24)$$

and the cross-spectral density, $\Phi_{y_2,y_1}$, is given in terms of the PSD of $y_1$ by

$$\Phi_{y_2,y_1} = Q^2 \, \Phi_{y_1,y_1} \qquad (B\text{-}25)$$

These facts entail a result of fundamental importance when the gravity field on the surface of the earth is seen as a realization of a stationary random process. Since all quantities in Table B-1 are interrelated by transfer functions, the specification of the covariance function for any one of them determines completely the covariance structure for all of them.

It is convenient to develop a matrix notation for expressing the cross-spectral density matrix of the vector processes $\underline{w}$ and $\underline{u}$ in terms of the PSD of the anomalous surface potential when the components of $\underline{w}$ and $\underline{u}$ are any field-related quantities. To this end, suppose that the k-th component of $\underline{w}$ is related to the anomalous surface potential, $T_o$, through a transfer function, $G_k(\underline{s})$; i.e.,

$$\hat{\underline{w}} = \underline{G} \, \hat{T}_o \qquad (B\text{-}26)$$

with

$$\underline{G}(\underline{s}) = \begin{pmatrix} G_1(\underline{s}) \\ G_2(\underline{s}) \\ \vdots \\ G_p(\underline{s}) \end{pmatrix} \qquad (B\text{-}27)$$

B-9

and that the j-th component of $\underline{u}$ is related to $T_o$ through the transfer function $F_j(\underline{s})$; i.e.,

$$\hat{\underline{u}} = \underline{F}\, \hat{T}_o \tag{B-28}$$

with

$$\underline{F}(\underline{s}) = \begin{pmatrix} F_1(\underline{s}) \\ F_2(\underline{s}) \\ \vdots \\ F_q(\underline{s}) \end{pmatrix} \tag{B-29}$$

Consider the $(k,j)$ entry, $\Phi_{w_k,u_j}$, of the cross-spectral density matrix $\Phi_{\underline{w},\underline{u}}$. From Eqs. B-26 and B-28, the transfer function from $u_j$ to $w_k$ is seen to be the quotient $G_k/F_j$. Thus, from Eq. B-25,

$$\Phi_{w_k,u_j} = (G_k/F_j)\, \Phi_{u_j,u_j} \tag{B-30}$$

However, from Eqs. B-24 and B-28,

$$\Phi_{u_j,u_j} = |F_j|^2\, \Phi_{T_o,T_o} \tag{B-31}$$

Therefore, combining the last two equations,

$$\Phi_{w_k,u_j} = G_k\, F_j^*\, \Phi_{T_o,T_o} \tag{B-32}$$

It then follows that the cross-spectral density matrix, $\Phi_{\underline{w},\underline{u}}$, is given in terms of the PSD of the anomalous surface potential, $\Phi_{T_o,T_o}$, by

$$\Phi_{\underline{w},\underline{u}} = \underline{G} \ \underline{F}^* \ \Phi_{T_o,T_o} \qquad \text{(B-33)}$$

with the vector transfer functions $\underline{G}$ and $\underline{F}$ as in Eqs. B-27 and B-29.

A similar expression can be obtained for the spectral density matrix $\Phi_{\underline{w},\underline{w}}$. Replacing $\underline{u}$ by $\underline{w}$ and $\underline{F}$ by $\underline{G}$ in Eq. B-33, the following equation is obtained:

$$\Phi_{\underline{w},\underline{w}} = \underline{G} \ \underline{G}^* \ \Phi_{T_o,T_o} \qquad \text{(B-34)}$$

## APPENDIX C
## MULTISENSOR SURVEY ERROR ANALYSIS

This appendix presents a complete derivation of the expressions for the statistics of the errors in the estimates of the gravity field obtained from multisensor data. The problem of determining the errors in the estimation of the gravity field from multisensor survey data can be formulated in the following manner: It is desired to characterize the differences (estimation errors)

$$\delta \underline{w}(\underline{x}) = \underline{w}(\underline{x}) - \underline{w}^O(\underline{x}) \qquad (C-1)$$

between the true values of the process $\underline{w}(x)$, and the best estimates[*] $\underline{w}^O(\underline{x})$. The components of $\underline{w}$ are any collection of field-related quantities.

The estimates, $\underline{w}^O(\underline{x})$, are obtained from q data sets

$$\Xi_k = \{\psi_k(\underline{x}) | \underline{x} \varepsilon M_k\} \quad ; \quad k=1,2,\ldots,q \qquad (C-2)$$

corresponding to the measurements that constitute the survey. The set $\Xi_k$ represents a collection of scalar measurements of a single data type in which all measurement points form a rectangular grid $M_k$. Later in this appendix (Section C.3), these q data sets will be classified according to the grids on which measurements are taken. As a result, n classes will be formed, where each class contains $q_\beta$ sets of measurements on a common grid $M_\beta(\beta=1,2,\ldots,n)$. Within the flat-earth approximation, the

---

[*]In the mean-square sense.

measurement geometry adapts to the description given above in most practical cases. Examples of data sets, $\Xi_k$, are

- Gravimeter readings collected at equal time intervals by a survey ship traveling at constant speed along equally spaced East-West tracks

- Satellite radar-altimeter data on equally spaced ground tracks. One set, $\Xi_{k_1}$, for ascending passes; another set, $\Xi_{k_2}$, for descending passes.

The measurements, $\psi_k$, represent a scalar linear combination of field-related quantities, $u_k$, corrupted by additive noise, $E_k$; i.e.,

$$\psi_k(\underline{x}) = u_k(\underline{x}) + E_k(\underline{x}); \quad \underline{x}\varepsilon M_k \qquad (C-3)$$

The measurement errors, $E_k$, k=1,2,...,q, are taken to be stationary gaussian processes independent of the gravity field.

Formulas for the spectral density matrix of the residuals, $\delta\underline{w}$, are derived in this appendix. The analysis begins in Section C.1 by considering the idealized case where the survey data consist of a collection of continuous measurements (i.e., $M_k = \{\underline{x}|\underline{x} = (x_1,x_2)^T, -\infty < x_1 < \infty, -\infty < x_2 < \infty\}$). A general formula for the spectral density matrix of the errors in the estimates obtained with the optimal linear processor is derived. In Section C.2 the effects of sampling the field at regular intervals are examined and a relation between the spectral density of the field and a sampled version of it is obtained. This relation is used in Section C.3 to obtain a practical solution to the general problem formulated above. The solution is exact when all sets $M_k$ agree with each other and is approximate when this is not the case. In Section C.4, the results are specialized to the

situation in which estimates are sought of <u>spatially averaged</u> <u>quantities</u>. <u>Section C.5</u> discusses the evaluation of the average errors in a map of gravity estimates obtained from multisensor data.


## C.1    CONTINUOUS MEASUREMENTS CASE

Consider the case in which the data consist of a vector of measurements $\underline{\psi} = (\psi_1, \psi_2, \ldots, \psi_p)^T$ at every point $\underline{x} = (x_1, x_2)^T$. The values of $\underline{\psi}$ are measurements of a vector of field-related quantities, $\underline{u}$, corrupted by stationary additive noise, $\underline{\zeta}$; i.e.,

$$\underline{\psi}(\underline{x}) = \underline{u}(\underline{x}) + \underline{\zeta}(\underline{x}) \qquad (C-4)$$

The noise process $\underline{\zeta}$ is taken to be independent of the gravity field.

It is desired to determine

- The best linear estimator, $\underline{w}^o$, of another vector of field-related quantities $\underline{w} = (w_1, w_2, \ldots, w_q)^T$ jointly stationary with $\underline{u}(\underline{x})$

- The spectral density matrix of the estimation errors, $\delta\underline{w} = \underline{w} - \underline{w}^o$.

These questions are dealt with in Subsections C.1.1 and C.1.2, respectively.

### C.1.1    Derivation of the Optimal Smoother

By a linear estimator it is meant that the estimate of $\underline{w}$ at any point $\underline{x}_o$ must be given by a suitable linear combination

of the data $\underline{\psi}(\underline{x})$. The most general linear estimator has the form

$$\underline{w}^o(\underline{x}_o) = \iint\limits_{-\infty}^{\infty} K(\underline{x}_o,\underline{x})\, \underline{\psi}\,(\underline{x})\, dx_1 dx_2 \qquad (C\text{-}5)$$

where K is a q×p matrix function of $\underline{x}_o$ and $\underline{x}$ to be determined.

The kernel $K(\underline{x}_o,\underline{x})$ indicates how to weight the measurement $\underline{\psi}$ at the point $\underline{x}$ in evaluating the estimate of $\underline{w}$ at the point $\underline{x}_o$. Because all the processes involved are stationary, for any $\underline{x}'$ the statistical relation between the measurement $\underline{\psi}$ at the point $\underline{x}+\underline{x}'$ and the field $\underline{w}$ at the point $\underline{x}_o+\underline{x}'$ is identical to the relation between the measurement at $\underline{x}$ and the field at $\underline{x}_o$. Therefore, in evaluating the estimate of $\underline{w}$ at $\underline{x}_o+\underline{x}'$ the measurement at the point $\underline{x}+\underline{x}'$ must be weighted in the same manner in which $\underline{\psi}(\underline{x})$ is weighted in the computation of $\underline{w}^o(\underline{x}_o)$. Thus for all $\underline{x}'$,

$$K(\underline{x}_o+\underline{x}',\ \underline{x}+\underline{x}') = K\,(\underline{x}_o,\underline{x}) \qquad (C\text{-}6)$$

This relation implies that K only depends on the difference between its arguments. Consequently, Eq. C-5 can be written as a convolution; i.e.,

$$\underline{w}^o(\underline{x}_o) = \iint\limits_{-\infty}^{\infty} K(\underline{x}_o-\underline{x})\, \underline{\psi}(\underline{x})\, dx_1 dx_2 \qquad (C\text{-}7)$$

The error or residual in the estimate of $w_n$ (the n-th component of $\underline{w}$) at the point $\underline{x}_o$ is

$$\delta w_n(\underline{x}_o) = w_n(\underline{x}_o) - w_n^o(\underline{x}_o) \qquad (C\text{-}8)$$

It is desired to determine K so that the variance of $\delta w_n(\underline{x}_o)$ is minimized for every $n=1,2,\ldots,q$.

Let $H_\psi$ be the Hilbert space generated[*] by the random variables $\psi_j(\underline{x})$ for $j=1,2,\ldots,p$ (Ref. 3). Since $w_n^o(\underline{x}_o)$ is a linear combination of the data, for each $\underline{x}_o$, $w_n^o(\underline{x}_o)\varepsilon H_\psi$. The scalar product between two elements of $H_\psi$, $y_1$ and $y_2$, is defined as the expectation of their product; i.e.,

$$\langle y_1,y_2\rangle = E(y_1 y_2) \tag{C-9}$$

and the norm of each element is its standard deviation:

$$||y|| = (\langle y,y\rangle)^{1/2} = [E(y^2)]^{1/2} \tag{C-10}$$

The Hilbert space $H_\psi$ is a linear subspace of the Hilbert space H generated by the components of the processes $\underline{w}$ and $\underline{\psi}$. From the Projection Theorem for Hilbert spaces (Ref. 20), it follows that the element, $w_n^o(\underline{x}_o)$, of $H_\psi$ that minimizes the standard deviation of the difference $\delta w_n(\underline{x}_o) = w_n(\underline{x}_o) - w_n^o(\underline{x}_o)$ is the projection of $w_n(\underline{x}_o)$ on the subspace $H_\psi$ and that the difference $\delta w_n(\underline{x}_o)$ must be orthogonal to every element of $H_\psi$; i.e.,

$$E[\delta w_n(\underline{x}_o)y] = 0 \tag{C-11}$$

for every $y\varepsilon H_\psi$. Since $H_\psi$ is generated by the components of $\underline{\psi}$, Eq. C-11 is equivalent to

---

[*]The space $H_\psi$ contains all linear combinations of $\underline{\psi}(\underline{x})$ and all limits in the mean-square sense of Cauchy sequences of such linear combinations.

$$E[\delta w_n(\underline{x}_o) \, \psi_j(\underline{x})] = 0 \qquad (C-12)$$

for all $\underline{x}$ and all $j=1,2,\ldots,p$.

From Eq. C-7,

$$w_n^o(\underline{x}_o) = \sum_{\ell=1}^{p} \iint_{-\infty}^{\infty} k_{n\ell}(\underline{x}_o - \underline{x}') \, \psi_\ell(\underline{x}') \, dx_1' dx_2' \qquad (C-13)$$

where $k_{n\ell}$ is the component of K in row n and column $\ell$. Therefore, the expectation on the left in Eq. C-12 can be written as

$$E[\delta w_n(\underline{x}_o)\psi_j(\underline{x})] = E[w_n(\underline{x}_o)\psi_j(\underline{x})]$$

$$- \sum_{\ell=1}^{p} \iint_{-\infty}^{\infty} k_{n\ell} \, (\underline{x}_o - \underline{x}') \, E[\psi_\ell(\underline{x}')\psi_j(\underline{x})] \, dx_1' dx_2'$$

$$(C-14)$$

Consequently, from Eq. C-12

$$R_{w_n, \psi_j}(\underline{x}_o - \underline{x}) = \sum_{\ell=1}^{p} \iint_{-\infty}^{\infty} k_{n\ell} \, (\underline{x}_o - \underline{x}') \, R_{\psi_\ell, \psi_j}(\underline{x}' - \underline{x}) \, dx_1' dx_2'$$

$$(C-15)$$

Setting $\underline{r} = \underline{x}_o - \underline{x}$ and changing integration variables through the transformation $\underline{r}' = \underline{x}' - \underline{x}$, Eq. C-15 becomes

$$R_{w_n, \psi_j}(\underline{r}) = \sum_{\ell=1}^{p} \iint_{-\infty}^{\infty} k_{n\ell} \, (\underline{r} - \underline{r}') \, R_{\psi_\ell, \psi_j}(\underline{r}') \, dr_1' dr_2'$$

$$(C-16)$$

Since Eq. C-12 is valid for all $\underline{x}$, Eq. C-16 is valid for all choices of $\underline{r}$. In matrix form, Eq. C-16 becomes a matrix convolution equation

$$R_{\underline{w},\underline{\psi}}(\underline{r}) = \iint_{-\infty}^{\infty} K(\underline{r}-\underline{r}') \, R_{\underline{\psi},\underline{\psi}}(\underline{r}') \, dr_1' dr_2' \qquad \text{(C-17)}$$

Taking Fourier transforms on both sides of Eq. C-17 results in

$$\Phi_{\underline{w},\underline{\psi}}(\underline{s}) = \hat{K}(\underline{s}) \, \Phi_{\underline{\psi},\underline{\psi}}(s) \qquad \text{(C-18)}$$

Therefore, the Fourier transform of the weighting matrix K in Eq. C-7 is found to be given in terms of the spectral densities of the measurement and estimated processes by

$$\hat{K} = \Phi_{\underline{w},\underline{\psi}} \Phi_{\underline{\psi},\underline{\psi}}^{-1} \qquad \text{(C-19)}$$

Condition C-11 is equivalent to the statement that the estimation errors are uncorrelated with the measurements. Any two gaussian random variables which are uncorrelated are also independent (Ref. 21). Thus, if $\underline{w}$ and $\underline{\psi}$ are gaussian, the errors in the best linear estimates are not only uncorrelated with the measurements but independent of them as well.

In the preceding derivation, the attention has been restricted to the class of linear estimators. Next, it is shown that no nonlinear estimator can further reduce the variance of the estimation errors if the process to be estimated and the measurements are gaussian.

Let $\underline{w}'(\underline{x}_0)$ be any nonlinear estimator of $\underline{w}(\underline{x}_0)$ [i.e., $\underline{w}'(\underline{x}_0)$ is some nonlinear functional of the data $\underline{\psi}(\underline{x})$] and let $\delta w_n'$ be the error associated with the use of $\underline{w}'$ in the estimation of the n-th component of $\underline{w}$:

C-7

$$\delta w_n'(\underline{x}_o) = w_n(\underline{x}_o) - w_n'(\underline{x}_o) \qquad \text{(C-20)}$$

The variance of $\delta w_n'(x_o)$,

$$\sigma^2_{\delta w_n', \delta w_n'} = E \{ [w_n(x_o) - w_n'(x_o)]^2 \} \qquad \text{(C-21)}$$

can be written as

$$\sigma^2_{\delta w_n', \delta w_n'} = E \left\{ [(w_n(\underline{x}_o) - w_n^o(\underline{x}_o)) + (w_n^o(\underline{x}_o) - w_n'(\underline{x}_o))]^2 \right\}$$

$$\text{(C-22)}$$

where $w_n^o$ is the best linear estimator of $w_n$. From Eq. C-8,

$$\sigma^2_{\delta w_n', \delta w_n'} = E \left\{ [\delta w_n(\underline{x}_o) + (w_n^o(\underline{x}_o) - w_n'(\underline{x}_o))]^2 \right\} \qquad \text{(C-23)}$$

The expression on the right-hand side of Eq. C-23 is the vari-
ance of the sum of two random variables. The first random
variable is $\delta w_n(x_o)$, the error in the linear estimates. The
second random variable is the difference between the linear
and nonlinear estimates of $w_n(\underline{x}_o)$. Since both estimators are
functions of the data $\underline{\psi}$ and since $\underline{\psi}$ and $\delta w_n$ are independent
because of the gaussian assumption, it follows that

$$\sigma^2_{\delta w_n', \delta w_n'} = \sigma^2_{\delta w_n, \delta w_n} + E \left\{ [w_n^o(\underline{x}_o) - w_n'(\underline{x}_o)]^2 \right\} \qquad \text{(C-24)}$$

Therefore,

$$\sigma^2_{\delta w_n', \delta w_n'} \geq \sigma^2_{\delta w_n, \delta w_n} \qquad \text{(C-25)}$$

proving the assertion.

C-8

## C.1.2 Spectral Density Matrix of the Residuals

The covariance matrix of the residuals is defined as

$$E[\delta \underline{w}(\underline{x}_o) \delta \underline{w}^T(\underline{x}_o - \underline{x})] = E\left\{[\underline{w}(\underline{x}_o) - \underline{w}^o(\underline{x}_o)] \ [\underline{w}(\underline{x}_o - \underline{x}) - \underline{w}^o(\underline{x}_o - \underline{x})]^T\right\} \tag{C-26}$$

which can be rewritten as

$$E[\delta \underline{w}(\underline{x}_o) \delta \underline{w}^T(\underline{x}_o - \underline{x})] = E\left\{[\underline{w}(\underline{x}_o) - \underline{w}^o(\underline{x}_o)] \ \underline{w}^T(\underline{x}_o - \underline{x})\right\}$$

$$- E\left\{[\underline{w}(\underline{x}_o) - \underline{w}^o(\underline{x}_o)] \ [(\underline{w}^o(\underline{x}_o - \underline{x})]^T\right\} \tag{C-27}$$

The second term on the right is $E\{\delta \underline{w}(x_o) \ [\underline{w}^o(\underline{x}_o - \underline{x})]^T\}$. Since $\underline{w}^o$ is a function of the measurements $\psi$, Eq. C-11 implies that this expectation is zero. Hence, Eq. C-27 reduces to

$$E[\delta w(\underline{x}_o) \delta w^T(\underline{x}_o - \underline{x})] = E[\underline{w}(\underline{x}_o) \underline{w}^T(\underline{x}_o - \underline{x})] - E[\underline{w}^o(\underline{x}_o) \underline{w}^T(\underline{x}_o - \underline{x})] \tag{C-28}$$

But

$$E[\underline{w}(\underline{x}_o) \underline{w}^T(\underline{x}_o - \underline{x})] = R_{\underline{w},\underline{w}}(\underline{x}) \tag{C-29}$$

and, from Eq. C-7

$$E[\underline{w}^o(\underline{x}_o) \underline{w}^T(\underline{x}_o - \underline{x})] = \iint\limits_{-\infty}^{\infty} K(\underline{x}_o, \underline{x}') \ E[\underline{\psi}(\underline{x}') \underline{w}^t(\underline{x}_o - \underline{x})] \ dx_1' dx_2'$$

$$= \iint\limits_{-\infty}^{\infty} K(\underline{x}_o - \underline{x}') R_{\underline{\psi},\underline{w}}[\underline{x} - (\underline{x}_o - \underline{x}')] \ dx_1' dx_2' \tag{C-30}$$

Changing integration variables, Eq. C-30 becomes

$$E[\underline{w}^o(\underline{x}_o)\underline{w}^T(\underline{x}_o-\underline{x})] = \int\!\!\int_{-\infty}^{\infty} K(\underline{x}'') \, R_{\underline{\psi},\underline{w}}(\underline{x}-\underline{x}'')dx_1''dx_2'' \quad (C-31)$$

Therefore, from Eqs. C-28, C-29 and C-31,

$$E[\delta\underline{w}(\underline{x}_o)\delta\underline{w}^T(\underline{x}_o-\underline{x})] = R_{\underline{w},\underline{w}}(\underline{x}) - \int\!\!\int_{-\infty}^{\infty} K(\underline{x}'')R_{\underline{\psi},\underline{w}}(\underline{x}-\underline{x}'')dx_1''dx_2''$$

$$(C-32)$$

which shows that the residuals are stationary and that their covariance $R_{\delta\underline{w},\delta\underline{w}}(\underline{x})$ is given by the expression in the right-hand side of Eq. C-32.

The spectral density matrix of the residuals is the Fourier transform of their covariance. From Eq. C-32,

$$\Phi_{\delta\underline{w},\delta\underline{w}}(\underline{s}) = \Phi_{\underline{w},\underline{w}}(\underline{s}) - \hat{K}(\underline{s}) \, \Phi_{\underline{\psi},\underline{w}}(\underline{s}) \quad (C-33)$$

Since,

$$\Phi_{\underline{\psi},\underline{w}}(\underline{s}) = \Phi_{\underline{w},\underline{\psi}}^{*}(\underline{s}) \quad (C-34)$$

it follows from Eq. C-19 that

$$\Phi_{\delta\underline{w},\delta\underline{w}} = \Phi_{\underline{w},\underline{w}} - \Phi_{\underline{w},\underline{\psi}} \, \Phi_{\underline{\psi},\underline{\psi}}^{-1} \, \Phi_{\underline{w},\underline{\psi}}^{*} \quad (C-35)$$

This expression for the spectral density of the residuals is considerably simplified when the independence of the measurements noise from the gravity field is incorporated into the formulation, and when the relations among the quantities being measured and estimated are taken into account. From the

C-10

independence of the field and measurement errors and from Eq. C-4 it follows that

$$\Phi_{\underline{w},\underline{\psi}} = \Phi_{\underline{w},\underline{u}} \qquad (C-36)$$

and

$$\Phi_{\underline{\psi},\underline{\psi}} = \Phi_{\underline{u},\underline{u}} + \Phi_{\underline{\zeta},\underline{\zeta}} \qquad (C-37)$$

Therefore, Eq. C-35 can be written as

$$\Phi_{\delta\underline{w},\delta\underline{w}} = \Phi_{\underline{w},\underline{w}} - \Phi_{\underline{w},\underline{u}}[\Phi_{\underline{u},\underline{u}} + \Phi_{\underline{\zeta},\underline{\zeta}}]^{-1} \Phi_{\underline{w},\underline{u}}^{*} \qquad (C-38)$$

Now, the estimated variables, $\underline{w}$, and the measured quantities, $\underline{u}$, are related to the anomalous surface potential, $T_o$, through vector transfer functions $\underline{G}$ and $\underline{F}$ as in Eqs. B-26 and B-28. Consequently, from Eqs. B-33 and B-34,

$$\Phi_{\underline{w},\underline{w}} = \underline{G}\ \underline{G}^{*}\ \Phi_{T_o,T_o} \qquad (C-39)$$

$$\Phi_{\underline{u},\underline{u}} = \underline{F}\ \underline{F}^{*}\ \Phi_{T_o,T_o} \qquad (C-40)$$

and

$$\Phi_{\underline{w},\underline{u}} = \underline{G}\ \underline{F}^{*}\ \Phi_{T_o,T_o} \qquad (C-41)$$

Combining Eqs. C-38 through C-41 the following expression for the spectral density matrix of the residuals is obtained:

$$\Phi_{\delta\underline{w},\delta\underline{w}} = \underline{G}\ \underline{G}^{*}\ \{[1 - \underline{F}^{*}\ (\underline{F}\ \underline{F}^{*} + \Phi_{\underline{\zeta},\underline{\zeta}}/\Phi_{T_o,T_o})^{-1}\ \underline{F}]\Phi_{T_o,T_o}\}$$

$$(C-42)$$

C-11

There are two important observations with respect to the above formula. First, for any multisensor survey the vector transfer functions $\underline{F}$ and $\underline{G}$ are readily obtained from the entries in Table 2.1-1. Thus, to evaluate the spectral density of the residuals, one need only specify the spectral density matrix of the measurement errors, $\Phi_{\underline{\zeta},\underline{\zeta}}$, and the (a priori) PSD of the surface anomalous potential, $\Phi_{T_o,T_o}$. Second, the spectral density of the residuals given by Eq. C-42 has the same form as the expression for the (a priori) spectral density of the estimated quantities, $\Phi_{\underline{w},\underline{w}}$, as given by Eq. C-39; i.e., $\underline{G}\,\underline{G}^{*}$ multiplied by a scalar. Thus, the residuals bear the same relations among themselves as the original quantities do. Moreover, if $\underline{w} = T_o$, then $\underline{G} = 1$ and, therefore, the PSD of the residual anomalous surface potential, $\Phi_{\delta T_o,\delta T_o}$, is given by the expression in braces in Eq. C-42; i.e.,

$$\Phi_{\delta T_o,\delta T_o} = [1 - \underline{F}^{*}(\underline{F}\,\underline{F}^{*} + \Phi_{\underline{\zeta},\underline{\zeta}}/\Phi_{T_o,T_o})^{-1}\underline{F}]\Phi_{T_o,T_o}\}$$

(C-43)

and Eq. C-42 can be written as

$$\Phi_{\delta\underline{w},\delta\underline{w}} = \underline{G}\,\underline{G}^{*}\,\Phi_{\delta T_o,\delta T_o}$$

(C-44)

An equivalent expression for the matrix inverse in Eq. C-43 can be obtained from the Matrix Inversion Lemma (Ref. 22)

$$(\underline{F}\ \underline{F}^* + \Phi_{\underline{\zeta},\underline{\zeta}}/\Phi_{T_o,T_o})^{-1} = (\Phi_{\underline{\zeta},\underline{\zeta}}/\Phi_{T_o,T_o})^{-1}$$

$$- \frac{(\Phi_{\underline{\zeta},\underline{\zeta}}/\Phi_{T_o,T_o})^{-1}\underline{F}\ \underline{F}^*(\Phi_{\underline{\zeta},\underline{\zeta}}/\Phi_{T_o,T_o})^{-1}}{1 + \underline{F}^*(\Phi_{\underline{\zeta},\underline{\zeta}}/\Phi_{T_o,T_o})^{-1}\underline{F}}$$

$$(C-45)$$

Replacing the matrix inverse in Eq. C-43 by the right-hand side of Eq. C-34 and simplifying the resulting expression yields the following formula for the PSD of the residual surface anomalous potential:

$$\Phi_{\delta T_o,\delta T_o} = \frac{1}{\underline{F}^* \Phi_{\underline{\zeta},\underline{\zeta}}^{-1} \underline{F} + 1/\Phi_{T_o,T_o}} \qquad (C-46)$$

## C.2    SAMPLING EFFECTS - ALIASING

In order to analyze the general problem formulated in the introduction to this appendix, it is necessary to account for the fact that the survey data consist of a discrete collection of measurements. The purpose of this section is to obtain expressions for the spectral and cross-spectral density matrices of sampled (aliased) versions of vector processes in terms of those corresponding to the underlying continuous processes. The problem is more precisely formulated below.

Denote by $\underline{U}$ the discrete vector random process corresponding to having sampled the process $\underline{u}$ on a rectangular grid $M_o$. The axes of the grid $M_o$ are parallel to the axes of a primed reference frame obtained by rotating the original (East-North) frame by an angle $\theta$ as shown in Fig. C-1. The

C-13
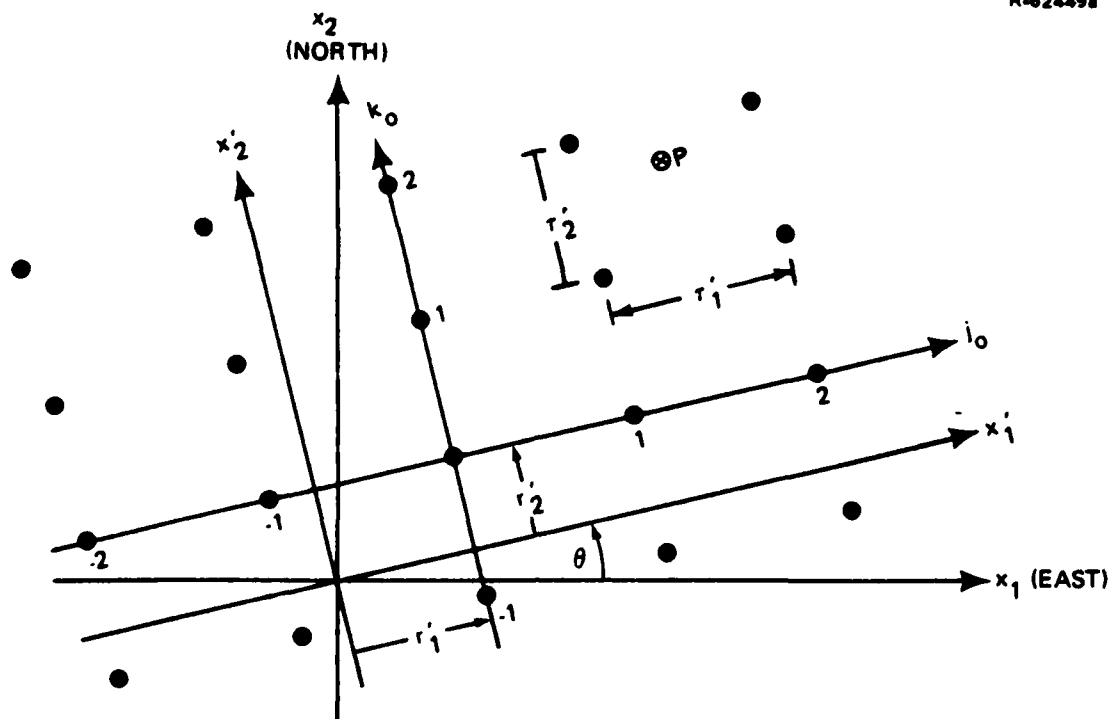
Figure C-1

Figure C-1    Relations Among the Grid $M_o$, $(j_o,k_o)$,
the Primed Coordinates, $(x_1',x_2')$, and
the Original Frame $(x_1,x_2)$

spacings of the grid $M_o$ are $\tau_1'$ and $\tau_2'$ in the $x_1'$ and $x_2'$ direc-
tions, respectively. The grid points are represented by pairs
of integers $(j_o, k_o)$. The origin of the grid $(j_o=0, k_o=0)$ is
located at the point $\underline{r}' = (r_1',r_2')^T$ of the primed frame.

Similarly, let $\underline{W}$ represent the process $\underline{w}$ sampled on a
grid $M_c$ parallel to and having the same grid spacings as the
grid $M_o$ but displaced from it by a vector $\underline{c}' = (c_1',c_2')^T$ as
measured in the primed reference frame (see Fig. C-2).

Two formulas are sought. <u>First</u>, an expression for
the cross-spectral density matrix of the processes $\underline{W}$ and $\underline{U}$ in
terms of the cross-spectral density matrix of $\underline{w}$ and $\underline{u}$. <u>Second</u>,
an expression for the spectral density matrix of $\underline{U}$ in terms of
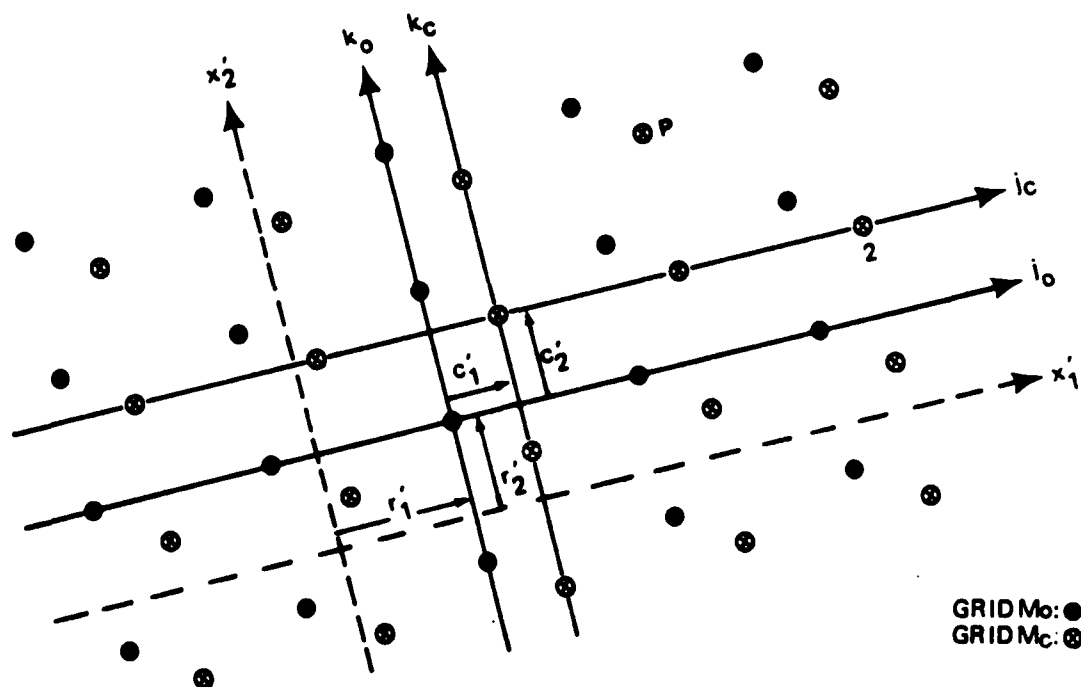
Figure C-2    Relations Among the Grid $M_c$, $(j_c, k_c)$
the Grid $M_o$, $(j_o, k_o)$, and the Primed
Coordinates $(x_1', x_2')$

the spectral density of $\underline{u}$. The second formula follows from
the first by taking the process $\underline{w}$ equal to the process $\underline{u}$ and
by setting the displacement vector between the two grids equal
to zero. Thus, the analysis below is restricted to the first
formula.

Some definitions are in order. Let $\underline{w}'$, $\underline{u}'$ and $R'_{\underline{w},\underline{u}}$
denote the values of the processes $\underline{w}$ and $\underline{u}$ and their covariance
as functions of the primed coordinates. Similarly, let $\Phi'_{\underline{w},\underline{u}}$
denote the cross-spectral density matrix of $\underline{w}$ and $\underline{u}$ as a func-
tion of frequencies measured in the $x_1'$ and $x_2'$ directions.

In the primed reference frame the physical position,
$\underline{x}_o'$, of a point with coordinates $\underline{\Omega} = (j,k)^T$ in the grid $M_o$ is

$$\underline{x}'_o = \underline{r}' + J\underline{\Omega} \qquad\qquad (C-47)$$

where J is the spacing matrix given by

$$J = \begin{pmatrix} \tau'_1 & 0 \\ 0 & \tau'_2 \end{pmatrix} \qquad\qquad (C-48)$$

while the same integer coordinates in the grid $M_c$ represent the point

$$x'_c = \underline{c}' + \underline{r}' + J\underline{\Omega} \qquad\qquad (C-49)$$

Defining the rotation matrix

$$\theta = \begin{pmatrix} \cos\theta & -\sin\theta \\ \sin\theta & \cos\theta \end{pmatrix} \qquad\qquad (C-50)$$

the corresponding points in the original (east-north) frame are

$$\underline{x}_o = \underline{r} + \theta J\underline{\Omega} \qquad\qquad (C-51)$$

$$\underline{x}_c = \underline{c} + \underline{r} + \theta J\underline{\Omega} \qquad\qquad (C-52)$$

with $\underline{r} = \theta\underline{r}'$ and $\underline{c} = \theta\underline{c}'$ representing the position of the origin of the grid $M_o$ and the shift between the two grids as measured in the original frame.

The processes $\underline{U}$ and $\underline{W}$ are given in terms of $\underline{u}'$ and $\underline{w}'$ by

$$\underline{U}(\underline{\Omega}) = \underline{u}'(\underline{r}' + J\underline{\Omega}) \qquad\qquad (C-53)$$

$$\underline{W}(\underline{\Omega}) = \underline{w}'(\underline{c}' + \underline{r}' + J\underline{\Omega}) \qquad (C\text{-}54)$$

Their covariance,

$$R_{\underline{W},\underline{U}}(\underline{\Omega}) = E[\underline{W}(\underline{\Omega}''+\underline{\Omega})\ \underline{U}^T(\underline{\Omega}'')] \qquad (C\text{-}55)$$

is easily related to the covariance of the continuous processes $\underline{w}$ and $\underline{u}$ through the use of Eqs. C-53 and C-54. The result is

$$R_{\underline{W},\underline{U}}(\underline{\Omega}) = R'_{\underline{w},\underline{u}}(\underline{c}'+J\underline{\Omega}) \qquad (C\text{-}56)$$

Spectral and cross-spectral densities of discrete processes are denoted by a superimposed tilde. The cross-spectral density matrix of $\underline{W}$ and $\underline{U}$ is defined as the finite Fourier transform of their covariance (see Appendix A, Eq. A-62)[*]

$$\tilde{\Phi}'_{\underline{W},\underline{U}}(\underline{s}') = \Delta(J) \sum_{\underline{\Omega}} R_{\underline{W},\underline{U}}(\underline{\Omega})\ e^{-i2\pi<J\underline{\Omega},\underline{s}'>} \qquad (C\text{-}57)$$

where $\underline{s}' = (s'_1, s'_2)^T$ with $s'_1$ and $s'_2$ frequencies measured in the $x'_1$ and $x'_2$ directions, respectively. The relation inverse to Eq. C-57 is

$$R_{\underline{W},\underline{U}}(\underline{\Omega}) = \int_{-\bar{s}'_2}^{\bar{s}'_2} \int_{-\bar{s}'_1}^{\bar{s}'_1} \tilde{\Phi}'_{\underline{W},\underline{U}}(\underline{s}')\ e^{i2\pi<J\underline{\Omega},\underline{s}'>}\ ds'_1 ds'_2 \qquad (C\text{-}58)$$

---

[*] $\displaystyle\sum_{\underline{\Omega}}$ stands for $\displaystyle\sum_{j=-\infty}^{\infty} \sum_{k=-\infty}^{\infty}$ and $\Delta(J)$ is the determinant of $J$.

C-17

where

$$\bar{s}_1' = 1/2\tau_1'$$

$$\bar{s}_2' = 1/2\tau_2' \tag{C-59}$$

are the Nyquist frequencies in the $x_1'$ and $x_2'$ directions, respectively. The cross-spectral density matrix $\tilde{\phi}_{\underline{W},\underline{U}}'$ is periodic in $s_1'$ and $s_2'$ with periods $2\bar{s}_1'$ and $2\bar{s}_2'$, respectively.

The relation between the cross-spectral density matrices of the sampled and continuous processes is derived next. The basic idea of the derivation given below is to use the equality between the crosscovariances of the continuous and discrete processes given by Eq. C-56 to obtain a relation between the spectral densities.

For the discrete processes $\underline{W}$ and $\underline{U}$, the covariance matrix $R_{\underline{W},\underline{U}}$ is given in terms of the spectral density $\tilde{\phi}_{\underline{W},\underline{U}}'$ in Eq. C-58. For the continuous processes $\underline{w}$ and $\underline{u}$, the analogous relation is

$$R_{\underline{w},\underline{u}}'(\underline{x}') = \iint\limits_{-\infty}^{\infty} \phi_{\underline{w},\underline{u}}'(\underline{s}')\ e^{i2\pi<\underline{x}',\underline{s}'>}\ ds_1'ds_2' \tag{C-60}$$

It then follows by combining Eqs. C-56 and C-60 that

$$R_{\underline{W},\underline{U}}(\underline{\Omega}) = \iint\limits_{-\infty}^{\infty} \phi_{\underline{w},\underline{u}}'(\underline{s}')\ e^{i2\pi<\underline{c}'+J\underline{\Omega},\underline{s}'>}\ ds_1'ds_2' \tag{C-61}$$

Thus, two different expressions for $R_{\underline{W},\underline{U}}(\underline{\Omega})$ have been obtained. In Eq. C-58 the integration is over a finite range, while in Eq. C-61 the integration takes place over the whole

C-18

plane. To compare integrands it is necessary to reduce both integrations to the same domain. The integral in Eq. C-61 can be written as an infinite sum of integrals over equal-size rectangles as

$$
R_{\underline{W},\underline{U}}(\underline{\Omega}) = \sum_{\underline{\Lambda}} \int_{(2m-1)\bar{s}_2'}^{(2m+1)\bar{s}_2'} \int_{(2\ell-1)\bar{s}_1'}^{(2\ell+1)\bar{s}_1'} \phi'_{\underline{w},\underline{u}}(\underline{s}')
$$

$$
\times \; e^{i2\pi<\underline{c}'+J\underline{\Omega},\underline{s}'>} \; ds_1' ds_2' \qquad (C-62)
$$

where $\underline{\Lambda} = (\ell,m)^T$. Changing integration variables in such a way that all integrals are taken over the domain $[-\bar{s}_1', \bar{s}_1'] \times [-\bar{s}_2', \bar{s}_2']$, Eq. C-62 reduces to

$$
R_{\underline{W},\underline{U}}(\underline{\Omega}) = \int_{-\bar{s}_2'}^{\bar{s}_2'} \int_{-\bar{s}_1'}^{\bar{s}_1'} \sum_{\underline{\Lambda}} \phi'_{\underline{w},\underline{u}}(\underline{s}'+J^{-1}\underline{\Lambda})
$$

$$
\times \; e^{i2\pi<\underline{c}'+J\underline{\Omega},\underline{s}'+J^{-1}\underline{\Lambda}>} \; ds_1' ds_2' \qquad (C-63)
$$

The complex exponential can be rewritten as

$$
e^{i2\pi<\underline{c}'+J\underline{\Omega},\underline{s}'+J^{-1}\underline{\Lambda}>} = e^{i2\pi<\underline{c}',\underline{s}'+J^{-1}\underline{\Lambda}>} \times e^{i2\pi<J\underline{\Omega},\underline{s}'>}
$$

$$
(C-64)
$$

because the scalar product $<J\underline{\Omega},J^{-1}\underline{\Lambda}> = <\underline{\Omega},\underline{\Lambda}>$ is an integer. Thus, Eq. C-63 becomes

$$R_{\underline{W},\underline{U}}(\underline{\Omega}) = \int\limits_{-\bar{s}_2'}^{\bar{s}_2'} \int\limits_{-\bar{s}_1'}^{\bar{s}_1'} [\sum_{\underline{\Lambda}} \Phi_{\underline{w},\underline{u}}'(\underline{s}'+J^{-1}\underline{\Lambda})\ e^{i2\pi<\underline{c}',\underline{s}'+J^{-1}\underline{\Lambda}>}]$$

$$\times\ e^{i2\pi<J\underline{\Omega},\underline{s}'>}\ ds_1'ds_2' \tag{C-65}$$

From the uniqueness of the Fourier transformation, it follows by comparing Eqs. C-58 and C-65 that the desired relation between the cross-spectral densities of the discrete and continuous processes is

$$\tilde{\Phi}_{\underline{W},\underline{U}}'(\underline{s}') = \sum_{\underline{\Lambda}} \Phi_{\underline{w},\underline{u}}'(\underline{s}'+J^{-1}\underline{\Lambda})\ e^{i2\pi<\underline{c}',\underline{s}'+J^{-1}\underline{\Lambda}>} \tag{C-66}$$

where $\underline{\Lambda} = (\ell,m)^T$ as before.

The corresponding relations for the spectral density matrices of processes $\underline{W}$ and $\underline{U}$ are:

$$\tilde{\Phi}_{\underline{W},\underline{W}}'(\underline{s}') = \sum_{\underline{\Lambda}} \Phi_{\underline{w},\underline{w}}'(\underline{s}'+J^{-1}\underline{\Lambda}) \tag{C-67}$$

$$\tilde{\Phi}_{\underline{U},\underline{U}}'(\underline{s}') = \sum_{\underline{\Lambda}} \Phi_{\underline{u},\underline{u}}'(\underline{s}'+J^{-1}\underline{\Lambda}) \tag{C-68}$$

Since the processes $\underline{w}$ and $\underline{u}$ are interconnected by transfer functions which have simple representations when the frequencies are measured in the east and north directions, it is convenient to rewrite Eqs. C-66 through C-68 in the original reference frame. These equations become

$$\tilde{\Phi}_{\underline{W},\underline{U}}(\underline{s}) = \sum_{\underline{\Lambda}} \Phi_{\underline{w},\underline{u}}(\underline{s}+\theta J^{-1}\underline{\Lambda})\ e^{i2\pi<\underline{c},\underline{s}+\theta J^{-1}\underline{\Lambda}>} \tag{C-69}$$

$$\tilde{\Phi}_{\underline{W},\underline{W}}(\underline{s}) = \sum_{\underline{\Lambda}} \Phi_{\underline{w},\underline{w}}(\underline{s}+\theta J^{-1}\underline{\Lambda}) \qquad\qquad (C-70)$$

$$\tilde{\Phi}_{\underline{U},\underline{U}}(\underline{s}) = \sum_{\underline{\Lambda}} \Phi_{\underline{u},\underline{u}}(\underline{s}+\theta J^{-1}\underline{\Lambda}) \qquad\qquad (C-71)$$

where $\theta$ is the rotation matrix of Eq. C-50 and $\underline{c} = \theta\underline{c}'$ is the displacement from the origin of the grid $M_O$ to the origin of the grid $M_S$ as measured in the east-north frame.

A graphical interpretation of Eqs. C-70 and C-71 is given in Fig. C-3. The spectral density matrix of a sampled version of a process, e.g., $\tilde{\Phi}_{\underline{U},\underline{U}}$, is obtained as an infinite superposition of matrix functions of frequency, $\Phi_{\underline{u},\underline{u}}(\underline{s}+\theta J^{-1}\underline{\Lambda})$, each of which corresponds to the spectral density matrix of the underlying continuous process translated to the points $\underline{s} = -\theta J^{-1}\underline{\Lambda}$ in the frequency domain. These points are marked with solid dots in Fig. C-3. It is clear from Fig. C-3 that the spectrum $\tilde{\Phi}_{\underline{U},\underline{U}}$ is periodic and that one period is represented by any of the rectangles in Fig. C-3.

A similar interpretation applies to the cross-spectral density matrix of the processes $\underline{U}$ and $\underline{W}$ (Eq. C-66). In this case the cross-spectral density, $\Phi_{\underline{w},\underline{u}}(\underline{s})$, is multiplied by the factor $e^{i2\pi<\underline{c},\underline{s}>}$ which accounts for the displacement between the grids $M_O$ and $M_c$. The product function is then translated to each of the points $\underline{s} = -\theta J^{-1}\underline{\Lambda}$. The sum of all these functions yields $\tilde{\Phi}_{\underline{W},\underline{U}}$.

## C.3 AVERAGE SPECTRAL DENSITY OF POST-SURVEY GRAVITY RESIDUALS

A general solution to the problem of characterizing the errors in the estimates of gravity from multisensor survey
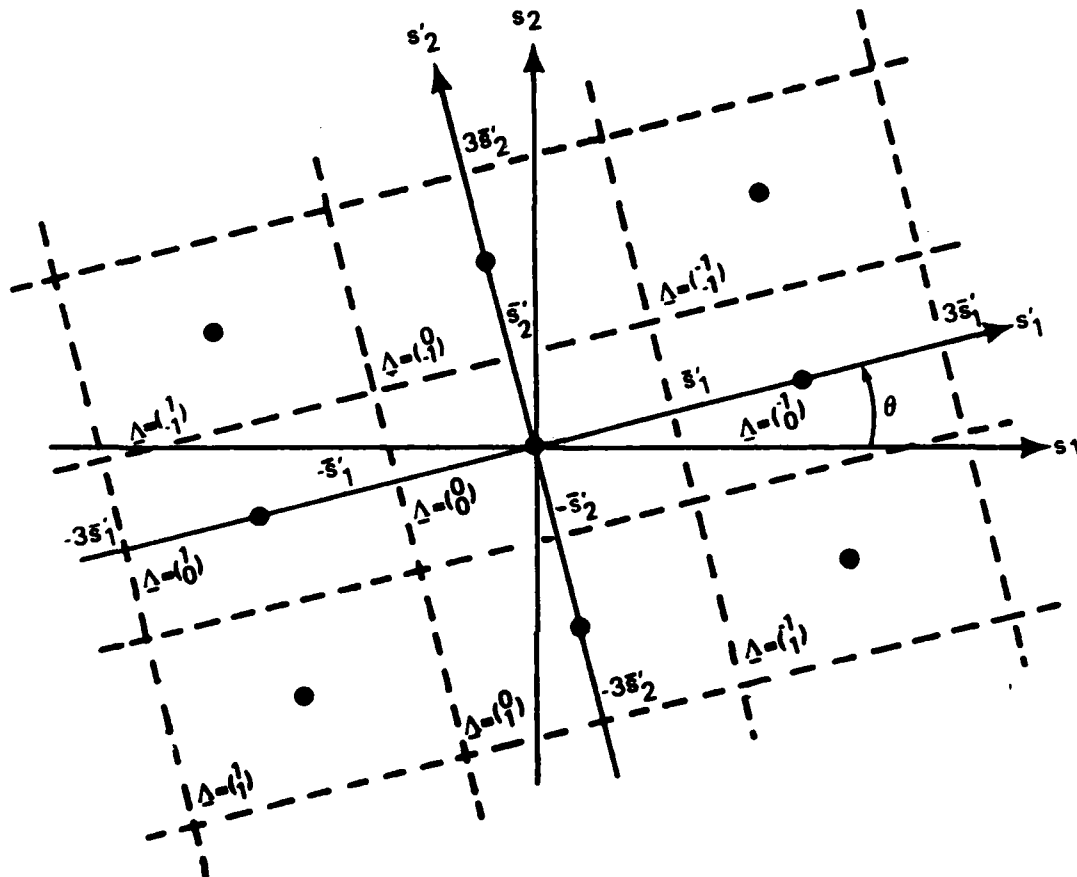
Figure C-3    Graphical Interpretation of the Effects
of Sampling on the Spectrum

data is given in this subsection.  An exact solution is found
for the case in which data from various sensors are collected
on a common rectangular grid $M_o$.  A modification of the result-
ing expression for the average spectral density of the post-
survey gravity residuals yields an approximate formula for the
case in which the data lie on different grids.

Consider the situation in which the survey data con-
sist of a measurement vector, $\underline{\psi}(\underline{x}_o)$, at every point $\underline{x}_o$ on a

grid $M_o$ as in Fig. C-1. As before, the measurements correspond to a vector of field-related quantities, $\underline{u}$, corrupted by additive noise, $\underline{E}$; i.e.,

$$\underline{\psi}(\underline{x}_o) = \underline{u}(\underline{x}_o) + \underline{E}(\underline{x}_o); \quad x_o \varepsilon M_o \tag{C-72}$$

Let the primed coordinate system be defined as in the last subsection, and let $\underline{\psi}$ and $\underline{U}$ be the measurements and the measured quantities as functions of the integer coordinates $\underline{\Omega}_o = (j_o, k_o)^T$ of the grid $M_o$.

Since the process to be estimated, $\underline{w}$, and the measurements, $\underline{\psi}$, are gaussian, the best estimate of $\underline{w}$, $\underline{w}^o$, at an arbitrary point $\underline{x}_a$ is given by some (unknown) linear combination of the data, i.e.,

$$\underline{w}^o(\underline{x}_a) = \sum_{\underline{\Omega}_o} \bar{K}(\underline{x}_a, \underline{\Omega}_o) \, \underline{\psi} \, (\underline{\Omega}_o) \tag{C-73}$$

In contrast with the continuous measurements case analyzed in Section C.1 of this appendix, the weighting coefficients $\bar{K}(\underline{x}_a, \underline{\Omega}_o)$ depend on the specific position of the point $\underline{x}_a$ on the plane. In fact, the estimation errors

$$\delta\underline{w}(\underline{x}_a) = \underline{w}(\underline{x}_a) - \underline{w}^o(\underline{x}_a) \tag{C-74}$$

are no longer stationary. This is not surprising since, intuitively, it is to be expected that the rms value of the estimation error gets smaller as the point $\underline{x}_a$ moves closer to a point on the measurement grid $M_o$. However, if another point, $\underline{x}_b$, is chosen so that it occupies the same relative position with respect to the grid points as $\underline{x}_a$ does (see Fig. C-4), then the weights $\bar{K}(\underline{x}_b, \underline{\Omega}_o)$ are identical to the weights $\bar{K}(\underline{x}_a, \underline{\Omega}_o)$ except for a shift in the integer coordinates. Thus, if $\underline{W}$

C-23
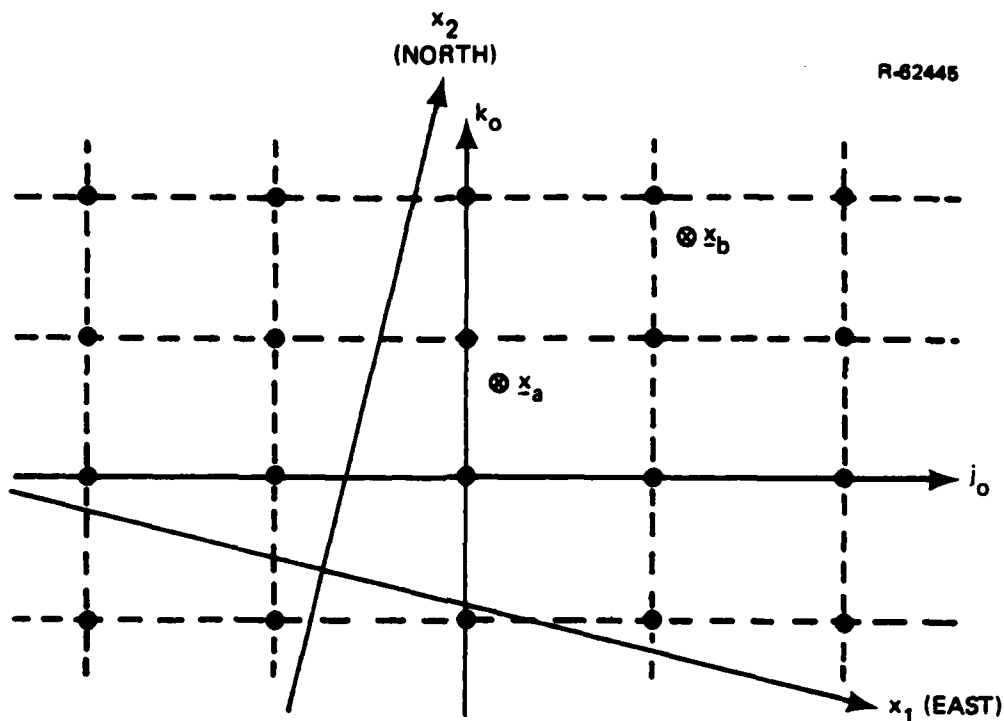
Figure C-4    Points Having the Same Relative Position
with Respect to the Grid $M_o$

represents the values of the field $\underline{w}$ as a function of the inte-
ger coordinates of a grid $M_c$ parallel to the grid $M_o$ as in
Section C.2 (see Fig. C-2), the best estimates of $\underline{W}$ can be
written as

$$\underline{W}^o(\underline{\Omega}_c) = \sum_{\underline{\Omega}_o} K(\underline{\Omega}_c - \underline{\Omega}_o) \ \underline{\psi}(\underline{\Omega}_o) \qquad (C-75)$$

where $\underline{\Omega}_c = (j_c, k_c)^T$ is an arbitrary point of the grid $M_c$ and
where $K(\underline{\Omega})$ is to be determined.

A derivation parallel to that of Section C.1 shows
that formulas similar to those obtained in the continuous meas-
urements case apply to the discrete case as well.  In particu-
lar, the errors in the estimates

$$\delta \underline{W}(\underline{\Omega}_c) = \underline{W}(\underline{\Omega}_c) - \underline{W}^o(\underline{\Omega}_c) \qquad (C-76)$$

are stationary and have an unnormalized spectral density matrix given by

$$\tilde{\Phi}'_{\delta \underline{W}, \delta \underline{W}}(\underline{c}', \underline{s}') = \tilde{\Phi}'_{\underline{W}, \underline{W}} - \tilde{\Phi}'_{\underline{W}, \underline{U}} [\tilde{\Phi}'_{\underline{U}, \underline{U}} + \tilde{\Phi}'_{\underline{E}, \underline{E}}]^{-1} (\tilde{\Phi}'_{\underline{W}, \underline{U}})^{*}$$

$$(C-77)$$

where all the spectral densities in the right-hand side are functions of $\underline{s}'$ but, in addition, $\tilde{\Phi}'_{\underline{W}, \underline{U}}$ depends on the displacement $\underline{c}'$ between the grids $M_o$ and $M_c$ as indicated by Eq. C-66.

It is of interest to determine the spectral density of the errors on a grid $M$ whose absolute position on the plane is chosen at random. It suffices to consider displacement vectors $\underline{c}' = (c_1', c_2')^T$ for which $0 \leq c_1' < \tau_1'$ and $0 \leq c_2' < \tau_2'$. The spectral density of the errors in a random grid is

$$\tilde{\Phi}'_{\delta \underline{W}, \delta \underline{W}}(\underline{s}') = \frac{1}{\Delta(J)} \int_0^{\tau_2'} \int_0^{\tau_1'} \tilde{\Phi}'_{\delta \underline{W}, \delta \underline{W}}(\underline{c}', \underline{s}') dc_1' dc_2' \qquad (C-78)$$

where $\Delta(J) = \tau_1' \tau_2'$ is the determinant of the matrix $J$ of Eq. C-48.

All spectral densities appearing on the right-hand side of Eq. C-77 are independent of $\underline{c}'$ except for the cross-spectral density matrix $\tilde{\Phi}'_{\underline{W}, \underline{U}}$. Substituting the right-hand side of Eq. C-77 for $\Phi'_{\delta \underline{W}, \delta \underline{W}}(\underline{c}', \underline{s}')$ in Eq. C-78 and using Eq. C-66 results in

C-25

$$\widetilde{\Phi}'_{\delta\underline{W},\delta\underline{W}}(\underline{s}') = \widetilde{\Phi}'_{\underline{W},\underline{W}}(\underline{s}')$$

$$- \sum_{\underline{\Lambda}} \sum_{\underline{\Lambda}'} \{\Phi'_{\underline{w},\underline{u}}(\underline{s}'+J^{-1}\underline{\Lambda})[\widetilde{\Phi}'_{\underline{U},\underline{U}}(\underline{s}')+\widetilde{\Phi}'_{\underline{E},\underline{E}}(\underline{s}')]^{-1}[\Phi'_{\underline{w},\underline{u}}(\underline{s}'+J^{-1}\underline{\Lambda}')]^{*}$$

$$\times \frac{1}{\Delta(J)} \int_{0}^{\tau'_2} \int_{0}^{\tau'_1} e^{i2\pi<\underline{c}',J^{-1}(\underline{\Lambda}-\underline{\Lambda}')>} dc'_1 dc'_2\}$$

$$\text{(C-79)}$$

However,

$$\frac{1}{\Delta(J)} \int_{0}^{\tau'_1} \int_{0}^{\tau'_2} e^{i2\pi<\underline{c}',J^{-1}(\underline{\Lambda}-\underline{\Lambda}')>} dc'_1 dc'_2 = \begin{cases} 0 & \text{if } \underline{\Lambda} \neq \underline{\Lambda}' \\ 1 & \text{if } \underline{\Lambda} = \underline{\Lambda}' \end{cases}$$

$$\text{(C-80)}$$

Therefore Eq. C-79 becomes

$$\widetilde{\Phi}'_{\delta\underline{W},\delta\underline{W}}(\underline{s}') = \widetilde{\Phi}'_{\underline{W},\underline{W}}(\underline{s}')$$

$$- \sum_{\underline{\Lambda}} \Phi'_{\underline{w},\underline{u}}(\underline{s}'+J^{-1}\underline{\Lambda})[\widetilde{\Phi}'_{\underline{U},\underline{U}}(\underline{s}')+\widetilde{\Phi}'_{\underline{E},\underline{E}}(\underline{s}')^{-1}[\Phi'_{\underline{w},\underline{u}}(\underline{s}'+J^{-1}\underline{\Lambda})]^{*}$$

$$\text{(C-81)}$$

Replacing $\widetilde{\Phi}'_{\underline{W},\underline{W}}(\underline{s}')$ by the series on the right-hand side of Eq. C-67, Eq. C-81 becomes

$$\widetilde{\Phi}'_{\delta\underline{W},\delta\underline{W}}(\underline{s}') = \sum_{\underline{\Lambda}} \{\Phi'_{\underline{w},\underline{w}}(\underline{s}'+J^{-1}\underline{\Lambda})$$

$$- \Phi'_{\underline{w},\underline{u}}(\underline{s}'+J^{-1}\underline{\Lambda})[\widetilde{\Phi}'_{\underline{U},\underline{U}}(\underline{s}')+\widetilde{\Phi}'_{\underline{E},\underline{E}}(\underline{s}')]^{-1}[\widetilde{\Phi}'_{\underline{w},\underline{u}}(\underline{s}'+J^{-1}\underline{\Lambda})]^{*}\}$$

$$\text{(C-82)}$$

C-26

But $\tilde{\Phi}'_{\underline{U},\underline{U}}$ and $\tilde{\Phi}'_{\underline{E},\underline{E}}$ are periodic; i.e., for all $\underline{\Lambda}$

$$\tilde{\Phi}'_{\underline{U},\underline{U}}(\underline{s}') = \tilde{\Phi}'_{\underline{U},\underline{U}}(\underline{s}'+J^{-1}\underline{\Lambda}) \qquad (C-83)$$

$$\tilde{\Phi}'_{\underline{E},\underline{E}}(\underline{s}') = \tilde{\Phi}'_{\underline{E},\underline{E}}(\underline{s}'+J^{-1}\underline{\Lambda}) \qquad (C-84)$$

Consequently, the spectral density of the errors in a random grid can be written as

$$\tilde{\Phi}'_{\delta\underline{w},\delta\underline{w}}(\underline{s}') = \sum_{\underline{\Lambda}} \Phi'_{\delta\underline{w},\delta\underline{w}}(\underline{s}'+J^{-1}\underline{\Lambda}) \qquad (C-85)$$

where

$$\Phi'_{\delta\underline{w},\delta\underline{w}} = \Phi'_{\underline{w},\underline{w}} - \Phi'_{\underline{w},\underline{u}} [\tilde{\Phi}'_{\underline{U},\underline{U}} + \tilde{\Phi}'_{\underline{E},\underline{E}}]^{-1}(\Phi'_{\underline{w},\underline{u}})^{*} \qquad (C-86)$$

Equation C-85 admits an important interpretation. The errors in a random grid can be viewed as the sampled version of a continuous process, $\delta\underline{w}$, whose spectral density is given by Eq. C-86. The spectral density $\Phi'_{\delta\underline{w},\delta\underline{w}}$ represents the errors in a map of gravity estimates when no information is given concerning the position of the measurements from which the map was obtained. Even if this information is provided it is shown in Section C.5 that rms values of the residuals computed on the basis of Eq. C-86 yield the average rms of the map errors.

The function $\Phi'_{\delta\underline{w},\delta\underline{w}}$ given by Eq. C-86 is called the average spectral density of the residuals. The spectral densities in Eq. C-86 are all functions of frequencies, $\underline{s}'$, measured in the directions of the primed axes. However, Eq. C-86 is invariant under rotations. Thus, when all spectral densities

C-27

are expressed as functions of frequencies in the east and north directions, $\underline{s}$, the relation remains unchanged; i.e.,

$$\Phi_{\delta\underline{w},\delta\underline{w}} = \Phi_{\underline{w},\underline{w}} - \Phi_{\underline{w},\underline{u}} \, [\tilde{\Phi}_{\underline{U},\underline{U}} + \tilde{\Phi}_{\underline{E},\underline{E}}]^{-1} \, \Phi^*_{\underline{w},\underline{u}} \qquad (C-87)$$

Using Eq. C-71, the average spectral density of the residuals can be written as

$$\Phi_{\delta\underline{w},\delta\underline{w}} = \Phi_{\underline{w},\underline{w}} - \Phi_{\underline{w},\underline{u}} [\Phi_{\underline{u},\underline{u}} + \tilde{\Phi}_{\underline{E},\underline{E}} + \Phi_{\underline{a},\underline{a}}]^{-1} \, \Phi^*_{\underline{w},\underline{u}} \qquad (C-88)$$

where

$$\Phi_{\underline{a},\underline{a}}(\underline{s}) = \sum_{\underline{\Lambda}\neq\underline{0}} \Phi_{\underline{u},\underline{u}}(\underline{s}+\theta J^{-1}\underline{\Lambda}) \qquad (C-89)$$

Equation C-88 can be compared with the analogous expression for the spectral density of the residuals in the continuous measurements case given by Eq. C-38. The two expressions are identical when the spectral density of the errors in the continuous measurements case, $\Phi_{\underline{\zeta},\underline{\zeta}}$ is identified with

$$\Phi_{\underline{\zeta},\underline{\zeta}} = \tilde{\Phi}_{\underline{E},\underline{E}} + \Phi_{\underline{a},\underline{a}} \qquad (C-90)$$

The first term on the right-hand side of Eq. C-90 is the finite Fourier transform of the covariance of the measurement errors. The second term corresponds to the sampling (or aliasing) errors. Note that the aliasing errors appear in Eq. C-88 as if they were independent of the gravity field. This, of course, is not the case. The aliasing errors at frequency $\underline{s}$ are correlated with the components of the field at frequency $\underline{s}+\theta J^{-1}\underline{\Lambda}$ for any integer vector $\underline{\Lambda} \neq 0$. However, the aliasing errors at frequency s are, indeed, independent of the components of the field at that same frequency. This is because the spectral representation of a process is an orthogonal decomposition. Thus, spectral components at different frequencies

are independent (Ref. 3). Since the aliasing errors at frequency $\underline{s}$ arise from field components at frequencies $\underline{s}+\Theta J^{-1}\underline{\Lambda}$ for $\underline{\Lambda} \neq 0$, aliasing errors and field components at the same frequency are independent.

Following the same procedure used in Section C.1, it can be shown that the average spectral density of the residuals is given by

$$\Phi_{\delta\underline{w},\delta\underline{w}} = \underline{G}\ \underline{G}^* \ \Phi_{\delta T_o,\delta T_o} \tag{C-91}$$

where $\underline{G}$ is the vector transfer function from anomalous surface potential to the quantities being estimated and where

$$\Phi_{\delta T_o,\delta T_o} = \frac{1}{\underline{F}^* \Phi_{\underline{\zeta},\underline{\zeta}}^{-1} \underline{F} + 1/\Phi_{T_o,T_o}} \tag{C-92}$$

is the average power spectral density of the residual anomalous surface potential. In Eq. C-92, $\underline{F}$ is the vector transfer function from anomalous surface potential to the quantities being measured and $\Phi_{T_o,T_o}$ is the a priori PSD of the anomalous surface potential.

The error spectral density matrix $\Phi_{\underline{\zeta},\underline{\zeta}}$ in Eq. C-92 is given by Eq. C-90. The aliasing contribution, $\Phi_{\underline{a},\underline{a}}$, is expressed in terms of the spectral density of the measured quantities in Eq. C-89. For computational purposes, it is convenient to obtain it directly from the spectral density of the unsurveyed anomalous surface potential, $\Phi_{T_o,T_o}$. Using the results of Appendix B.2, Eq. C-89 can be rewritten as

$$\Phi_{\underline{a},\underline{a}}(\underline{s}) = \sum_{\underline{\Lambda} \neq \underline{0}} \underline{F}(\underline{s}+\Theta J^{-1}\underline{\Lambda})\ \underline{F}^*(\underline{s}+\Theta J^{-1}\underline{\Lambda})\ \Phi_{T_o,T_o}(\underline{s}+\Theta J^{-1}\underline{\Lambda})$$

$$\tag{C-93}$$

A discussion on practical approximations to this infinite sum is given next.

Equation C-93 indicates that the value of the spectral density matrix of the aliasing errors at frequency $\underline{s}$ is given by the infinite superposition of translates of the function $\underline{F}\ \underline{F}^{*}\phi_{T_0,T_0}$ to the points $\underline{s}_0 = -\theta J^{-1}\underline{\Lambda}$ with $\underline{\Lambda}\neq 0$. This is illustrated in Fig. C-5. The function $\underline{F}\ \underline{F}^{*}\phi_{T_0,T_0}$ is centered at each of the points denoted by a solid dot in Fig. C-5. The aliasing spectral density at any point $\underline{s}$ is obtained by adding up the contribution of all the translates of $\underline{F}\ \underline{F}^{*}\phi_{T_0,T_0}$.
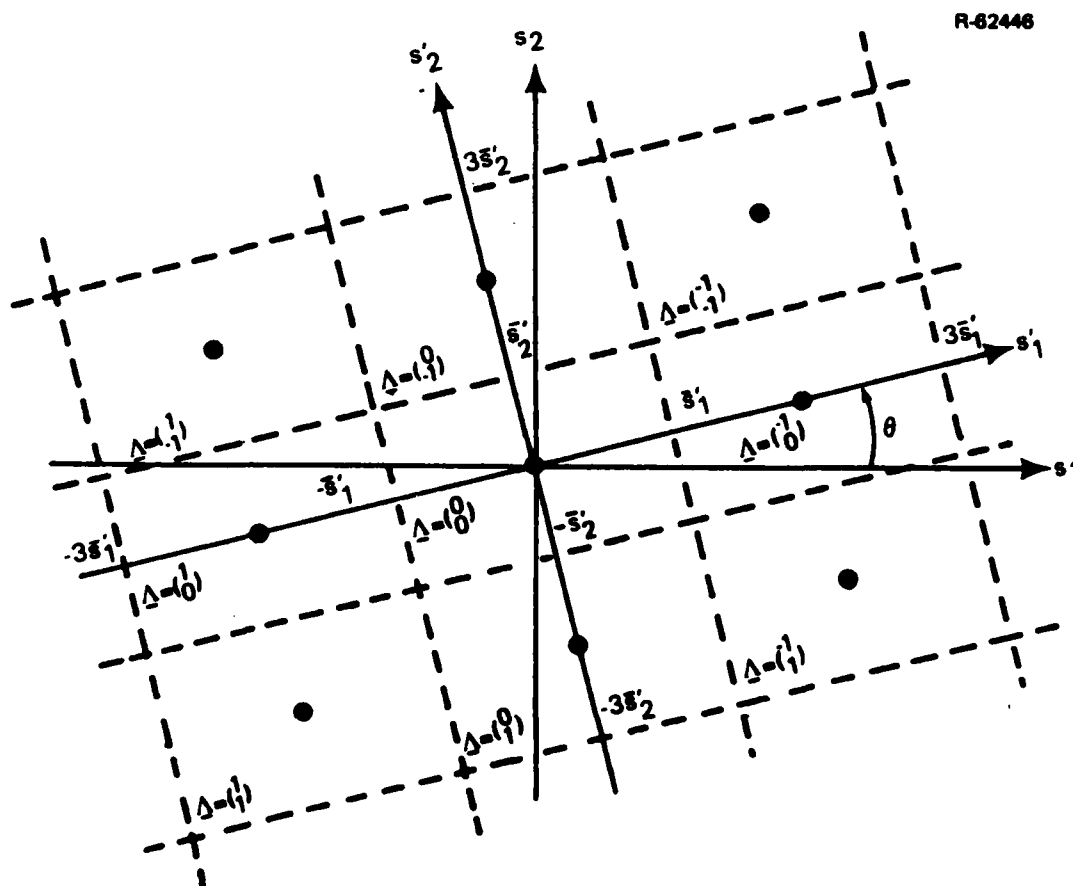


Figure C-5    Graphical Interpretation of Eq. C-93

Since gravity spectra exhibit a rapid decay with frequency (Refs. 23 and 24), in all practical situations there is negligible contribution to the sum in Eq. C-93 from terms other than the translates of $\underline{F}\ \underline{F}^*\Phi_{T_o,T_o}$ which are centered at those points $\underline{s}_o = -\theta J^{-1}\underline{\Lambda}$ in the neighborhood of $\underline{s}$. In general, it is sufficient to take the terms corresponding to the values of $\underline{\Lambda}$ belonging to the set

$$Q = \{\underline{\Lambda}|\underline{\Lambda} \neq \underline{0},\ ||\underline{s}+\theta J^{-1}\underline{\Lambda}|| < 2\ ||\underline{\bar{s}}'||\} \tag{C-94}$$

where $\underline{\bar{s}}' = (\bar{s}'_1,\bar{s}'_2)$ is the vector of Nyquist frequencies associated with the survey. Thus, Eq. C-93 is approximated by

$$\Phi_{\underline{a},\underline{a}}(\underline{s}) = \sum_{\underline{\Lambda}\varepsilon Q} \underline{F}(\underline{s}+\theta J^{-1}\underline{\Lambda})\ \underline{F}^*(\underline{s}+\theta J^{-1}\underline{\Lambda})\ \Phi_{T_o,T_o}(\underline{s}+\theta J^{-1}\underline{\Lambda})$$

$$\tag{C-95}$$

with Q as in Eq. C-94.

Note that the product $\underline{F}\ \underline{F}^*$ of the vector transfer functions from surface anomalous potential to measured quantities appearing in Eq. C-95 yields a full matrix. Thus, the spectral density matrix of the aliasing errors, $\Phi_{\underline{a},\underline{a}}$, is full. This means that aliasing errors in different measurement types are correlated. The reason for this correlation is that these errors originate from the same spectral components of the field. This point is of importance in the approximation of the expression for the residual spectral density given below for the case in which different data types lie on nonoverlapping grids. This case is considered next. An expression similar to Eq. C-92 for the residual anomalous surface potential is given and the approximations involved in its use are discussed.

First, classify the q data sets $\Xi_k$ of Eq. C-2 according to the grids on which measurements are taken. In this fashion, n classes result, each of them containing $q_\beta$ sets of measurements on a common grid $M_\beta$ with $\beta = 1, 2, \ldots, n$. Thus,

$$q = q_1 + q_2 + \ldots + q_n \qquad (C-96)$$

If necessary, relabel the data sets $\Xi_k$ so that all sets within the same class are consecutively numbered. The class identified with the index $\beta$ consists of a vector of measurements, $\underline{\psi}_\beta$, of dimension $q_\beta$,

$$\underline{\psi}_\beta = \begin{pmatrix} \psi_{q_1 + \ldots + q_{\beta-1} + 1} \\ \psi_{q_1 + \ldots + q_{\beta-1} + 2} \\ \vdots \\ \psi_{q_1 + \ldots + q_{\beta-1} + q_\beta} \end{pmatrix} \qquad (C-97)$$

at every point of the grid $M_\beta$. Let $\underline{U}_\beta$ and $\underline{E}_\beta$ be the measured quantities and the errors in the measurements of class $\beta$, and let $\underline{F}_\beta$ be the vector transfer function from anomalous surface potential to the quantities being measured on the grid $M_\beta$. Similarly, let $\Theta_\beta$ and $J_\beta$ be the rotation and spacing matrices of the grid $M_\beta$ defined as in Eqs. C-50 and C-48, respectively.

The approximation to the average spectral density matrix of the residual anomalous surface potential is given by an expression of the same form as Eq. C-92:

$$\Phi_{\delta T_o, \delta T_o} = \frac{1}{\underline{F}^* \, \Phi_{\underline{\zeta}, \underline{\zeta}}^{-1} \, \underline{F} + 1/\Phi_{T_o, T_o}} \qquad (C-98)$$

C-32

where

$$
\Phi_{\underline{\zeta},\underline{\zeta}} = \begin{pmatrix}
\Phi_{\underline{\zeta}_1,\underline{\zeta}_1} & 0 & . & . & . & 0 \\
0 & \Phi_{\underline{\zeta}_2,\underline{\zeta}_2} & . & . & . & 0 \\
. & . & . & & & . \\
. & . & & . & & . \\
. & . & & & . & . \\
0 & 0 & . & . & . & \Phi_{\underline{\zeta}_n,\underline{\zeta}_n}
\end{pmatrix}
$$

(C-99)

with $\Phi_{\underline{\zeta}_\beta,\underline{\zeta}_\beta}$ the spectral density of the errors of class $\beta$ given by

$$
\Phi_{\underline{\zeta}_\beta,\underline{\zeta}_\beta}(\underline{s}) = \tilde{\Phi}_{\underline{E}_\beta,\underline{E}_\beta}(\underline{s}) + \Phi_{\underline{a}_\beta,\underline{a}_\beta}(\underline{s})
$$

(C-100)

In Eq. C-100, $\tilde{\Phi}_{\underline{E}_\beta,\underline{E}_\beta}$ is the finite Fourier transform of the covariance of the measurement errors $E_\beta$ and $\Phi_{\underline{a}_\beta,\underline{a}_\beta}$ is the spectral density of the aliasing errors of class $\beta$ obtained from a formula analogous to Eq. C-95:

$$
\Phi_{\underline{a}_\beta,\underline{a}_\beta}(\underline{s}) = \sum_{\underline{\Lambda} \varepsilon Q_\beta} \underline{F}_\beta(\underline{s}+\theta_\beta J_\beta^{-1}\underline{\Lambda}) \, \underline{F}_\beta^*(\underline{s}+\theta_\beta J_\beta^{-1}\underline{\Lambda}) \, \Phi_{T_o,T_o}(\underline{s}+\theta_\beta J_\beta^{-1}\underline{\Lambda})
$$

(C-101)

where $Q_\beta$ is defined for each class as in Eq. C-94.

In writing the error spectral density matrix, $\Phi_{\underline{\zeta},\underline{\zeta}}$, as in Eq. C-99, it has been assumed that the errors in the measurements of class $\beta$, $\underline{E}_\beta$, are independent of the errors in the measurements of all other classes. This assumption is not necessary to obtain an expression for the average spectral density matrix of the residuals but it is satisfied by the error models given in Section 2.3, and it simplifies the resulting expressions.

Equations C-99 and C-100 indicate that aliasing errors from different classes are uncorrelated. This, indeed, is the case if any pair of grids, $M_{\beta_1}$ and $M_{\beta_2}$, whose axes are parallel have different spacings along each axis, because in that case the aliasing errors in classes $\beta_1$ and $\beta_2$ arise from different spectral components of the field.

The only approximation involved in the use of Eqs. C-98 through C-101 (aside from the flat-earth approximation) is that the correlation between aliasing errors of a given class and field measurements of a different class has been neglected. The energy at frequency $\underline{s}+\Theta_\beta J_\beta^{-1}\underline{\Lambda}$ for $\underline{\Lambda}\neq\underline{0}$ causes aliasing errors of frequency $\underline{s}$ in class $\beta$. However, information about the spectral component at frequency $\underline{s}+\Theta_\beta J_\beta^{-1}\underline{\Lambda}$ can be obtained from measurements in another class and used to correct for the aliasing at frequency $\underline{s}$ in class $\beta$. It is this possible use of the data which is discounted by neglecting the correlation between aliasing errors and measurements in different classes. In most practical cases, this approximation has little effect on the computed residuals because the spectral components affected by (correctable) aliasing in class $\beta$ are usually much better recovered from measurements in another class.

Since the vector transfer function $\underline{F}$ in Eq. C-98 can be expressed as

$$\underline{F} = \begin{pmatrix} \underline{F}_1 \\ \underline{F}_2 \\ \cdot \\ \cdot \\ \cdot \\ \underline{F}_n \end{pmatrix} \qquad (C\text{-}102)$$

where $\underline{F}_\beta$ is the vector transfer function from anomalous surface potential to the measured quantities in class $\beta$ ($\beta = 1, 2, \ldots, n$), Eq. C-98 can be rewritten in a more convenient form as

$$\Phi_{\delta T_o, \delta T_o} = \frac{1}{\displaystyle\sum_{\beta=1}^{n} \underline{F}_\beta^* \, \Phi_{\underline{\zeta}_\beta, \underline{\zeta}_\beta}^{-1} \, \underline{F}_\beta + 1/\Phi_{T_o, T_o}} \qquad (C\text{-}103)$$

Each of the terms in the summation in the denominator of Eq. C-103 arises from a single class of measurements.

The various measurement classes considered in this report are listed in Section 2.2. Note that by taking as many terms as appropriate in the summation of Eq. C-103, any combination of survey alternatives can be analyzed. In addition, for any scalar-measurement class $\beta$, the contribution to the sum of the denominator in Eq. C-103 is a product of scalar quantities which can be written as $|F_\beta|^2/\Phi_{\zeta_\beta, \zeta_\beta}$. Thus, for all scalar-measurement classes, there is no need to carry out a matrix inversion to evaluate the residuals.


C.4    RESIDUALS OF SPATIALLY AVERAGED QUANTITIES

In this section, the formulas given in Section 2.4 for the average spectral density of the residuals of spatially averaged quantities are derived.

Consider a square block whose sides are parallel to the east and north directions and have length a. Let $\underline{x} = (x_1, x_2)^T$ be the center of the block. The a-mean, $\bar{y}^a$, of a field-related quantity y at the point $\underline{x}$ is the average of y on this block, i.e.,

$$\bar{y}^a(\underline{x}) = \frac{1}{a^2} \int_{x_2-a/2}^{x_2+a/2} \int_{x_1-a/2}^{x_1+a/2} y(\underline{x}') \, dx_1' dx_2' \qquad (C-104)$$

where $\underline{x}' = (x_1', x_2')^T$. It is customary to define a-means only at the grid points of a square grid whose axes are oriented towards the east and north directions. However, it is convenient to see Eq. C-104 as defining $\bar{y}^a$ for all $\underline{x}$. The usual collection of a-means is, simply, a sampled version of $\bar{y}^a$.

The quantities $\bar{y}^a$ and y are related by a transfer function. This can be seen by writing Eq. C-104 as a convolution, i.e.,

$$\bar{y}^a(\underline{x}) = \iint_{-\infty}^{\infty} h(\underline{x}-\underline{x}') \, y(\underline{x}') \, dx_1' dx_2' \qquad (C-105)$$

with

$$h(\underline{x}'') = \begin{cases} 1/a^2 & \text{if } |x_1''| < a/2 \text{ and } |x_2''| < a/2 \\ 0 & \text{otherwise} \end{cases} \qquad (C-106)$$

where $\underline{x}'' = (x_1'',x_2'')^T$. Thus, the transfer function from y to $\bar{y}^a$ is

$$\hat{h}(\underline{s}) = \iint_{-\infty}^{\infty} h(\underline{x}'') \, e^{i2\pi<\underline{x}'',\underline{s}>} \, dx_1'' dx_2'' \qquad (C-107)$$

C-36

The evaluation of this integral is straightforward. The result is

$$\hat{h}(\underline{s}) = \frac{\sin\pi as_1}{\pi as_1} \; \frac{\sin\rho as_2}{\pi as_2} \qquad\qquad (C-108)$$

Next, suppose that the vector of quantities to be estimated from the data consists exclusively of a-means. Let $\underline{\bar{w}}^a$ be the vector of a-means to be estimated. The vector transfer function from anomalous surface potential to the estimated vector is $\hat{h}\,\underline{G}$ where $\underline{G}$ is the vector transfer function from anomalous surface potential to the vector $\underline{w}$ whose a-means yield $\underline{\bar{w}}^a$.

According to Eq. C-91, the average spectral density of the residuals in the a-means, $\Phi_{\delta\underline{\bar{w}}^a,\delta\underline{\bar{w}}^a}$ is

$$\Phi_{\delta\underline{\bar{w}}^a,\delta\underline{\bar{w}}^a} = \underline{G}\,\underline{G}^* \; |\hat{h}|^2 \; \Phi_{\delta T_o,\delta T_o} \qquad\qquad (C-109)$$

where $\Phi_{\delta T_o,\delta T_o}$ is the average spectral density of the residual anomalous surface potential given by Eq. C-103. Since the residuals in the estimates of $\underline{w}$ have an average spectral density given by

$$\Phi_{\delta\underline{w},\delta\underline{w}} = \underline{G}\,\underline{G}^* \; \Phi_{\delta T_o,\delta T_o} \qquad\qquad (C-110)$$

the average spectral density in the a-means, $\underline{\bar{w}}^a$, is obtained from that of the residuals in $\underline{w}$ by

$$\Phi_{\delta\underline{\bar{w}}^a,\delta\underline{\bar{w}}^a} = |\hat{h}|^2 \; \Phi_{\delta\underline{w},\delta\underline{w}} \qquad\qquad (C-111)$$

## C.5    AVERAGE MAP ERRORS

The purpose of this section is to prove that, as claimed in Section C.3 of this appendix, rms values of the residuals computed on the basis of Eq. C-86 yield the average rms of the errors in a map of gravity, even in the case in which information concerning the specific location of the measurement grid is available.

Let the measurement grid $M_o$ be as in Section C.2 and suppose it is desired to evaluate the rms of the errors in the estimation of the vector of field-related quantities $\underline{w}$ at a point P as shown in Fig. C-6. It is clear that it is always possible to find a measurement point with respect to which P is displaced by less than $\tau_1'$ units of distance in the positive direction of the $x_1'$ axis and less than $\tau_2'$ in the positive direction of the $x_2'$ axis. Let the displacements in the $x_1'$ and $x_2'$ directions be $c_1'$ and $c_2'$ with $0 \leq c_1' < \tau_1'$ and $0 \leq c_2' < \tau_2'$. Define another grid, $M_c$, parallel to and having the same spacings as the grid $M_o$ but displaced from it by the amounts $c_1'$ and $c_2'$ as in Fig. C-7. The point P belongs to the grid $M_c$.

As shown in Section C.2, the errors in the estimation of $\underline{w}$ at the points belonging to the grid $M_c$ are stationary and their spectral density matrix $\tilde{\Phi}'_{\delta\underline{w},\delta\underline{w}}(\underline{c}',\underline{s}')$ is given by Eq. C-77. Their covariance is the inverse finite Fourier transform of $\tilde{\Phi}'_{\delta\underline{w},\delta\underline{w}}(\underline{c}',\underline{s}')$; i.e.,

$$R_{\delta\underline{w},\delta\underline{w}}(\underline{c}',\underline{\Omega}) = \int_{-\bar{s}_2'}^{\bar{s}_2'} \int_{-\bar{s}_1'}^{\bar{s}_1'} \tilde{\Phi}'_{\delta\underline{w},\delta\underline{w}}(\underline{c}',\underline{s}') \, e^{-i2\pi<J\underline{\Omega},\underline{s}'>} \, ds_1' ds_2'$$
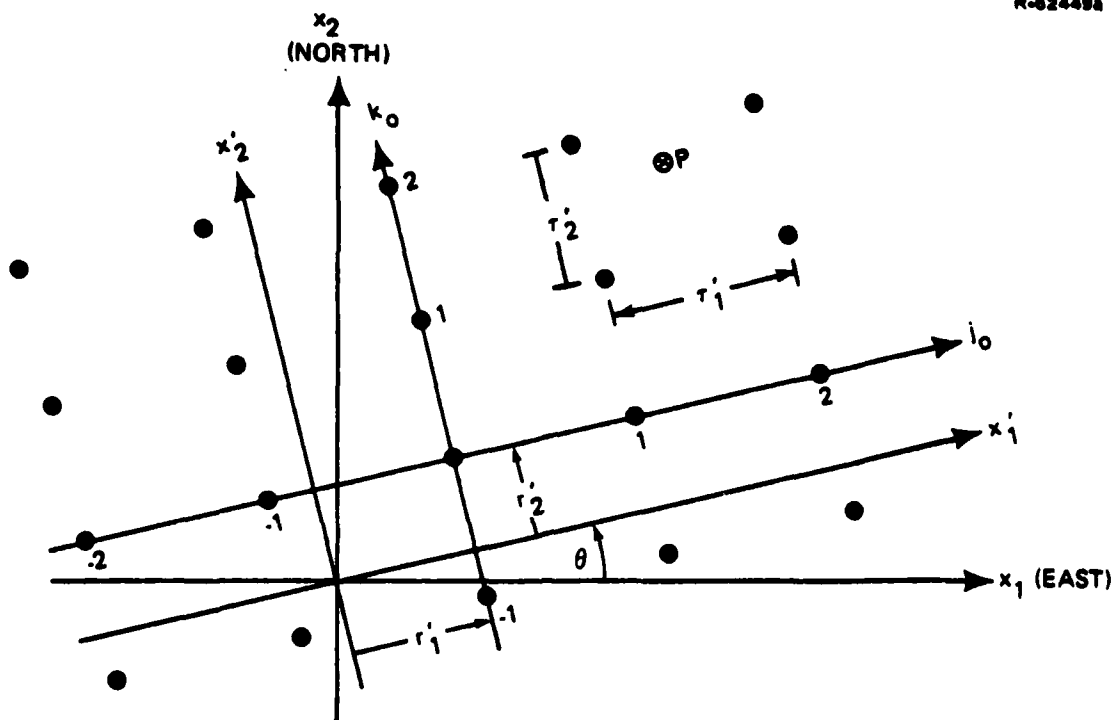
$$(C-112)$$

C-38

Figure C-6    Position of the Point P in Relation
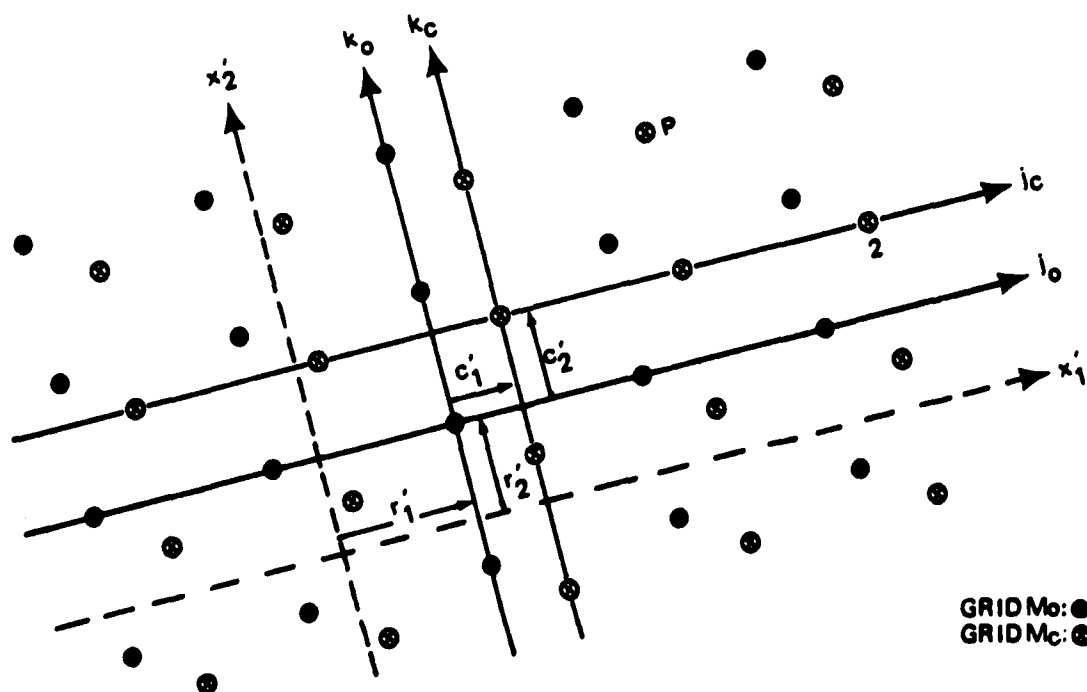              to the Measurement Grid $M_o$

Figure C-7    Definition of the Grid $M_c$

where $\bar{s}_1'$, $\bar{s}_2'$ and J are defined in Section C.2, $\underline{\Omega}$ is the integer vector coordinate difference in the grid $M_c$ and the argument $\underline{c}'$ of the covariance emphasizes its dependence on the shift between the estimation and measurement grids.

The variance of the estimation errors at any point on the grid $M_c$, $\underline{\sigma}^2(\underline{c}')$, is given by the diagonal elements of the covariance matrix evaluated at an integer vector coordinate difference of zero; i.e.,

$$\underline{\sigma}^2(\underline{c}') = \text{diag }[R_{\delta\underline{W},\delta\underline{W}}(\underline{c}',\underline{0})] \qquad\qquad \text{(C-113)}$$

Consequently, from Eq. C-112

$$\underline{\sigma}^2(\underline{c}') = \int_{-\bar{s}_2'}^{\bar{s}_2'} \int_{-\bar{s}_1'}^{\bar{s}_1'} \text{diag}[\tilde{\Phi}_{\delta\underline{W},\delta\underline{W}}'(\underline{c}',\underline{s}')] \, ds_1' ds_2' \quad \text{(C-114)}$$

The average variance of the errors in the estimates is defined as

$$\underline{\sigma}^2 = \frac{1}{\tau_1\tau_2} \int_0^{\tau_1} \int_0^{\tau_2} \underline{\sigma}^2(\underline{c}') \, dc_1' dc_2' \qquad\qquad \text{(C-115)}$$

Replacing $\underline{\sigma}^2(\underline{c}')$ by the expression in the right-hand side of Eq. C-114 and interchanging integrations with respect to displacements and frequencies results in

$$\underline{\sigma}^2 = \text{diag} \left\{ \int_{-\bar{s}_2'}^{\bar{s}_2'} \int_{-\bar{s}_1'}^{\bar{s}_2'} \left[ \frac{1}{\tau_1\tau_2} \int_0^{\tau_1} \int_0^{\tau_2} \tilde{\Phi}_{\delta\underline{W},\delta\underline{W}}'(\underline{c}',\underline{s}') dc_1' dc_2' \right] ds_1' ds_2' \right\}$$

$$\text{(C-116)}$$

The quantity in brackets is readily recognized as the spectral density of the errors in a random grid defined in Eq. C-78. Thus,

$$\underline{\sigma}^2 = \text{diag} \left[ \int_{-\bar{s}_2'}^{\bar{s}_2'} \int_{-\bar{s}_1'}^{\bar{s}_1'} \tilde{\Phi}'_{\delta\underline{w},\delta\underline{w}}(\underline{s}') \, ds_1' ds_2' \right] \qquad \text{(C-117)}$$

It was shown in Section C.3 that $\Phi'_{\delta\underline{w},\delta\underline{w}}$ can be written as the aliased version of a continuous process whose spectral density, $\Phi'_{\delta w,\delta w}$, is given by Eq. C-86. From Eqs. C-85 and C-117 it follows that the average variance of the errors in the estimates is

$$\underline{\sigma}^2 = \text{diag} \left[ \int_{-\bar{s}_2'}^{\bar{s}_2'} \int_{-\bar{s}_1'}^{\bar{s}_1'} \sum_{\underline{\Lambda}} \Phi'_{\delta\underline{w},\delta\underline{w}}(\underline{s}'+J^{-1}\underline{\Lambda}) \, ds_1' ds_2' \right]$$

$$\text{(C-118)}$$

where $\underline{\Lambda} = (\ell,m)^T$ is a vector of integers. Interchanging the operations of summation and integration, Eq. C-118 becomes

$$\underline{\sigma}^2 = \text{diag} \left[ \sum_{\ell} \sum_{m} \int_{-\bar{s}_2'}^{\bar{s}_2'} \int_{-\bar{s}_1'}^{\bar{s}_1'} \Phi'_{\delta\underline{w},\delta\underline{w}}(\underline{s}'+J^{-1}\underline{\Lambda}) \, ds_1' ds_2' \right]$$

$$\text{(C-119)}$$

Consider the integral $I(\ell,m)$ associated with the indices $\ell$ and $m$ in Eq. C-119. This integral can be written as

C-41

$$I(\ell,m) = \int_{-\bar{s}_2'}^{\bar{s}_2'} \int_{-\bar{s}_1'}^{\bar{s}_1'} \Phi'_{\delta\underline{w},\delta\underline{w}} \left[(s_1'+2\ell\bar{s}_1', s_2'+2m\bar{s}_2')^T\right] ds_1' ds_2'$$

$$(C-120)$$

where use of Eqs. C-48 and C-59 has been made. Changing integration variables

$$I(\ell,m) = \int_{(2m-1)\bar{s}_2'}^{(2m+1)\bar{s}_2'} \int_{(2\ell-1)\bar{s}_1'}^{(2\ell+1)\bar{s}_1'} \Phi'_{\delta\underline{w},\delta\underline{w}}(\underline{s}') \, ds_1' ds_2'$$

$$(C-121)$$

Consequently, combining Eqs. C-119 and C-121,

$$\underline{\sigma}^2 = \text{diag}\left[\sum_\ell \sum_m \int_{(2m-1)\bar{s}_2'}^{(2m+1)\bar{s}_2'} \int_{(2\ell-1)\bar{s}_1'}^{(2\ell+1)\bar{s}_1'} \Phi'_{\delta\underline{w},\delta\underline{w}}(\underline{s}') \, ds_1' ds_2'\right]$$

$$(C-122)$$

The integrals in Eq. C-122 are taken over disjoint domains of the frequency plane whose union equals the whole plane. Thus,

$$\underline{\sigma}^2 = \text{diag}\left[\int_{-\infty}^{\infty} \Phi'_{\delta\underline{w},\delta\underline{w}}(\underline{s}') \, ds_1' ds_2'\right] \qquad (C-123)$$

This last equation is the result that was sought. It shows that the average variance of the residuals, defined by Eq. C-115, can be computed as the total power under the diagonal elements of the average spectral density matrix of residual gravity.

C-42

# REFERENCES

1. Wiener, N., _The Extrapolation, Interpolation and Smoothing of Stationary Time Series_, John Wiley & Sons, Inc., New York, 1949.

2. Heiskanen, W.A., and Moritz, H., _Physical Geodesy_, W.H. Freeman and Co., Inc., San Francisco, 1967.

3. Wong, E., _Stochastic Processes in Information and Dynamical Systems_, McGraw-Hill Book Co., Inc., New York, 1971.

4. Jordan, S.K., and Sherman, G.N., "Spatial Gauss-Markov Models of Ocean Currents," _IEEE Transactions on Aerospace and Electronic Systems_, Vol. AES-15, No. 6, November 1979.

5. Gelb, A. (Editor), _Applied Optimal Estimation_, MIT Press, Cambridge, 1974.

6. Lee, V., and Wunsch, C., _Atlas of the Mid-Ocean Dynamics Experiment (MODE-1)_, MIT Press, Cambridge, 1977.

7. Schwiderski, E.W., "On Charting Global Ocean Tides," _Reviews of Geophysics and Space Physics_, Vol. 18, No. 1, February 1980.

8. Heller, W.G., "Error Models for Prototype Moving-Base Gravity Gradiometers," The Analytic Sciences Corporation, Technical Report TR-823-1, April 1977.

9. White, J.V., "Error Models for Gravity Gradiometers in Airborne Surveys," The Analytic Sciences Corporation, Technical Report TR-868-2, January 1980.

10. "Gravity Gradiometer Instrument (GGI) and the Gravity Gradiometer System (GGS) Definition Studies Program GGI Analyses and Studies Report," Bell Aerospace Textron, Report No. 6441-927014, May 1979.

11. "Moving Base Gravity Gradiometer Review," Bell Aerospace Textron, Air Force Academy Report No. 6441-927018, February 1979.

<u>REFERENCES</u> (Continued)

12.  "Bell GGI Test Procedure No. TP5, Temperature Sensitiv-
     ity," Bell Aerospace Textron, Report No. 6441-928005,
     Issue C, February 1978.

13.  Heller, W.G., and Jordan, S.K., "Attenuated White Noise
     Statistical Gravity Model," <u>Journal of Geophysical Re-
     search</u>, Vol. 84, No. B9, August 1979.

14.  Jordan, S.K., "Self-Consistent Statistical Models for
     the Gravity Anomaly, Vertical Deflections and Undula-
     tion of the Geoid," <u>Journal of Geophysical Research</u>,
     Vol. 77, No. 20, July 1972.

15.  Gihman, I.I., and Skorohod, A.V., <u>The Theory of Stochas-
     tic Processes I</u>, Springer-Verlag, New York, 1974.

16.  Butzer, D.L., and Nessel, R.J., <u>Fourier Analysis and
     Approximation</u>, Vols. I and II, Academic Press, New York,
     1971.

17.  Donoghue, W.R., Jr., <u>Distributions and Fourier Trans-
     forms</u>, Academic Press, New York, 1969.

18.  Abramowitz, M., and Stegun, I.A., <u>Handbook of Mathemati-
     cal Functions</u>, Dover Publications, Inc., New York, 1972.

19.  Erdélyi, A. (Editor), <u>Tables of Integral Transforms</u>,
     Vol. II, McGraw-Hill Book Co., Inc., New York, 1954.

20.  Friedman, B., <u>Principles and Techniques of Applied
     Mathematics</u>, John Wiley and Sons, Inc., New York, 1956.

21.  Davenport, W.B., Jr., and Root, W.L., <u>An Introduction
     to the Theory of Random Signals and Noise</u>, McGraw-Hill
     Book Co., Inc., New York, 1958.

22.  Jazwinski, A.H., <u>Stochastic Processes and Filtering
     Theory</u>, Academic Press, New York, 1970.

23.  Larimore, W.E., Thomas, S.W., and Baumgartner, S.L.,
     "Statistical Modeling of Gravity Disturbances Using
     Measured Anomaly Data," The Analytic Sciences Corpo-
     ration, Technical Report TR-776-1, May 1977.

24.  Davis, T.J., "Theory and Practice of Geophysical Survey
     Design," Naval Oceanographic Office, Report No. NOORP-13,
     Washington, D.C., October 1974.

# END

# FILMED

11-85

# DTIC